Activation and Utilization of DNA Damage Signaling by Murine Polyomavirus

Katie Heiser

B.S. University of Maryland, 2007

A thesis submitted to the

Faculty of the Graduate School of the

University of Colorado in partial fulfillment

of the requirement for the degree of

Doctor of Philosophy

Department of Molecular, Cellular, and Developmental Biology

2016

This thesis entitled:

Activation and Utilization of DNA Damage Signaling by Murine Polyomavirus
Written by Katie Heiser

Has been approved for the Department of Molecular, Cellular, and Developmental Biology

_____

(Dr. Robert L. Garcea)

Date _____

_____

(Dr. Bradley Olwin)

Date _____

The final copy of this thesis has been examined by the signatories, and we find that both the content and the form meet acceptable presentation standards of scholarly work in the above mentioned discipline.

Abstract

Katie Heiser, Department of Molecular, Cellular, and Developmental Biology

Activation and Utilization of DNA Damage Signaling by Murine Polyomavirus

Thesis directed by Professor Robert L. Garcea

Nuclear replication of DNA viruses activates DNA damage repair (DDR) pathways, which may detect and inhibit viral replication. However, many DNA viruses also depend on these pathways in order to optimally replicate their genomes. I investigated the relationship between murine polyomavirus (MuPyV) and components of DDR signaling pathways including CHK1, CHK2, H2AX, ATR, ATM, RPA, MRN, and DNAPK. I found that recruitment and retention of DDR proteins at viral replication centers was independent of H2AX, as well as the viral small and middle T-antigens. Additionally, infectious virus production required ATR kinase activity, but was independent of CHK1, CHK2, or DNAPK signaling. ATR inhibition did not reduce the total amount of viral DNA accumulated, but affected the amount of virus produced, indicating a defect in virus assembly. Additionally, by creating a mutant virus (E320A), I found large T-antigen binding to RPA was required for appropriate viral genome resolution. The E320A mutant virus produced approximately 5-fold less infectious virus than WT and replicated viral DNA that was concatemerized. Taken together, these data suggest that MuPyV may utilize a subset of DDR proteins or non-canonical DDR signaling pathways in order to efficiently replicate and assemble. Specifically, these results demonstrate the requirement for DDR proteins in appropriate resolution and packaging of the viral genome. Finally, I utilized an optimized set-up for Stochastic Optical Reconstruction Microscopy (STORM) to interrogate the sub-nuclear domains of MuPyV replication and assembly. I observed an exclusionary relationship between T-antigen and the host cell protein, PML. I was also able to visualize MuPyV “factories” and virions formed by viral protein, VP1 for the first time using a light microscopy based technique. This technique will greatly enhance our

ability to observe and study the composition of these sub-nuclear structures. These findings expanded to our understanding of the mechanisms of PyV replication and assembly.

Table of Contents:

Chapter 1
Introduction to Polyomaviruses

1.1 Introduction:

1.1.1 DNA Tumor Viruses and Disease

The *Adenoviridae, Polyomaviridae* and *Papillomaviridae* are families of small double-stranded DNA viruses that cause tumors. These viruses manipulate conserved cellular pathways, including those that control cellular proliferation, apoptosis, cell cycle regulation, and mitogenic signaling. Studies of the interaction of these viruses with host cell pathways greatly enhanced our understanding of cell signaling and oncogenesis.

The first adenoviruses (Ads) were isolated from adenoids and are the causal agent of respiratory disease in humans (Rowe, et al. 1953). The Ads are a family of double-stranded DNA viruses with a linear, approximately 36 kb genome (Davison, et al. 2003). The Ad capsid is non-enveloped, icosahedral, and comprised of three major and five minor capsid proteins (Russell 2009). The study of Ad early proteins and their targets has greatly aided our understanding of cellular functions including DNA replication, transcriptional regulation, and cell cycle control (Levine 2009, O'Shea 2005). In addition to the contributions made by Ad research to our understanding of basic cell biology, Ads are also used as gene transfer vectors (Ginn, et al. 2013).

The papillomaviruses (PVs) can induce papillomas in their host (Shope and Hurst 1933). PVs have a double stranded circular genome of approximately 8kb and protein capsid comprised of late viral proteins, L1 and L2. Human Papillomavirus (HPV) causes cervical and other types of cancer in humans. High risk HPV serotypes HPV 16 and 18 are responsible for the majority of

these cases (Walboomers, et al. 1999). These viruses encode E6 and E7 proteins, which bind to and inhibit p53 and phosphorylated retinoblastoma protein (pRb) (Dyson, et al. 1989, Werness, et al. 1990). Interactions with p53 and pRb aid viral replication by driving cell proliferation, but also contribute to oncogenic transformation (Yim and Park 2005).

1.1.2 Discovery of polyomaviruses (PyVs) and their genome structure

The two founding viruses in the family *Polyomaviridae* were Simian virus 40 (SV40) and murine polyomavirus (MuPyV). In the 1950s, MuPyV was identified as an agent in a filtered extract that caused tumors in baby mice (Gross 1953, Stewart, et al. 1957). SV40 was discovered in 1960 as a contaminating agent in the monkey kidney cells used to produce the Polio vaccine (Sweet and Hilleman 1960). Following this discovery the potential role for SV40 in cancer and human disease was extensively studied (Garcea 2001, Garcea and Imperiale 2003, Mutti, et al. 1998).

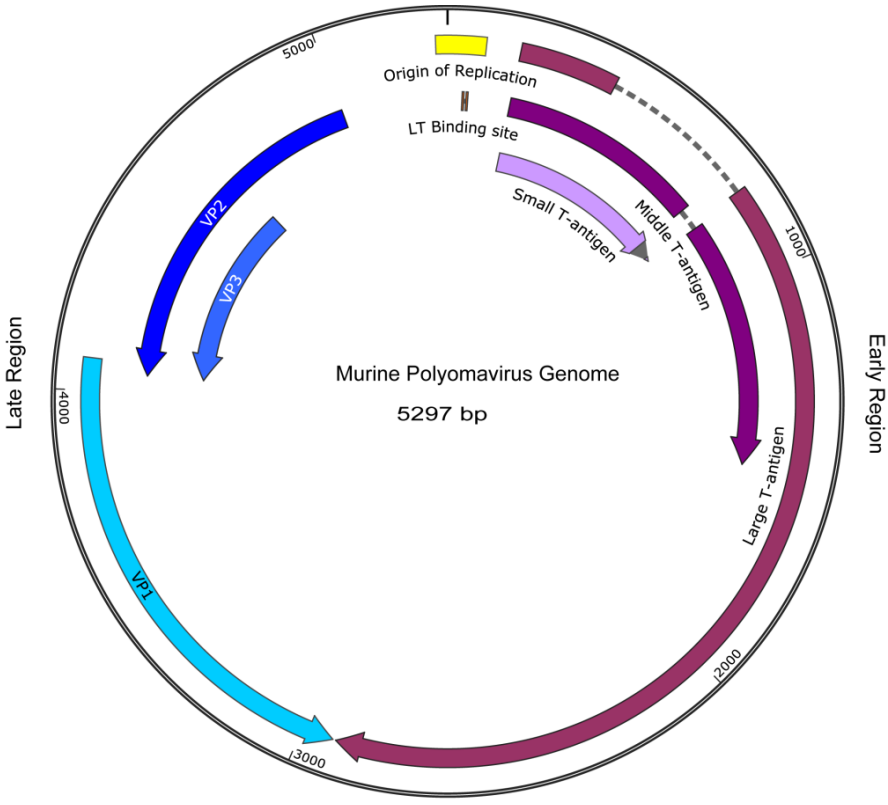

Figure 1.1 MuPyV genome: The MuPyV genome encodes three Tag proteins in the early region and VP1, VP2 and VP3 in the late region

The PyV genome is divided into an early region, a late region, and an origin of replication or a non-coding regulatory region. The early region encodes the T-antigen

proteins, small (ST), large (LT), and some PyVs also encode a middle T-antigen (MT) or a T'(Treisman, et al. 1981). The late region encodes the viral capsid proteins VP1, VP2, VP3 and some PyVs encode a VP4. Several PyVs also encode a small multifunctional protein, agnoprotein, which is involved in many stages of infection including, transcriptional regulation, virion release and DNA replication. The viral genome is circular, approximately 5 kb, and incorporates roughly 24 host nucleosomes (Saragosti, et al. 1980). The PyV genome is encaspidated in an icosahedral virion comprised of pentameric subunits of VP1 or capsomeres. The minor capsid proteins (VP2/3) interact with the internal face of the VP1 capsomers and are believed to play roles in capsid stability and host cell entry (Daniels, et al. 2006, Mannova, et al. 2002).

1.1.3 Human polyomaviruses and disease

Human PyVs establish persistent infections and have a seroprevelance of 70-90% in adults. Seroepidemiology studies suggest that exposure to most PyVs occurs at a young age (Kean, et al. 2009). Two human PyVs were discovered in the 1960s and 1970s and they were named for the index case patients (JC and BK).

Virus	Associated Disease
JCPyV	Progressive Multifocal Leukoencephalopathy (PML)
BKPyV	Polyomavirus-Associated Nephropathy (PVAN)
MCPyV	Merkel Cell Carcinoma
TSPyV	Trichodysplasia spinulosa-associated polyomavirus

Table 1: Human PyVs and their associated diseases

BK polyomavirus (BKPyV) was originally isolated from a renal transplant patient in 1971(Gardner, et al. 1971). BK infection is a contributing factor to PyV-associated nephropathy (PVAN) in renal transplant patients (Kuypers 2012). PVAN is dangerous to the patient and can cause loss of the transplant in many cases. However, in non-immunosuppressed individuals,

BKPyV and other human PyVs likely establish latent infection in the kidneys and other tissues without causing significant disease.

JC polyomavirus (JCPyV) was discovered in 1965 in brain tissue from a patient with Progressive Multifocal Leukoencephalopathy (Padgett, et al. 1971, Zurhein and Chou 1965). JCPyV was later found to be the causative agent of PML in immunocompromised patients (Ferenczy, et al. 2012). Although most human PyVs have a seroprevalence of 70-90%, JCPyV antibodies are present in only 40-60% of the adult population (Egli, et al. 2009, Kean, et al. 2009). A new class of immunosuppressive drugs to treat MS and other disorders is associated with in increased risk of PML in JCPyV positive individuals (Major 2010).

Merkel cell polyomavirus (MCPyV) is the causative agent of at least 80% of Merkel cell carcinoma cases (Rodig, et al. 2012). Like other PyV induced diseases, Merkel cell carcinoma (MCC) has an increased prevalence in immunocompromised patients (Koljonen, et al. 2009, Toker 1972). Interestingly, MCPyV induced MCCs contain a clonal integration of the viral genome with mutations in the DNA binding domain of the LT gene (Schmitt, et al. 2012). Therefore, MCC is caused by a replication incompetent form of the MCPyV genome, similar to cancers caused by HPV and other DNA tumor viruses.

1.1.4 Polyomavirus entry into host cells

Gangliosides are the primary cell surface receptor for PyVs (Taube, et al. 2010). MuPyV utilizes a range of ganglioside receptors including GD1a and GT1b in order to enter cells, whereas the primary ganglioside receptor for SV40 is GM1 (Low, et al. 2004, Smith, et al. 2003, Tsai, et al. 2003). In addition to gangliosides, most PyVs also utilize a protein receptor or co-receptor. MuPyV interacts with the alpha4/beta1 integrin heterodimer in a secondary binding

event following ganglioside interactions (Caruso, et al. 2003). Differences in receptor specificity between viruses likely contribute to species and cell type specificity of PyVs.

Once PyVs are endocytosed, they traffic to the endoplasmic reticulum (ER) where protein disulfide isomerases (PDIs) partially disassemble the capsid (Magnuson, et al. 2005). Although the precise mechanism is not well understood, the viral genome and remaining capsid proteins are translocated out of the ER into the cytosol, likely utilizing components of the ER-associated degradation (ERAD) pathway (Lilley, et al. 2006). The remaining viral proteins and the viral genome are trafficked to the nucleus through recognition of the nuclear localization sequence (NLS) on the capsid proteins by importin, and transcription of early proteins begins (Nakanishi, et al. 2007).

1.1.5 The T-antigen proteins

Expression of the T-antigen (Tag) proteins occurs during early PyV infection and the Tag proteins then prime the cell for replication of viral DNA, through interactions with host cell proteins. MuPyV encodes three Tag proteins ST, MT and LT which are alternatively spliced from the early gene transcript (Treisman, et al. 1981). All three Tag proteins encode a common 79 amino acid N-terminal J-domain that interacts with host cell chaperones Hsc70/Hsp70 (Campbell, et al. 1997, Srinivasan, et al. 1997). The MuPyV ST and MT both interact with subunits of the cellular phosphatase 2A (PP2A) complex (Pallas, et al. 1990).

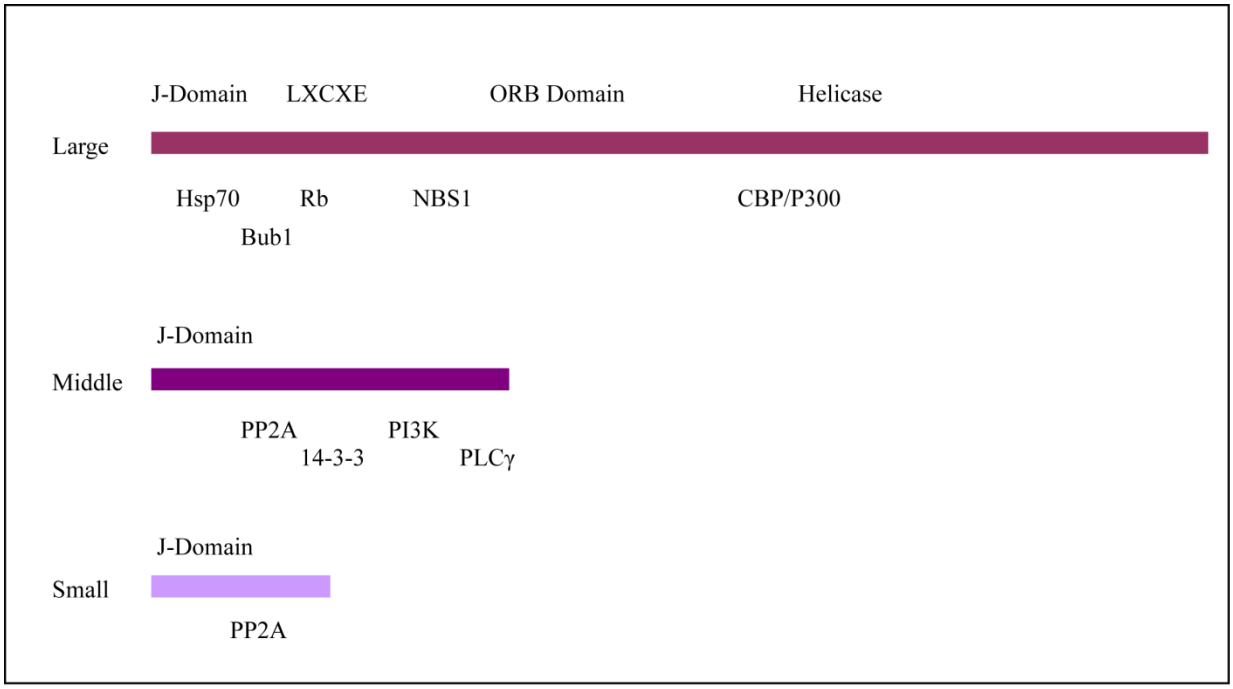

Figure 1.2: T-antigens of MuPyV and select cellular binding partners

PyV ST interacts with PP2A and alters its activity towards targets (Pallas, et al. 1990, Pallas, et al. 1992). ST activates mitogen-activated protein kinase (MAPK) signaling by modulating the phosphorylation level of multiple targets (Sontag, et al. 1993). Additionally, ST plays a role in increasing the acetylation and phosphorylation of histones incorporated into the viral genome (Dahl, et al. 2007, Schaffhausen and Benjamin 1976).

MuPyV and hamster PyV are the only two PyV that encode a MT, which contains a transmembrane domain (Andrews, et al. 1993). MuPyV MT is sufficient to transform some cell types and is widely used to transform cell lines for use as cancer models (Aguzzi, et al. 1990, Bautch, et al. 1987, Fluck and Schaffhausen 2009). MT activates growth factor-like signaling through interactions with the src family kinases (Cheng, et al. 1988, Kornbluth, et al. 1987). This interaction is required for the transforming properties of MT(Guy, et al. 1994). MT also interacts

with PI3K and PLCγ to activate AKT and suppress apoptotic signaling of the host cell (Dahl, et al. 1998, Meili, et al. 1998, Su, et al. 1995, Summers, et al. 1998).

LT is a highly multifunctional viral protein responsible for replicating the viral genome (Topalis, et al. 2013). The LT drives the cell into S-phase of the cell cycle through interactions with phosphorylated retinoblastoma protein (Rb) (DeCaprio, et al. 1988, Dyson, et al. 1990). This interaction activates the E2F family of transcription factors, which induce transcription of host genes responsible for the transition into S-phase and DNA replication. The LT from many PyVs, such as SV40, binds to p53 and inhibits apoptosis of the host cell (Lane and Crawford 1979). MuPyV LT does not directly interact with p53, but ST and MT may inhibit downstream signaling from p53 to functionally inhibit the pathway (Qian and Wiman 2000).

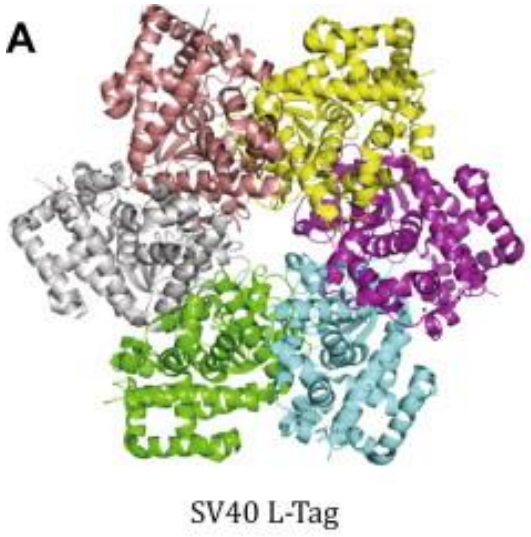

Figure 1.3: Structure of the SV40 LT as a hexameric helicase: The SV40 LT adopts a hexameric conformation to form a ring around the origin of replication of the PyV DNA. Two hexamers are needed to unwind the circular double-stranded genome before the cellular DNA polymerase can begin to duplicate the viral DNA. Figure adapted from Topalis, et al. 2013.

In addition to its roles in modulating the cell cycle, LT forms a hexameric helicase that drives viral DNA replication (Borowiec and Hurwitz 1988, Stahl, et al. 1986). LT forms two helicase complexes that progress bi-directionally around the viral genome (Wessel, et al. 1992). The SV40 LT replisome is the most extensively studied *in vitro* DNA replication system (Fanning and Zhao 2009). LT encodes an origin-binding domain (OBD) that recognizes GAGGC repeat sequences in the PyV origin of replication (Bochkareva, et al. 2006). LT recruits the required cellular proteins to viral DNA, including the DNA polymerase and primase complexes along with replication protein A (RPA) (Malkas and Hickey 1996, Weisshart, et al. 2000, Wold and Kelly 1988).

1.1.6 Late protein expression and virus structure

Large T-antigen induces the switch between early and late protein expression by suppressing transcription of the early promoter and activating transcription of late genes (Brady, et al. 1984). MiRNAs and transcriptional interference may also play a role in regulating this gene transcription "switch" for some PyVs (Sullivan, et al. 2005). Translation of VP1 occurs in the cytoplasm, where it forms pentamers associated with the minor capsid proteins, VP2 and VP3. These pentameric subunits, called capsomers, are then imported into the nucleus, where progeny virions are formed.

The PyV capsid is comprised of 72 pentameric subunits of the major capsid protein, VP1 (Liddington, et al. 1991). VP1 pentamers interact through the C-terminus of VP1 and calcium binding stabilizes this interaction. The minor capsid proteins, VP2 and VP3 associate with the internal face of the VP1 pentamers, interact with the viral genome, and stabilize the virion

structure (Sapp and Day 2009). A single PyV genome is encapsidated in the approximately 50 nm virion.

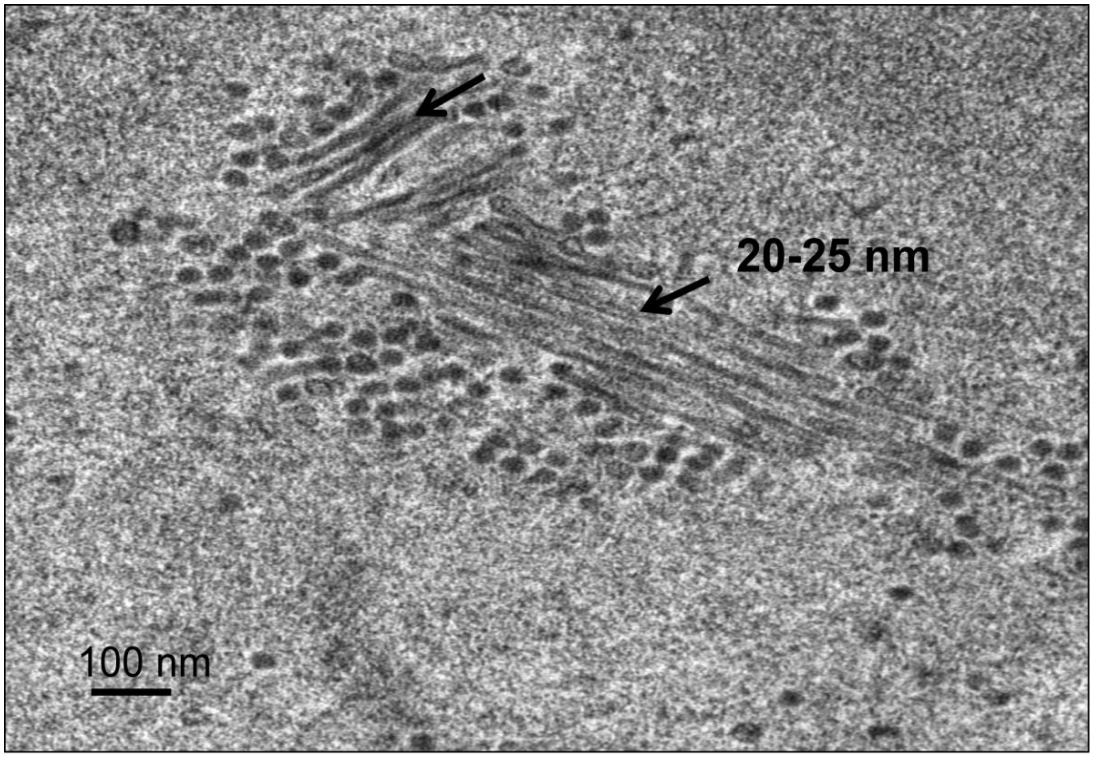

Figure 1.4: Virus Factories in MuPyV infected nuclei. 3T3 cells were infected with PyV (MOI of 10–20 pfu/cell) and harvested at 32 hours post infection (HPI). 70 nm thin section of Epon-embedded cells showing tubular structures adjacent to a virus cluster. (Black arrowheads indicate tubular structures). Figure adapted from Erickson, et al, 2012.

The method of encaspidation of viral genomes during replication of PyVs is not well understood. However, a recent model proposed that PyV VP1 might form tubes that "bud off" progeny virions (Erickson, et al. 2012). Tube-like structures were observed during MuPyV infection and in the brain tissue of a PML patient (Nagashima, et al. 1982). This proposed model for PyV assembly suggests that PyV DNA is packed into these tubes, and then fully formed

viruses bud off the ends or middle. MuPyV infection is generally lytic, so newly formed virions are released when the cell lyses.

1.1.7 Virus-host interactions

Viruses encode proteins that manipulate the host cell environment in order to replicate the viral genome and assembly progeny virions. Viruses form centers to tightly couple the replication of the viral genome and production of virions. These replication centers likely increase the efficiency of virus assembly by concentrating viral proteins and genomes in one location (Novoa, et al. 2005). For example, poliovirus reorganizes the membranes of the ER to create a scaffold for the production of progeny virions in the cytoplasm (Suhy, et al. 2000). However, DNA viruses form replication centers in the nucleus of host cells to facilitate viral DNA replication and assembly of progeny virions (Schmid, et al. 2014).

Host cells utilize adaptive and innate antiviral pathways and proteins in order to suppress or inhibit viral infection. Some of these antiviral agents are constitutively active, whereas others activate in response to viral infection. Interferon responsive genes are activated by pattern recognition receptors, which induce a network of proteins and pathways that suppress infection (Thompson, et al. 2011). Viruses have evolved to suppress many of these antiviral agents, in order to efficiently replicate. Additionally, different viruses will require different pathways to facilitate the replication of viral DNA and assembly of progeny virions. Although there are cellular pathways activated by many types of viral infections, the role of these pathways frequently varies between different types of viruses.

1.1.8 PML-NBs and virus infection

Tri-partite motif (TRIM) proteins acts as antiviral agents that recognize and inhibit viral infections (Rajsbaum, et al. 2014). Promyelocytic leukemia protein (PML) is TRIM family protein with a ring finger domain, two b boxes and a coiled-coil domain (Jensen, et al. 2001). PML forms discrete nuclear dots, known as PML-nuclear bodies (PML-NBs). During adenovirus infection, viral protein E4ORF3 functionally inhibits and reorganizes PML intro tracks throughout the nucleus (Carvalho, et al. 1995, Doucas, et al. 1996). This inhibition is required for efficient replication and assembly of adenovirus. The HSV-1 protein, ICP0, also disrupts PML-NBs and targets PML and PML-NB associated protein, Daxx, for degradation (Maul, et al. 1993).

In contrast to the antiviral activity of PML, some viruses may utilize PML-NBs as replication centers. Adenovirus, human papillomavirus (HPV), and SV40 viral genomes localize near PML-NBs during infection (Ishov and Maul 1996, Maul, et al. 1996). Additionally, papillomavirus early proteins, E1and E2, and late proteins, L1 and L2, co-localize at PML-NB-associated foci (Day, et al. 1998, Heino, et al. 2000). Knockout of PML protein reduces bovine papillomavirus (BPV) infection efficiency and viral DNA replication (Day, et al. 2004). These data suggest that PML protein enhances papillomavirus infection and may act as a site to establish viral replication centers.

1.1.9 DNA damage repair (DDR) and virus infection

DNA damage repair (DDR) pathways protect the cellular genome from mutation by repairing lesions from endogenous and exogenous DNA damage. In mammalian cells, ataxia-telangiectasia mutated (ATM) kinase, ataxia-telangiectasia and Rad3 related (ATR) kinase and

DNA dependent protein kinase (DNA-PK) are the phosphatidylinositol 3-kinase-related kinases (PIKKs) that activate DDR proteins and induce checkpoint signaling when cellular DNA damage occurs (Ciccia and Elledge 2010). The ATM and DNA-PK pathways are activated primarily in response to double strand breaks, which are detected and bound by the Mre11-Rad50-Nbs1 (MRN) or Ku70/80 complex (Lee and Paull 2004, Mahaney, et al. 2009, Stracker and Petrini 2011). ATR kinase activates in response to single stranded DNA lesions bound by the replication protein A (RPA) complex (Cimprich and Cortez 2008, Zou and Elledge 2003). ATM, ATR and DNA-PK also phosphorylate H2AX (γH2AX), to maintain repair enzymes around break sites, and checkpoint kinases, CHK1 and CHK2, to prevent progression of the cell cycle while repair occurs (Bassing, et al. 2002, Celeste, et al. 2003, Cimprich and Cortez 2008, Matsuoka, et al. 2007)

In addition to their role in cellular DNA damage, DDR pathways activate when viruses replicate and assemble in the nucleus, resulting in a complex interplay between DDR pathways and viral replication. These cellular DDR pathways can both promote and inhibit viral replication and assembly. For example, Herpes Simplex Virus 1 (HSV-1) utilizes a subset of DDR proteins, including ATM kinase and Mre11, to replicate its viral genome, while degrading others such as RNF8 and RNF168 (Lilley, et al. 2005, Lilley, et al. 2011). Similarly, PyVs such as SV40 and MuPyV utilize ATM signaling to efficiently replicate (Dahl, et al. 2005, Sowd, et al. 2013).

DDR pathways may act as a host cell defense that distinguishes between viral genomes and cellular DNA. For example, during adenovirus (Ad5) infection, the cellular MRN complex acts as a potent inhibitor of viral DNA replication that likely recognizes broken ends of the viral genome and suppresses DNA replication. Specific adenovirus gene products, E4ORF3 and E1B55k, counteract this inhibition by degrading the MRN complex (Carson, et al. 2003, Evans

and Hearing 2005, Stracker, et al. 2002). Similarly, SV40 LT binds to NBS1, and facilitates its proteasome dependent degradation (Wu, et al. 2004, Zhao, et al. 2008).The different interactions between DNA viruses and DDR proteins are related both to the structure of the viral genome (circular *versus* linear) and the phase of the cell cycle during which these viruses replicate (Chaurushiya and Weitzman 2009, Lilley, et al. 2007).

In the case of PyVs, some members of the ATM signaling pathway, including ATM kinase, enhance viral replication and some members may act as antiviral agents, such as NBS1. These complex interactions make it difficult to discern the role for DDR pathways in PyV infection. A more complex analysis of individual components of these pathways is required to understand the mechanism behind their interaction with viral replication.

1.1.10 Specific aims

In my thesis work I aimed to better understand the complex interaction between cellular pathways and MuPyV infection. Specifically, I aim to better understand the functional role of cellular pathways activated by MuPyV as well as, the spatial organization of viral and cellular proteins within the nucleus. In the experiments summarized in the second chapter, I analyzed the role of PML protein and PML-NB associated pathways during MuPyV infection. In the experiments discussed in the third and fourth chapters, I interrogated the functional role of individual components of DDR pathways in MuPyV DNA replication and assembly. The fifth chapter discusses the optimization and utilization of a super resolution imaging technique to describe the spatial organization of MuPyV infection at the nanoscale.

Chapter 2

Role of PML-NBs associated proteins during MuPyV infection

2.1: Introduction

2.1.1 PML-NB description, discovery, disease

Promyelocytic leukemia protein (PML) is tri-partite motif (TRIM) family protein with a ring finger domain, two b boxes and a coiled-coil domain (Jensen, et al. 2001). Many ring finger proteins are ubiquitin ligases, but PML is an E3 SUMO ligase that interacts with SUMO E2 ligase, UBC9 (Chu and Yang 2011, Duprez, et al. 1999). The PML protein was discovered at the boundary of a chromosomal translocation common in acute promyelocytic leukemia patients, which resulted in a PML protein fusion protein with retinoic acid receptor alpha (RARα) (de The, et al. 1990, de The, et al. 1991). Acute promyelocytic leukemia, which is caused by this fusion protein, can be treated with arsenic trioxide, which induces the degradation of the fusion protein (Zhu, et al. 2001). In non-disease states PML forms PML-NBs, which are multifunctional bodies associated with many cellular pathways including, interferon response, transcriptional regulation, and nuclear proteasomes. PML and other PML-NB associated proteins are highly sumoylated. Current models suggest that interactions between proteins and these SUMO chains help form the nuclear body.

PML nuclear bodies, also called "ND10s" are operationally defined as nuclear dots that are immuno-positive for the PML protein (Dyck, et al. 1994). PML is the scaffold protein necessary to form PML-NBs, therefore knockout of PML results in a loss of the nuclear body structure (Ishov, et al. 1999). Interestingly, PML null mice are viable, but show an increased incidence of tumors, suggesting PML is not essential but plays a more subtle role in the cellular response to stress (Wang, et al. 1998). Through interactions with SUMO-1 and sumoylated

proteins, PML-NBs can recruit a wide variety of proteins (Ishov, et al. 1999, Lallemand-Breitenbach, et al. 2001). These interactions allow PML-NBs to modulate the function of DNA damage repair proteins, transcription factors, and apoptosis associated pathways. One well-studied component of PML-NBs is Daxx (death domain-associated protein 6), a transcriptional repressor associated with induction of apoptosis (Salomoni and Khelifi 2006, Torii, et al. 1999). Daxx associates with alpha-thalassemia retardation syndrome x-linked (ATRX) protein, an ATP-dependent chromatin remodeler (Xue, et al. 2003). Together these proteins can target loci and recruit and histone deacetylates (HDACs) to repress transcription of target genes (Hollenbach, et al. 2002).

2.1.2 Role of PML-NBs during viral infection

Many PML-NB proteins, including PML and Sp100 are interferon responsive. Interferon treatment alters the size and number of PML-NBs in a cell (Chelbi-Alix, et al. 1995, Grotzinger, et al. 1996, Regad and Chelbi-Alix 2001). Additionally, during adenovirus infection, PML is functionally inhibited and reorganized into tracks throughout the nucleus formed by viral protein E4ORF3 (Carvalho, et al. 1995, Doucas, et al. 1996). This inhibition is required for efficient replication and assembly of adenovirus. The HSV-1 protein, ICP0, also disrupts PML-NBs and targets PML and Daxx for degradation (Maul, et al. 1993). These data suggest that PML-NBs may function as antiviral agents.

Viral genomes from viruses such as adenovirus, human papillomavirus (HPV), and SV40, localize near PML-NBs during early infection (Ishov and Maul 1996, Maul, et al. 1996). Papillomavirus (PV) early proteins, E1and E2, and late proteins, L1 and L2, co-localize at PML-NB-associated foci (Day, et al. 1998, Heino, et al. 2000). PyV replication centers for adjacent to

PML-NBs and JCV VP1 co-localizes with PML-NBs (Shishido-Hara, et al. 2004). During infection by human PyV, BKPyV, newly replicated viral DNA accumulates at PML-NBs (Jul-Larsen, et al. 2004). These data combined led to the hypothesis that PML-NBs might serve as a scaffold for papillomavirus and PyV assembly.

2.1.3 Association of DNA damage repair pathways with PML-NBs

PML-NBs are implicated as part of the DNA damage repair (DDR) response partially because the number of PML-NBs increases in response to DNA damage (Dellaire, et al. 2006). Additionally, many DDR proteins including, Mre11, ATM, CHK2, and ataxia-telangiectasia and Rad3 related (ATR) kinase, co-localize with PML-NBs (Barr, et al. 2003, Dellaire, et al. 2006, Lombard and Guarente 2000). PML-null cells are resistant to apoptosis following irradiation, suggesting a role in activating the apoptotic response to DNA damage (Wang, et al. 1998). CHK2 directly phosphorylates PML, which induces a PML-dependent apoptotic signal following irradiation (Yang, et al. 2002). In response to DNA damage, CHK2 is activated by the ataxia-telangiectasia mutated (ATM) kinase.

2.1.4 Role of DDR proteins during infection

PyV replication activates and recruits members of the ATM signaling pathway, including the Mre11-NBS1-Rad50 (MRN) complex to viral replication centers in the nucleus (Zhao, et al. 2008). ATM signaling is required during SV40 and MuPyV infection for efficient production of virus. DDR pathways may allow for extended replication time by halting the infected cell in S- or G2-phase of the cell cycle (Dahl, et al. 2005, Orba, et al. 2010). Additionally, DDR proteins may aid the replication and resolution of PyV genomes (Dahl, et al. 2005, Sowd, et al. 2013).

In order to determine if PML-NB associated proteins might be required for PyV infection we analyzed viral replication and assembly in PML-null MEFs. Additionally, we visualized recruitment of DDR proteins and other PML-NB associated proteins to viral replication centers in PML-null MEFs. The relationship between PML-NBs and DDR then led me to test the requirement for ATM, Mre11 and CHK2 activity during MuPyV infection, as well.

2.2 Methods

Cells and Viruses (Adapted from Erickson et al 2012)

A31 3T3 fibroblasts were grown in DMEM (D6429; Sigma) supplemented with 10% bovine calf serum (BCS) and penicillin/streptomycin. C57 mouse embryonic fibroblasts (MEFs) were obtained from ATCC (SCRC-1008; Manassas, VA) and served as a wild-type MEF control. $PML^{-/-}$ MEFs were a gift of Gerd Maul (Ishov, et al. 1999, Wang, et al. 1998). Both MEFs were grown in DMEM supplemented with 20% fetal bovine calf serum (FBS) and antibiotics at 37°C with 5% CO_2. CHK2-null and syngeneic WT controls were a gift from Tak Mak. CHK2-null cells and their syngeneic WT cells were grown in DMEM supplemented with 10% bovine calf serum (BCS), 55 μM βME and penicillin/streptomycin at 37°C with 5% CO_2. Virus strain NG59RA (Feunteun, et al. 1976) was used for all cell culture infections and strain A2 (Griffin, et al. 1974) for mouse infections. Cell culture infections were carried out as described previously (Cripe, et al. 1995). Cells were infected at a multiplicity of infection of 10–20 plaque forming units (PFU) per cell for 22–24 hours for immunofluorescence analysis.

Immunofluorescence (Adapted from Erickson et al 2012)

T-antigen was detected using rat anti-T-antigen (E3, gift of Tom Benjamin) diluted 1:5000. PML was detected using mouse anti-PML (ALX-804-816; Enzo, Plymouth Meeting, PA) diluted

1:1000, MRE11 was detected using rabbit anti-MRE11a (B1447; LSBio) diluted1:1000, CBP was detected using rabbit anti-CBP (LSBio) diluted 1:1000, H4K12ac was detected using rabbit anti-H4K12ac (Epigentek) diluted 1:5000. Secondary antibodies were either AlexaFluor 488- or AlexaFluor 594-conjugated (Invitrogen) and were diluted 1:1000. All antibodies were diluted in 10% FBS/PBS.

Cells were plated on acid-etched coverslips and infected as described above. Coverslips were washed twice with 4 ºC phosphate buffered saline (PBS), pre-extracted with 0.5% Triton X-100 in CSK Buffer (10 mM piperazine-1,4-bis(2-ethanesulfonic acid) (PIPES), pH 6.8, 100 mM NaCl, 300 mM sucrose, 1 mM $MgCl_2$, 1 mM EGTA) on ice for 5 mins, washed twice with 4 ºC PBS, and fixed with 4% paraformaldehyde (PFA) for 10 mins at room temperature (RT). Following an overnight block in 10% BCS, coverslips were incubated with primary antibody at 37ºC for 1 hr, washed three times with 10% BCS in PBS, then incubated for 1 hr at RT with secondary antibodies. Slides were washed three times in PBS and then mounted in ProLong antifade reagent containing DAPI (Invitrogen) and allowed to cure at 22 ºC for 24-48 hrs.

Fluorescence *in situ* Hybridization (Adapted from Erickson et al 2012)

To detect MuPy viral genomes after infection, we used nick-translation to label DNA probes specific for MuPyV DNA. Briefly, the entire MuPy viral genome (NG59RA) was cloned into pUC18 at BamHI (pUC-PyV) and 2 µg plasmid DNA was labeled with SpectrumRed using the Vysis Nick Translation Kit (Abbott Molecular, Des Plaines, IL), according to the manufacturer protocol. Labeled DNA was ethanol-precipitated with herring sperm and human Cot-1 DNA and re-suspended in 20 µl cDen-Hyb (Insitus Biotechnologies, Albuquerque, NM) to yield a final probe concentration of 100 ng/µl.

FISH analysis was performed as described previously (Jul-Larsen, et al. 2004), with some modifications. Briefly, cells grown on coverslips were infected, fixed and immunostained for viral or host proteins, as described above. Immunostained cells were fixed a second time with 4% PFA in PBS to crosslink bound antibodies followed by treatment with 0.2 mg/ml RNase Type III (Sigma) in 2X SSC at 37°C for 15 min and washed in 2X SSC 3 times. The PyV DNA probe was diluted in cDenHyb and hybridized to samples for 2 min each at 90°C, 80°C, 70°C, 60°C, 50°C and 45°C followed by an overnight incubation at 37°C. Coverslips were washed at 45°C with 1.5X SSC, 50% formamide/1.5X SSC, and 1.5X SSC for 5 min each. Stained cells were mounted onto glass slides with ProLong anti-fade reagent containing Dapi (Invitrogen) and allowed to incubate at 22°C overnight.

Confocal Microscopy (Adapted from Erickson et al 2012)

Imaging of fixed cells was performed with an inverted fluorescence microscope (TE2000-U; Nikon) equipped with an electron-multiplying charge-coupled device camera (Cascade II; Photometrics) and a Yokogawa spinning disc confocal system (CSU-Xm2; Nikon). Images were taken with a 60X NA 1.4 oil objective using MetaMorph (version 7.0; MDS Analytical Technologies) software. The data from each channel (excitation wavelengths at 488, 543 and 633 nm) were collected sequentially using the appropriate band-pass filters built into the instrument. Data sets were processed using ImageJ (National Institutes of Health) software. Data shown are single z-plane confocal images.

Viral Release Assay (From Erickson et al 2012)

10^5 cells per 60mm dish were seeded 12–16 hrs before infection with NG59RA. At this density, the cells were 50–60% confluent at the time of infection. Virus preparation and infection was

carried out as described above. At times indicated, supernatants were transferred to 15 ml conical tubes and saved. Cells remaining on the plate were treated with neuraminidase (NA) Type V (Sigma) diluted in NA buffer (10 mM Hepes, pH 5.6/1 mM $CaCl_2$/1 mM $MgCl_2$/5 mM KCl) at 37°C for 30 min. The NA supernatant was collected and combined with the cell supernatant. The plates were washed with PBS 3 times and each wash was collected and combined with supernatants. The combined supernatants and washes were stored at −20°C and are referred to as the "viral supernatant."

Nuclease-Resistant Genome Quantitation (From Erickson et al 2012)

Viral DNA was isolated from viral supernatants using the method described for Ad supernatants (Thomas, et al. 2007) with some modifications. Briefly, 50 µl viral supernatant was digested with DNase (RQ1, Promega) at 37°C for 1 hr. DNase-treated samples were incubated with Proteinase K (Fermentas) for 37°C for 1 hr. The viral DNA was purified using the Wizard DNA Clean-up System (Promega) according to the manufacturer protocol except 80% ethanol was used in place of isopropanol during the wash. The viral DNA was eluted with 50 µl prewarmed (80°C) milli-Q water and stored at −20°C until ready for use.

Primer Express 3.0 software (Applied Biosystems, Warrington, UK) was used to design probes and primers for amplification of a 67-bp region of the mouse polyomavirus genome (NCBI accession # NC_001515). PCR primers were synthesized by IDT and the TaqMan probe was synthesized by Applied Biosystems. The following primers were used: PyV VP1 forward primer, 5′TGGGAGGCAGTCTCAGTGAAA3′; PyV VP1 reverse primer, 5′TGAACCCATGCACATCTAACAGT3′; PyV VP1 probe, 5′CCGAGGTGGTGGGCTCTGGC3′. The TaqMan probe was labeled with FAM (6-

carboxy-fluorescein) at the 5′ end and a quencher, TAMRA (6-carboxy-tetramethylrodamine) at the 3′ end. Optimal concentrations of probe and primer were determined using a concentration matrix, as described in Applied Biosystems protocols.

Quantitative PCR (qPCR) reactions were prepared in 96-well optical plates (Applied Biosystems) in a volume of 25 µl. Each reaction contained 200 nM TaqMan probe, 900 nM of each forward and reverse primer, 12.5 µl TaqMan Master Mix (Applied Biosystems) and 5 µl purified viral DNA or DNA standards. The intensity of fluorescence of the reporter label was normalized to the ROX Passive Reference, supplied in the master mix solution. DNA amplification was carried out using an Applied Biosystems 7500 Real-Time PCR Sequence Detection System using cycling conditions of 50°C for 2 min, 95°C for 10 min followed by 40 cycles of 95°C for 15 sec, 60°C for 1 min. For each run, duplicates of seven dilutions of the viral standard DNA (from 0.1 ng to 5×10^{-5} ng; pGEX-VP1 plasmid DNA), viral DNA samples and no template controls were simultaneously subjected to analysis. The number of genomes was determined as previously described(Thomas, et al. 2007) and is reported as "nuclease-resistant genomes (NRG) per ml."

Small molecule inhibitors:

All small molecule inhibitors were dissolved in DMSO and diluted in DMEM with 10% serum to indicated concentrations and added to cells at 2-4 HPI: Mirin (Tocris); PF477736 (Tocris); and KU55933 (Tocris).

Viral DNA Isolation:

Viral DNA was isolated by Hirt extraction (Hirt 1967), with modifications. Briefly, cellular DNA was precipitated in high salt and remaining supernatants were treated with 10 µg RNase,

followed by 25 µg of proteinase K. Viral DNA was purified by phenol-chloroform extraction and sodium acetate/ethanol precipitation. The DNA pellet was re-suspended in 50 µL Tris-EDTA, diluted 1:200, and analyzed by qPCR, using same primers and methods as described above for "nuclease-protected genomes".

Statistical analysis:

All error bars are standard error of the mean of three of more biological replicates. Statistical significance was calculated using a two-tailed student's t-test assuming unequal variance. p values of <0.05 indicated with *, p values of <0.01 indicated with **.

2.3 Results

2.3.1 Viral Replication centers form adjacent to PML-NBs in WT and PML-null MEFs

BKPyV replication centers form at PML-NBs, leading to the suggestion that these nuclear bodies may act to establish centers for viral replication. I found that MuPyV replication centers also formed adjacent to PML-NBs in MEFs (Fig 2.1A). These replication centers are marked by the presence of viral protein, Tag and MuPyV DNA (Fig 2.1B). Additionally, cellular DDR protein Mre11 was present at these nuclear sites (Fig 2.1C).

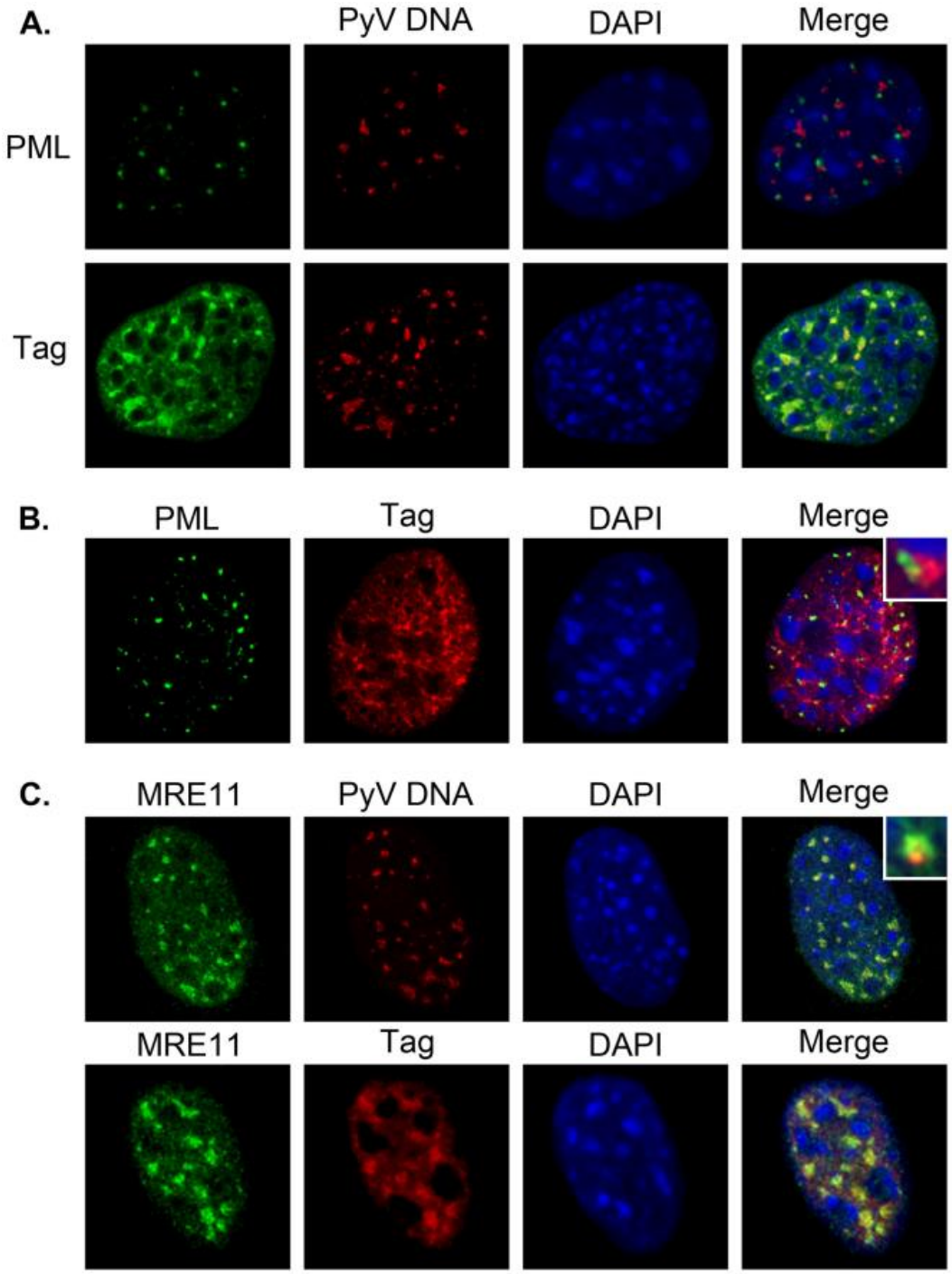

Figure 2.1: MuPyV DNA and T-antigen are localized near PML-NBs. C57 MEFs were infected at an MOI of 30–40 pfu/cell. At 24 or 28 HPI cells were fixed, permeabilized, and co-stained with either anti-PML, anti-Tag and/or anti-MRE11 antibodies followed by AlexaFluor-conjugated secondary antibodies, a fluorescently-labeled MuPyV DNA FISH probe, and DAPI staining of nuclei. A) MuPyV-infected C57 MEFs at 24 HPI stained for either PML (top) or Tag (bottom) followed by fluorescent in situ hybridization (FISH) for MuPyV DNA. B) PyV-infected C57 MEFs at 28 HPI co-stained for PML and Tag. C) C57 MEFs at 24 HPI co-stained for either MRE11 and MuPyV DNA (by FISH) or MRE11 and Tag. Insets show enlarged regions from image to illustrate the localization of proteins in relation to each other (B) or PyV DNA (C). **Figure from Erickson et al. 2012**

PML protein is required for the formation of PML-NBs in the nucleus. Knockout of PML results in loss of nuclear body formation and PML associated proteins no longer form foci in the nucleus. I analyzed viral replication centers in PML-null MEFs to determine the role for PML-NBs in MuPyV replication center formation. I found that MuPyV formed replication centers in the nucleus of infected PML-null MEFs similarly to WT cells (Fig. 2.2 A, B). Tag and MuPyV DNA co-localized in foci in nucleus and Mre11 was recruited to the replication centers in the absence of PML (Fig. 2.2 B).These results show that PML protein and PML-NBs were not required for formation of MuPyV replication centers in the nucleus.

2.3.2 PML-NB associated protein, Daxx, is diffusely localized during infection of PML-null MEFs

Daxx is a transcriptional repressor that associates with PML-NBs. In WT MEFs, Daxx co-localizes with PML in discrete nuclear bodies (Fig. 2.3 A). During MuPyV infection of WT MEFs, Daxx was localized in puncta in the nucleus that are adjacent to viral replication centers (Fig. 2.3 B). Since PML protein is required for PML-NB formation, Daxx was not localized to nuclear bodies in PML-null MEFs. In PML-null MEFs Daxx associated with heterochromatin, which can be visualized as bright foci stained by DAPI (Fig. 2.3 C). During MuPyV infection of PML-null MEFs, Daxx was diffusely localized throughout the nucleus, and was not co-localized with heterochromatin (Fig. 2.3 D). It is unclear why the localization of Daxx changed during infection of PML-null cells, but not WT cells.

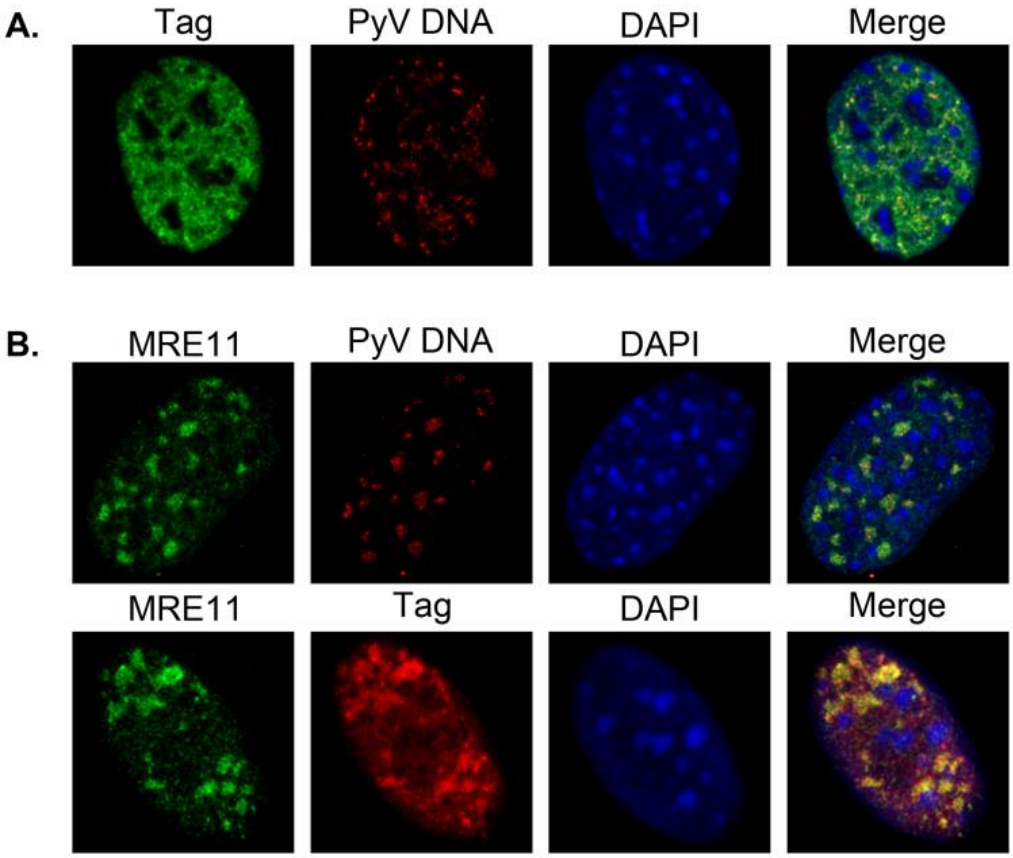

Figure 2.2: Mre11, MuPyV DNA and T-antigen localization in PyV-infected PML−/− MEFs. PML−/− MEFs were infected with MuPyV at an MOI of 30–40 pfu/cell. At 22 or 24 HPI cells were fixed, permeabilized, and co-stained with either anti-Tag and/or anti-MRE11a antibodies followed by AlexaFluor-conjugated secondary antibodies, a fluorescently-labeled MuPyV DNA FISH probe, and DAPI staining of nuclei. A) FISH for MuPyV DNA at 24 HPI followed by antibody staining for Tag. B) Infected cells were stained by FISH for MuPyV DNA at 22 HPI followed by antibody staining for MRE11 or co-stained for MRE11 and Tag. **Figure from Erickson et al. 2012**

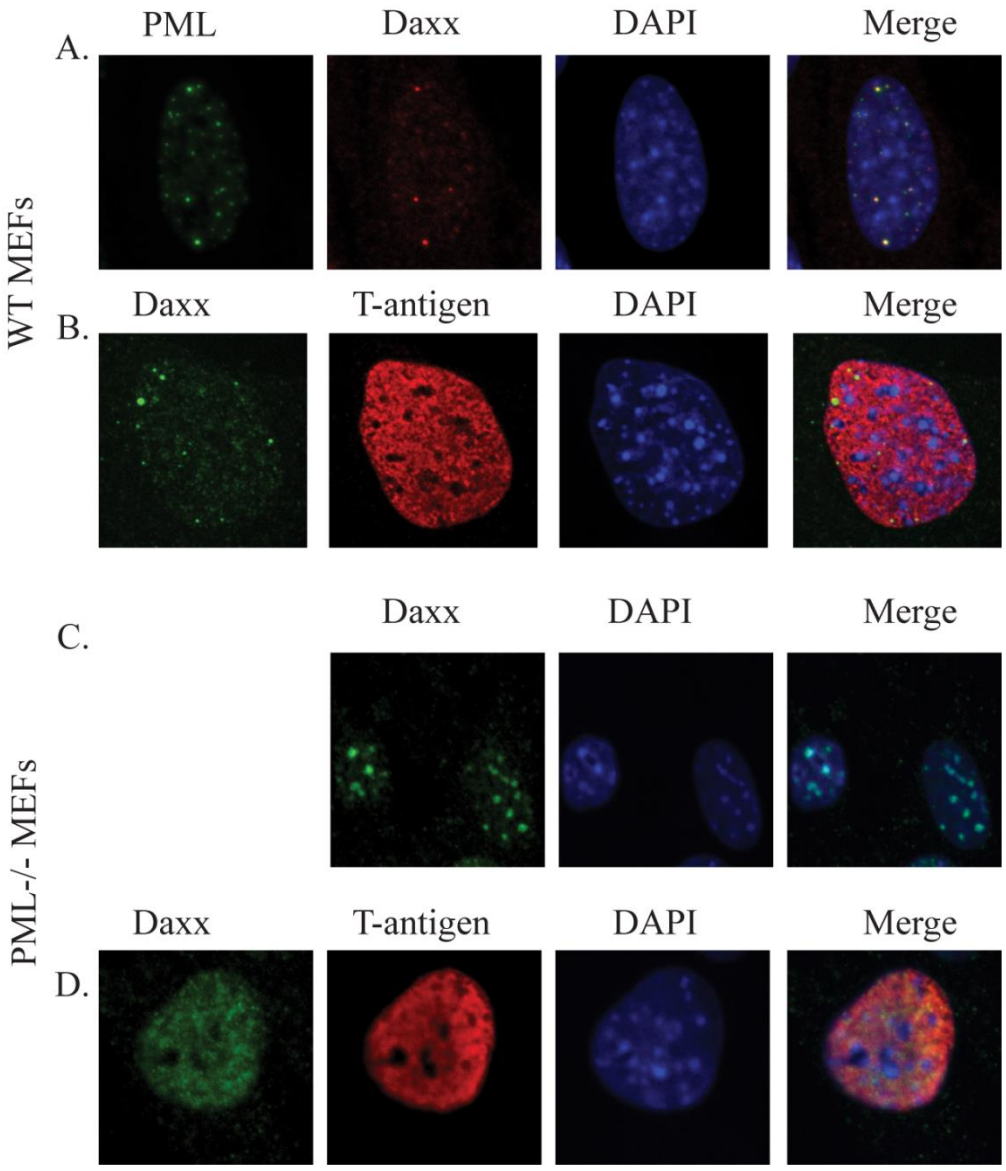

Figure 2.3: In PML -/- MEFs, Daxx localizes to chromatin and not Nuclear Bodies. A) Uninfected WT MEFs, fixed permeabilized and immunostained for PML and Daxx or B) WT MEFs infected with NG59RA at 28 HPI, immunostained for Daxx and Tag C) Uninfected PML -/- MEFs immunostained for Daxx and D) PML -/- MEFs infected with NG59RA at 28 HPI immunostained for Daxx and T-antigen. All images are single z-plane confocal images.

2.3.3 CREBBP (CBP) co-localizes with viral replication centers in WT and PML–null MEFs

CREB-binding protein (CBP) is a cellular histone-acetyltransferase (HAT) that localizes to PML-NBs (LaMorte, et al. 1998). MuPyV LT binds to CBP/P300 through a conserved motif and inhibits transactivation of some cellular targets. However, the LT interaction with CBP increases HAT activity and increases the abundance of H4K12ac and H3K56ac (Saenz Robles, et al. 2013). In uninfected MEFs, CBP was diffusely localized throughout the nucleus (Fig. 2.4 A) However, during infection CBP was reorganized to viral replication centers in the nucleus (Fig 2.4 B, C). CBP co-localized with Tag during infection, likely because it is directly bound by Tag (Fig 2.4 C). To determine if PML-NBs affect recruitment and retention of CBP to viral replication, I analyzed CBP localization in WT and PML-null MEFs. I found that CBP recruitment to replication centers was not affected by PML-NBs (Fig 2.4 C, D). Neither CBP nor Mre11 recruitment to MuPyV replication centers was affected PML knockout, suggesting that PML does not play a role is establishing these centers.

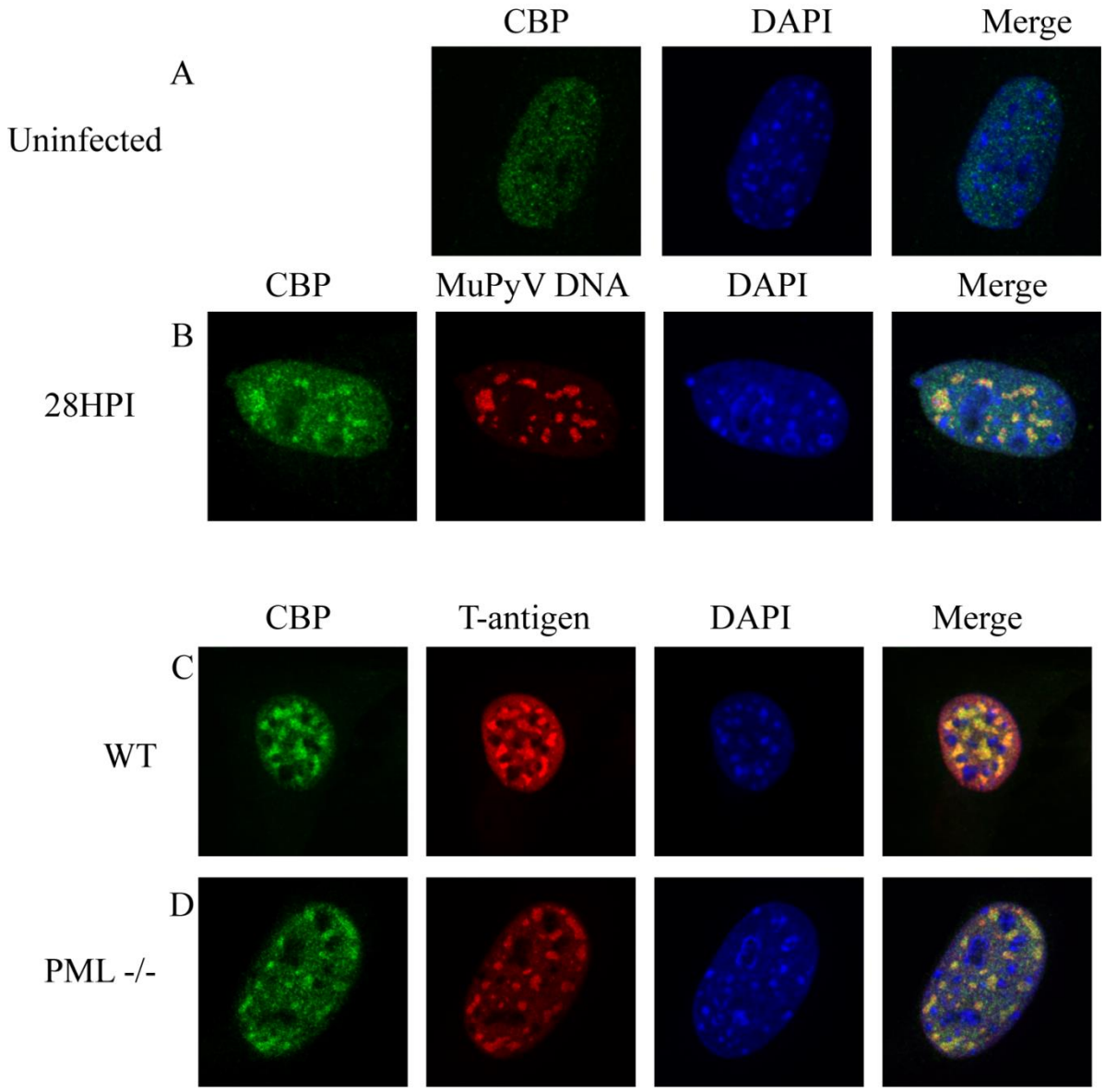

Figure 2.4: CBP localizes to viral replication centers in WT and PML-/- MEFs. **A**) Uninfected WT MEFs, fixed permeabilized and immunostained for CBP **B**) WT MEF infected with NG59RA at 28 HPI, stained for CBP and MuPyV DNA by FISH **C**) WT MEF infected with NG59RA at 28 HPI immunostained for CBP and Tag **D**) PML-/- MEF infected with NG59RA at 28 HPI immunostained for CBP and Tag

2.3.4 Histone H4K12 acetylation (H4K12ac) is enriched at MuPyV replication centers

Several cellular transcription factors, histone acetyltransferases (HATs), and HDACs associate with PML-NBs, leading to the hypothesis that the nuclear bodies may also regulate gene expression and transcription of some pathways (Takahashi, et al. 2004). Expression of LT stabilizes CBP/P300, a PML-NB associated HAT, and increases acetylation of cellular histones (Saenz Robles, et al. 2013). Additionally, histone acetylation which is regulated by the MuPyV ST, is important for viral gene expression and DNA replication (Schaffhausen and Benjamin 1976). In order to determine if H4K12ac was enriched at MuPyV replication centers, I analyzed H4K12ac localization during infection of MEFs. In mock infected cells, H4K12ac localized to euchromatin, but not heterochromatin, in the nucleus, as expected (Fig. 2.5 A). However during infection, H4K12ac is enriched at viral DNA replication centers and co-localized with Tag in nuclear foci (Fig. 2.5 B). This observation suggests that viral DNA that was present at these sites is likely highly acetylated.

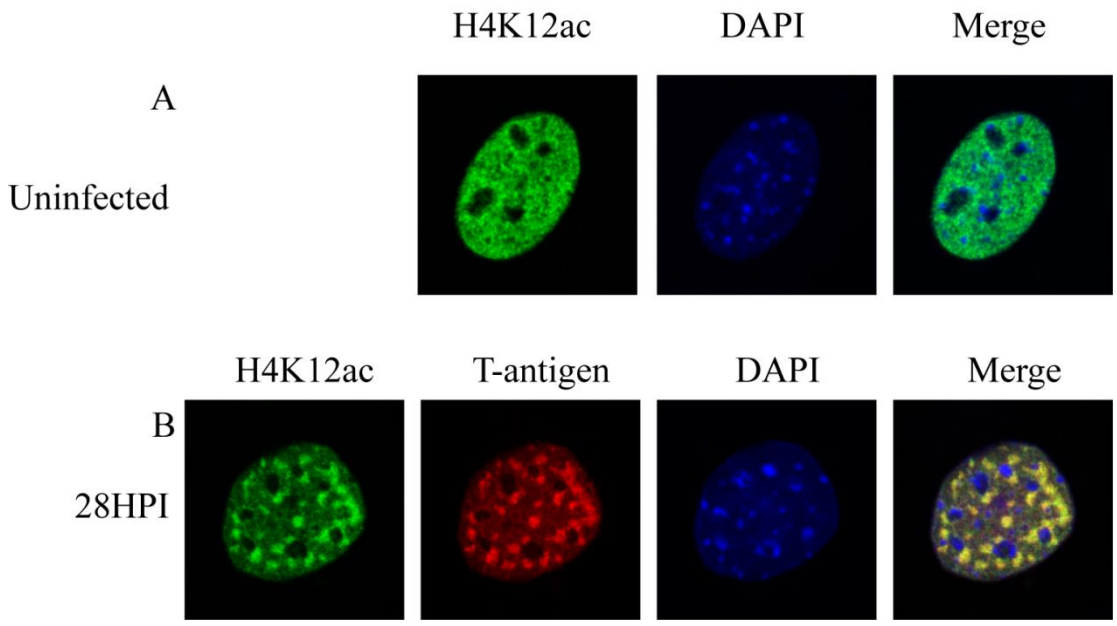

Figure 2.5: H4K12ac is enriched at viral replication centers. A) Uninfected WT MEFs were fixed, permeabilized and immunostained for H4K12ac. **B**) WT MEFs were infected with NG59RA at 28 HPI, fixed, permeabilized and immunostained for H4K12ac and Tag.

	Six days post-infection[a]		Fourteen days post-infection[a]	
Mouse Tissue	**Wild-Type**	**PML$^{-/-}$**	**Wild-Type**	**PML$^{-/-}$**
Spleen	2.8×10^{6}	2.7×10^{6}	5.1×10^{5}	8.0×10^{4}
Liver	1.1×10^{6}	2.6×10^{6}	1.1×10^{6}	1.2×10^{5}
Kidney	3.0×10^{6}	5.0×10^{6}	1.2×10^{5}	1.2×10^{5}
Lung	2.3×10^{5}	3.2×10^{5}	2.4×10^{5}	1.0×10^{4}

[a]Mean values shown as PyV genome copies/μg tissue DNA.
doi:10.1371/journal.ppat.1002630.t002

Figure 2.6: PML is dispensable for MuPyV replication *in vivo.* Viral titers from different tissues at six days or fourteen days post infection from PML null or WT mice. Figure form Erickson et al, 2012. **Experiment and figure by Eva Szomolanyi-Tsuda**.

2.3.5 PML Protein is not required for MuPyV infection

PML is required for efficient replication of some papillomaviruses, but its role in PyV infection remains unclear. *In vivo* studies of MuPyV replication and spread in mice showed that PML protein was not required for productive MuPyV infection (Fig 2.6). *In vitro* studies of MuPyV replication in WT and PML-null MEFs also showed no difference in viral outputs (Erickson et al, 2012). Therefore, PML protein is not required for MuPyV replication or assembly and does not affect formation of MuPyV replication centers in the nucleus.

2.3.6 Inhibition of DDR signaling during MuPyV reduced nuclease-protected genomes

Since PML was not required for MuPyV, but DDR proteins were still recruited to replication centers, I analyzed the requirement for DDR pathways using small molecule inhibitors. Previous reports show that ATM signaling is required during MuPyV infection and SV40 infection (Dahl, et al. 2005, Zhao, et al. 2008). Therefore, I targeted known members of the ATM pathway with drug inhibitors. Infection in the presence of an ATM inhibitor, KU55933, showed a dose responsive reduction in virus yield by a protected genomes assay at 48 HPI (Fig. 2.7 A). Additionally, inhibitors of Mre11 (Mirin) and CHK2 (CHK2 inhibitor II) showed dose responsive reductions in nuclease protected genomes (Fig. 2.7 B, C). In contrast, inhibition of CHK1 using PF477736 did not affect the amount of virus produced (Fig. 2.7 D). These results suggested that components of the ATM signaling pathway were required for MuPyV replication or assembly, but CHK1 signaling was not required.

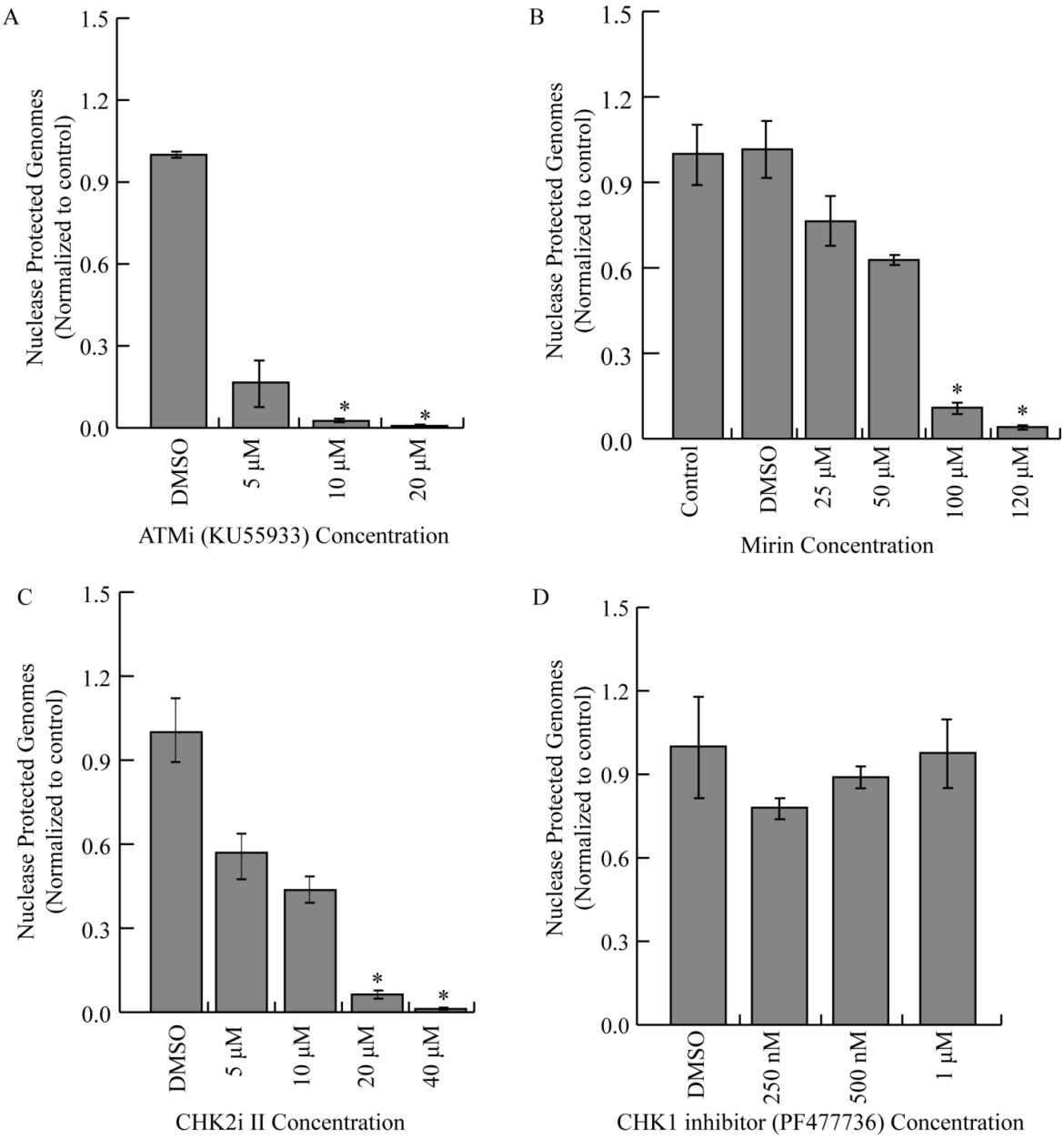

Figure 2.7: Inhibition of ATM, Mre11 or CHK2 during infection reduced viral outputs. Viral outputs from MEFs at 48 HPI quantified by nuclease protected genomes assay in the presence of increasing concentrations of **A**) ATM inhibitor, **B**) Mre11 inhibitor, **C**) CHK2 inhibitor, or **D**) CHK1 inhibitor. Normalized to DMSO control.

2.3.7 Mre11 inhibition, but not ATM or CHK inhibition, resulted in reduced viral DNA accumulation

In order to determine if ATM, CHK2 or Mre11 were required for viral DNA replication or assembly, I analyzed total viral DNA in infected cells at 30 HPI. Cells treated with an ATM inhibitor, a CHK2 inhibitor or a CHK1 inhibitor accumulated WT levels of viral DNA (Fig. 2.8). In contrast Mirin, an Mre11 nuclease inhibitor, reduced total viral DNA by about 80% (Fig. 2.8). These results suggested that Mre11 activity was required for viral DNA synthesis, but ATM and CHK2 activity were required for viral genome packaging.

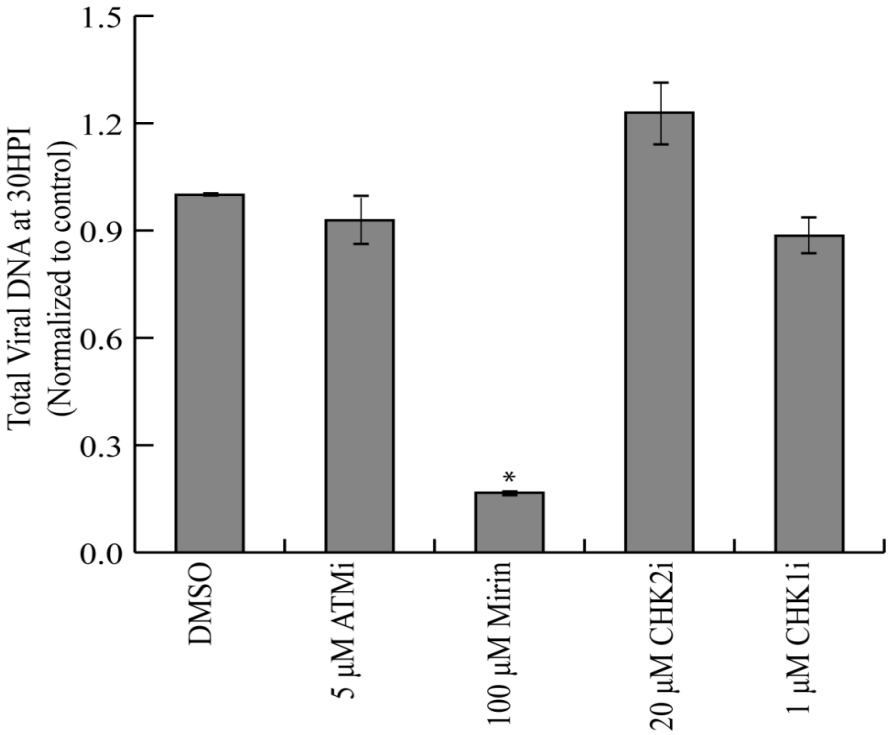

Figure 2.8: DNA accumulation is affected by Mre11 inhibition, but not ATM, CHK2 or CHK1 inhibition. Viral DNA was isolated by Hirt extraction from cells infected with NG59RA at 30 HPI. Viral DNA accumulation at 30 HPI was quantified by qPCR for VP1 gene of MuPyV genome, normalized to DMSO control.

2.3.8 CHK2 knockout cell line did not recapitulate inhibitor results

To confirm the specificity of the inhibitor results, I analyzed viral titers from CHK2 WT and null fibroblasts. CHK2 null cells produced similar viral titers to syngeneic WT cells (Fig. 2.9). Additionally, CHK2 null cells treated with CHK2 inhibitor II showed significant reductions in viral titer. Taken together, these results show that the effect of the CHK2 inhibitor was not specific and it is unclear why the reductions in viral titer occurred in the original experiments. Additionally, I created cell lines with knockdowns of ATM and members of the MRN complex, Mre11, and NBS1. The viral titers from these cell lines were variable between experiments and the results were therefore difficult to interpret (data not shown). Therefore, I was unable to genetically confirm the requirement for members of the ATM signaling pathway. However, the role and requirement for these pathways is more extensively tested and discussed in chapters three and four.

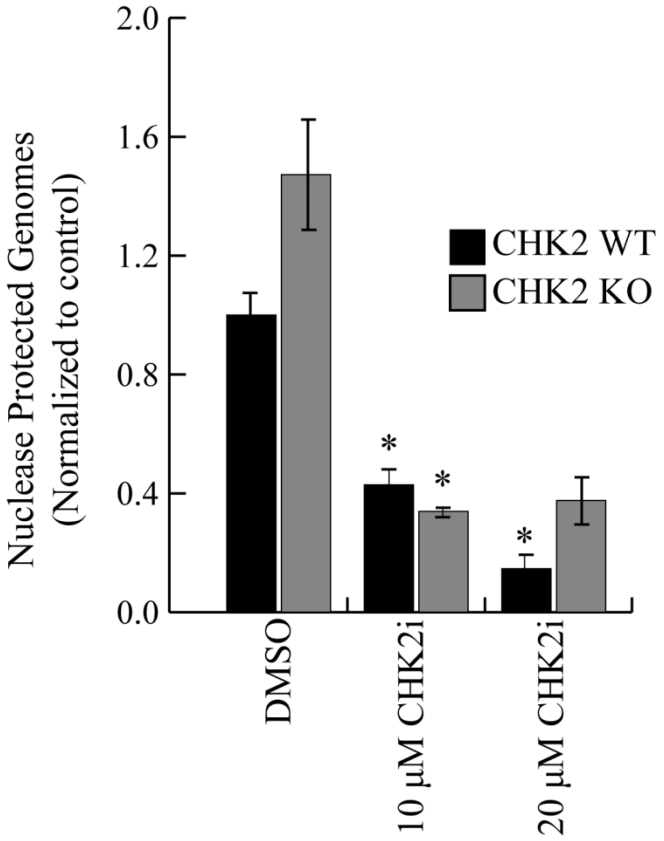

Figure 2.9: CHK2 inhibitor reduces viral titers in CHK2 null cells. Viral titers, quantified by protected genomes assay, produced by CHK2 WT and CHK2 null fibroblasts infected with NG59RA at 48 HPI in presence or absence of CHK2 inhibitor. Normalized to WT DMSO control.

2.4 Conclusions:

I characterized the formation of nuclear MuPyV replication centers and tested the requirement for several cellular pathways during infection. Although PML-NBs are required for productive infection by some papillomaviurses, they are not required during MuPyV infection. The knockout of the PML protein did not affect viral replication center formation, or viral titers *in vivo* or *in vitro*. I also tested the role of several DDR proteins during infection using small molecule inhibitors. Although the initial results of these experiments suggested a role for components of the ATM pathway, I was unable to confirm these results genetically. In order to better assay the requirement for cellular proteins during infection, I developed a new assay to analyze these experiments. This assay, referred to as an immunoplaque assay, is discussed and utilized in subsequent chapters.

2.5 Discussion:

PML-NBs are described as sites for the formation of PyV and papillomavirus replication centers, but we found that they were not required for MuPyV virus production, DNA replication, or recruitment of cellular proteins to replication centers. Therefore, PML-NBs must play a very different role in papillomavirus infection than in MuPyV infection. Although, I saw a change in the localization of PML-NB protein, Daxx during infection of PML-null fibroblasts, there were no changes in DDR protein localization. This observation coupled with the previously reported requirement for ATM signaling during PyV infection, made DDR proteins an obvious next target for analysis.

PML-NBs are associated with a wide variety of DDR proteins, including Mre11, ATM and CHK2. It is possible that PML-NBs localize at or adjacent to PyV replication centers

because DDR pathways are active at these sites. Since Mre11 co-localized with Tag and viral DNA at replication centers in WT and PML-null MEFs, we tested the requirement for these DDR proteins during infection. A limited screen of small molecule inhibitors to DDR proteins showed a reduction in viral titers following inhibition of proteins in the ATM pathway. I first attempted to confirm the requirement for CHK2 using a knockout cell line. I found that the CHK2 knockout cell lines did not have reduced viral outputs and the CHK2 inhibitor treatment reduced viral outputs in the knockout cells. These data strongly suggest that the CHK2 inhibitor results were due to an off target effect of the drug.

The unreliable nature of the inhibitor experiments, coupled with the variability I observed between experiments led to concerns about the significance of experiments done with the "protected genomes assay" utilized in these experiments. This problem led me to develop a new assay to quantify viral titers. The assay I developed, referred to as an "immunoplaque" assay is discussed in Chapters 3 and 4, along with further interrogation of DDR targets discussed in this chapter.

Chapter 3
Activation of DNA damage repair pathways by MuPyV

3.1 Introduction

3.1.1 Cellular DNA damage signaling

Robust replication and repair of DNA is required to maintain the integrity of the cellular genome. DNA damage repair (DDR) pathways protect the genome from mutation by repairing lesions from endogenous and exogenous DNA damage. In mammalian cells, ataxia-telangiectasia mutated (ATM) kinase, ataxia-telangiectasia and Rad3 related (ATR) kinase and DNA dependent protein kinase (DNA-PK) are the phosphatidylinositol 3-kinase-related kinases (PIKKs) that activate DDR proteins and induce checkpoint signaling when cellular DNA damage occurs (Ciccia and Elledge 2010). The ATM and DNA-PK pathways are activated primarily in response to double strand breaks, which are detected and bound by the Mre11-Rad50-Nbs1 (MRN) or Ku70/80 complex (Lee and Paull 2004, Mahaney, et al. 2009, Stracker and Petrini 2011). ATR kinase activates in response to single stranded DNA lesions bound by the replication protein A (RPA) complex (Cimprich and Cortez 2008, Zou and Elledge 2003). ATM, ATR and DNA-PK also phosphorylate H2AX (γH2AX), to maintain repair enzymes around break sites, and checkpoint kinases, CHK1 and CHK2, to prevent progression of the cell cycle while repair occurs (Bassing, et al. 2002, Celeste, et al. 2003, Cimprich and Cortez 2008, Matsuoka, et al. 2007).

3.1.2 DDR and viral replication

In addition to their role in cellular DNA damage, these DDR pathways often activate during viral replication and assembly in the nucleus, resulting in a complex interplay between

DDR pathways and viral replication. These cellular DDR pathways can both promote and inhibit viral replication and assembly. Herpes Simplex Virus 1 (HSV-1) utilizes a subset of DDR proteins, including ATM kinase and Mre11, to replicate its viral genome, while degrading others such as RNF8 and RNF168 (Lilley, et al. 2005, Lilley, et al. 2011). DDR pathways act as a host cell defense that distinguishes between viral genomes and cellular DNA. For example, during adenovirus (Ad5) infection, the cellular MRN complex acts as a potent inhibitor of viral DNA replication, but specific viral gene products, E4ORF3 and E1B55k, counteract this inhibition by degrading the MRN complex (Carson, et al. 2003, Evans and Hearing 2005, Stracker, et al. 2002). The different interactions between DNA viruses and DDR proteins are related both to the structure of the viral genome (circular *versus* linear) and the phase of the cell cycle during which these viruses replicate (Chaurushiya and Weitzman 2009, Lilley, et al. 2007).

3.1.3 Polyomaviruses and DDR proteins

Polyomaviruses (PyVs) are small dsDNA viruses with circular genomes that replicate in the nucleus. The murine polyomavirus (MuPyV) genome has six gene products, three early T-antigen proteins (small, middle, and large) and three late proteins (VP1, VP2, and VP3). The T-antigen (Tag) proteins prime the cell for viral DNA replication through interactions with host proteins. Small T-antigen (ST) binds to PP2A and modulates the phosphorylation of cellular proteins, including mitogen activated kinase (MAPK) and AKT (Andrabi, et al. 2007, Arroyo and Hahn 2005). Middle T-antigen (MT) is a membrane bound protein that activates signaling pathways through interactions with phosphatidylinositide 3-kinase (PI3K) and src family kinases (Courtneidge and Smith 1983, Fluck and Schaffhausen 2009). Large T-antigen (LT) drives cell cycle progression into S-phase through interactions with host proteins, such as phosphorylated retinoblastoma protein (Rb) (Sheng, et al. 1997, Zalvide, et al. 1998). Additionally, LT likely

binds to DDR proteins, including a component of the MRN complex, Nbs1, and the RPA complex to manipulate the host cell DDR to enhance viral DNA replication (Banerjee, et al. 2013, Wu, et al. 2004).

DDR pathways activate when PyVs replicate in the nucleus. For example, SV40, BKPyV, and MuPyV activate and utilize ATM kinase signaling for efficient replication (Dahl, et al. 2005, Jiang, et al. 2012, Sowd, et al. 2013). In cells infected by PyVs, DDR proteins co-localize at nuclear sites of viral DNA replication (Erickson, et al. 2012, Jiang, et al. 2012, Orba, et al. 2010, Tsang, et al. 2014). MuPyV utilizes ATM signaling to regulate the cell cycle and maintain a prolonged S-phase (Dahl, et al. 2005). SV40 requires both ATM and ATR kinase activity to replicate circular, monomeric viral genomes. Following inhibition of ATM or ATR, SV40 infected cells accumulate concatemerized and damaged viral genomes that cannot be packaged into virions (Sowd, et al. 2013, Sowd, et al. 2014). SV40 LT induces the proteasome-dependent degradation of the MRN complex, an activator of ATM kinase (Zhao, et al. 2008). These findings suggest that some proteins in the ATM pathway are required, while others may inhibit PyV replication.

The roles of DDR pathways and proteins during viral replication are complex because each virus may have particular requirements for replication and assembly. We investigated specific components of the ATM and ATR pathways in order to further elucidate the role of DDR proteins during MuPyV infection. We analyzed the recruitment of DDR proteins, such as Mre11and RPA32, to nuclear viral replication centers, as well as the functional requirement for ATR and checkpoint signaling in MuPyV virus production. Finally, we evaluated DDR signaling and viral replication center formation in cells infected with mutant viruses that do not express ST or MT.

3.2 Methods

Cell Lines and Infections: C57BL/6 mouse embryonic fibroblasts (MEF) were obtained from ATCC (SCRC-1008; Manassas, VA) and served as a wild-type (WT) MEF. MEFs were grown in DMEM (D6429, Sigma) supplemented with 10% fetal bovine calf serum (FBS; F0926, Sigma), and 55 μM β-mercaptoethanol (βME) at 37°C with 5% CO_2. Virus strain NG59RA (Feunteun, et al. 1976) was used for all WT virus infections. Cells were plated for 24 hrs, then cultured in DMEM supplemented with 0.5% serum for 24 hrs, before infections were carried out in adsorption buffer (Hanks Balanced Salt Solution (HBSS) with 10 mM HEPES, pH 5.6 and 0.5% BCS) as previously described (Cripe, et al. 1995). Cells were infected for 2 hrs at a multiplicity of infection of approximately 10-15 pfu/cell, and then cultured in DMEM supplemented with serum for the remainder of the experiment. CHK2-null and syngeneic WT controls were a gift from Tak Mak. H2AX-null and syngeneic WT controls were a gift from Andre Nussenzweig. CHK2 and H2AX-null cells and their syngeneic WT cells were grown in DMEM supplemented with 10% bovine calf serum (BCS), 55 μM βME and penicillin/streptomycin at 37°C with 5% CO_2.

Immunofluorescence: See Chapter 2

Immunofluorescence antibodies: Primary antibodies used for immunostaining were rat anti-Tag (E1, a gift from Tom Benjamin) (Goldman and Benjamin 1975) 1:5000; rabbit anti-VP1(Montross, et al. 1991) 1:5000, rabbit anti-pCHK1 (s345, Cell Signaling) 1:1000; mouse anti-pATM (ser1981, Abcam) 1:1000; rabbit anti-Mre11a (B1447; LSBio) 1:1000; rat anti-RPA32 (4E4, a gift from Heinz Nasheuer) 1:5; and rat anti-pSer23 RPA32 (a gift from Heinz Nasheuer) 1:20. For RPA32 co-staining with rat anti-Tag antibody, the E1 Tag antibody was

conjugated with AlexaFluor 647 (Invitrogen) and was used at a 1:1000 dilution. All other primary antibodies were detected using secondary antibodies, conjugated with AlexaFluor 488, AlexaFluor 546, or AlexaFluor 647 (Invitrogen), diluted 1:2000. All primary and secondary antibodies were diluted in 10% BCS in PBS.

Fluorescent in Situ Hybridization (FISH) of MuPyV DNA: The entire MuPyV genome (NG59RA) was cloned into pUC18 and a FISH probe was generated by nick translation of pUC18-MuPyV plasmid using Promofluor-550 NT Labeling Kit (PK-PF550-NTLK) according to manufacturer's instructions. FISH analysis was performed as described in Chapter 2, with the following modifications to wash steps. Coverslips were washed at 45ºC with 1.5x SSC, 50% formamide/1.5x SSC for 5 mins and 1.5x SSC for 5 mins. Coverslips were washed twice for 5 min in PBS at RT. Stained cells were mounted onto glass slides with ProLong antifade reagent containing Dapi (Invitrogen) and allowed to cure at 22 ºC for 24-48 hrs.

EdU labeling: EdU was added to media at final concentration of 10 μM at 28 HPI and allowed to incubate for 15 min at 37ºC. Coverslips were washed once in PBS and immediately fixed and stained, as described above. The fluorescent dye conjugation reaction was performed according to manufacturer's protocol (Invitrogen, C10340).

Microscopy: Confocal images were acquired on the Nikon A1R laser scanning confocal microscope, using a 1.45NA 100x objective and 405, 488, 561 and 638 laser lines. All images are a single z-plane through the center of the nucleus. Image processing and analysis were completed using ImageJ analysis software (NIH).

Western Blot Analysis (By Catherine Nicholas): Cells were lysed with 2X SDS lysis buffer with phosphatase inhibitors (25 mM Tris, pH 6.8 / 1% SDS / 6.25 mM EDTA with 1 mM

Na_3VO_4 and 25 mM NaF) on ice for 15 mins followed by a brief sonication to shear the DNA. The total protein concentration of each lysate was determined by BioRad DC Protein Assay. Samples were prepared by dilution in 4x SDS sample buffer (1 M Tris, pH 6.8 / 2% SDS / 12.5 mM EDTA / 40% glycerol / 600 mM βME / 0.02% Bromophenol Blue) and heated at 95 ºC for 5 mins. 25 µg total protein was resolved on 8% SDS-polyacrylamide gels and proteins were electrophoretically transferred to PVDF membranes. Membranes were blocked in 5% powered milk in TBST (10 mM Tris, pH 8.0, 150 mM NaCl, 0.1% Tween-20) with 1 mM Na_3VO_4 and 25 mM NaF. All antibodies except for pCHK1 were incubated at 37°C with rocking for 1 hr followed by three 20 min washes in TBST with rocking. The pCHK1 antibody was incubated at 4°C with rocking overnight, and then followed the same wash and secondary antibody protocol. Membranes were incubated with HRP-conjugated secondary antibodies (Promega) diluted 1:20,000 in TBST and washed as described for the primary antibodies. Proteins were detected using enhanced chemiluminescence (ECL, Pierce) detection and imaged on the LAS4000 Imager. Image processing and integrated density analysis were completed using ImageJ analysis software (NIH).

Western Blot Antibodies: Primary antibodies used for western blot were: rabbit anti-Rad50 (GeneTex, GTX119731) 1:1000; rabbit anti- pCHK1 S317 (Cell Signaling, 12302P) 1:200; rabbit anti-GAPDH (Abcam, 37168) 1:1000; mouse anti-Tag, PN116 (a gift from Brian Schaffhausen), 1:250; rabbit anti-VP1 (I58), 1:5000 (Montross, et al. 1991).

Small molecule inhibitors: All small molecule inhibitors were dissolved in DMSO and diluted in DMEM with 0.5% serum to working concentrations and added to cells at indicated time points: NU7441 (Tocris), 2 µM; PF477736 (Tocris), 1µM; and ATR inhibitor IV (VE-821, EMD Millipore), 5 µM.

Virus Supernatant Harvest: Cells ($4x10^4$ per well) were seeded on a six well dish ($9.5cm^2$ well) for 24 hrs, then starved in 0.5%FBS or BCS for 24 hrs before infection. At this time, the cells were 60-70% confluent. Virus preparation and infection was carried out as described above. After a 2 hr incubation with virus, 0.5% serum in DMEM was added for the remainder of the experiment. At times indicated, supernatants were transferred to 15 ml conical tubes and saved. Remaining cells on the plate were treated with 2 units of neuraminidase (NA) Type V (Sigma) that was diluted in NA buffer (10 mM Hepes, pH 5.6/1 mM $CaCl_2$/1 mM $MgCl_2$/5 mM KCl) for 30 min at 37°C. The NA supernatant was collected and combined with the original supernatant. The plates were washed three times with PBS and each wash was collected and combined with supernatants. The combined supernatants and washes were stored at −20°C.

Immunoplaque Assay: WT C57 cells were plated on a 96-well optical imaging dish (Costar, 9603) for 24 hrs, then cultured in 0.5% FBS for an additional 24 hrs. Cells were infected with viral supernatants diluted in adsorption buffer (as described above) at 1:100-1:1000 and infected in triplicate. Virus was removed after 2 hrs and DMEM with 0.5% FBS was added to cells. At 28-30 HPI, cells were fixed with 4% PFA/PBS at RT for 10 min, permeabilized with 0.5% Triton X-100/ PBS. Samples were then incubated with anti-Tag and anti-VP1 antibodies at dilutions described for immunofluorescence, followed by AlexaFluor 488 anti-rabbit, and AlexaFluor 546 anti-rat secondary antibodies. Nuclei were stained with Hoescht dye diluted in PBS. Plates were imaged on a Molecular Devices ImageXpress Micro XL High-Content Screener with a 10x objective. Tag and VP1 positive nuclei were determined based on the average pixel intensity within the nuclei, as defined by Hoescht dye staining. Image analysis was completed using ImageJ analysis software (NIH). An example of the analysis outlined in Figure M3.1.

Cell Line Normalization: For CHK2 WT and knockout, and H2AX WT and knockout comparisons, viral titers and viral DNA accumulation were normalized for the infection level of each individual cell line. Cell line normalization is described in Figure M3.2.

To address the requirement for CHK2 and H2AX during MPyV replication and assembly, we utilized knockout and syngeneic WT fibroblasts. Unfortunately, we found differences in the percent of cells able to be infected (infection efficiency) between cell lines during experiments. Stochastic changes in receptor expression likely account for these differences in infection efficiency. Since we were interested in interrogating the role of DDR proteins in viral replication and assembly, we normalized for these differences in infection efficiency across cell lines using an imaging based assay to quantify the number of cells infected during any given experiment (Fig. M 3.2).

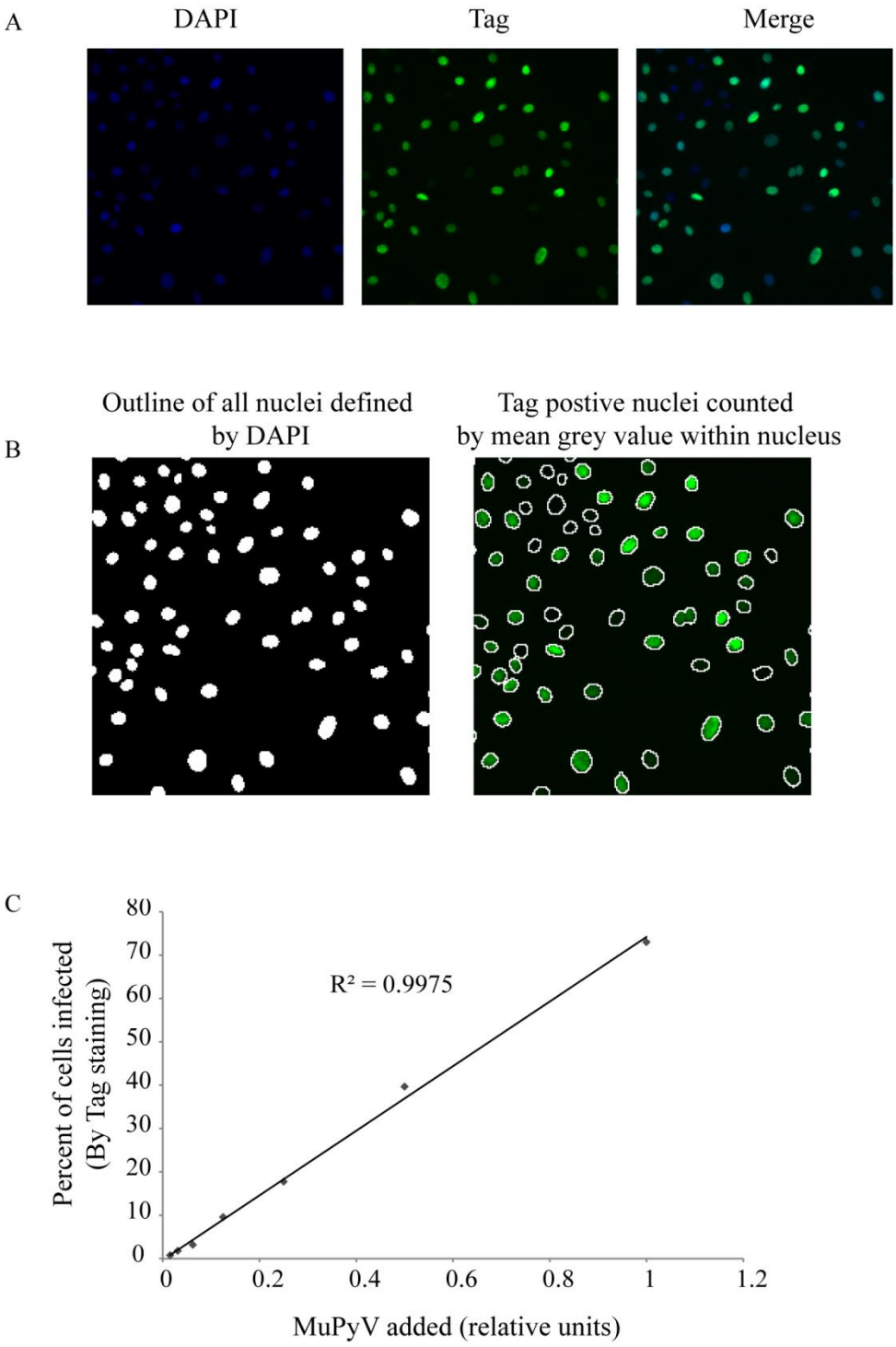

Figure M3.1 Quantification of viral titers using an immunoplaque assay. A) Example of DAPI (blue) and Tag (green) staining used in virus quantification. **B**) DAPI image with threshold applied to define outline of nucleus and Tag image with Regions of Interest (ROIs) outlined in white. **C**) Standard curve showing linear correlation between virus added and percent of cells infected.

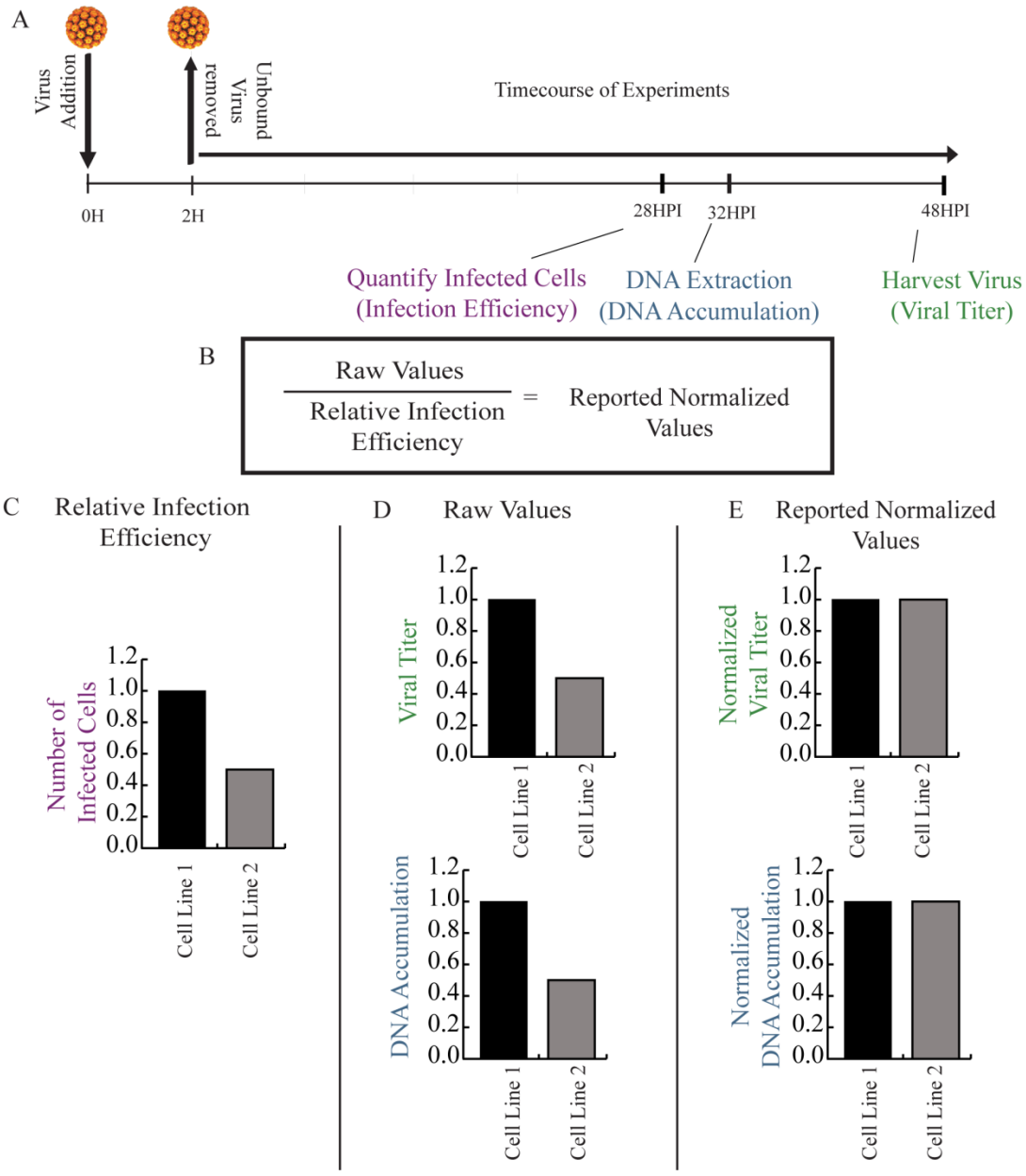

Figure M 3.2 Strategy for assessing MuPyV replication across cell types: In order to assess the role of DDR proteins in MuPyV replication and assembly, cell lines were normalized for the number of cells able to be infected or "infection efficiency". **A**) Timeline of viral titer and viral DNA accumulation assays. **B**) Equation used to calculate the normalized viral titer and DNA accumulation between cell lines of variable infection levels. **C**) Example graph of infection levels for cell lines quantified by high throughput imaging of Tag staining. **D**) Example raw values for viral titer, quantified by immunoplaque assay and viral DNA accumulation, quantified by qPCR. **E**) Example of calculated reported values for viral titer and viral DNA accumulation for each cell line, normalized for infection efficiency.

DNA Isolation: Viral DNA was isolated by Hirt extraction (Hirt 1967), with modifications. Briefly, cellular DNA was precipitated in high salt and remaining supernatants were treated with 10 µg RNase, followed by 25 µg of proteinase K. Viral DNA was purified by phenol-chloroform extraction and sodium acetate/ethanol precipitation. The DNA pellet was resuspended in 50 µL Tris-EDTA, diluted 1:200, and analyzed by qPCR.

Quantitative PCR (qPCR): Primers used for qPCR were the same as described in Chapter 2. qPCR reactions were prepared in 96-well optical plates (Applied Biosystems) in a volume of 25 µl. Each reaction contained 450 nM of each forward and reverse primer, 12.5 µl FastSYBR Master Mix (Applied Biosystems) and 5 µl purified viral DNA or DNA standards. DNA amplification was carried out using a Biorad CFX96 thermocycler using cycling conditions from Chapter 2. For each run, triplicates of five dilutions of the viral standard DNA (from 0.5 ng to 8×10−4 ng; pGEX-VP1 plasmid DNA), viral DNA samples and no template controls were simultaneously analyzed.

Statistical analysis: All error bars are standard error of the mean of three biological replicates. Statistical significance was calculated using a two-tailed student's t-test assuming unequal variance. p values of <0.05 indicated with *. Non-significant differences marked "n.s."

3.3 Results:

3.3.1 MuPyV recruits DDR proteins to viral DNA replication centers in the nucleus of infected cells

JCPyV, BKPyV, and SV40 activate and recruit host DDR proteins to sites of viral replication in the nucleus (Jiang, et al. 2012, Orba, et al. 2010, Zhao, et al. 2008). Therefore, we characterized nuclear MuPyV viral replication centers in infected mouse embryonic fibroblasts

(MEFs). DDR proteins are diffusely localized or slightly punctate throughout the nucleus of untreated MEFs (Fig 3.1 A-F). However, upon infection, these proteins were reorganized and co-localized with LT (Fig 3.1 G-M). The MuPyV LT formed "tracks" throughout the nucleus that co-localized with replicating viral DNA (Fig. 3.1G).We analyzed the localization of DNA repair proteins during infection and found many that were recruited to these viral replication centers, including RPA32, and Mre11 (Fig. 3.1H, K). Additionally, DDR signaling was active at replication centers, as evidenced by phosphorylated RPA32 (pSer23 RPA32), CHK1 (pCHK1), ATM (pATM) and H2AX (γH2AX) (Fig. 3.1 I, J, L, M). These data suggest that MuPyV activates and recruits DDR proteins similar to other PyVs.

Previous reports show that SV40 infection activates DDR signaling and induces the degradation of the MRN complex (Zhao, et al. 2008). We therefore analyzed immuno-blots of infected cell lysates to determine if levels of MRN proteins were affected during MuPyV infection. In contrast to SV40, we found that expression levels of Rad50, a member of the MRN complex, were similar in mock and infected samples (Fig. 3.1N). However, there was a striking increase in the amount of pCHK1 in infected cells (Fig. 3.1 N). Quantification of the immuno-blots revealed an approximately three-fold increase in pCHK1, but no change in Rad50 levels (Fig. 3.1 N). These data suggest that MuPyV activates and recruits DDR proteins, but does not affect their overall expression or stability, in contrast to observations during SV40 infection.

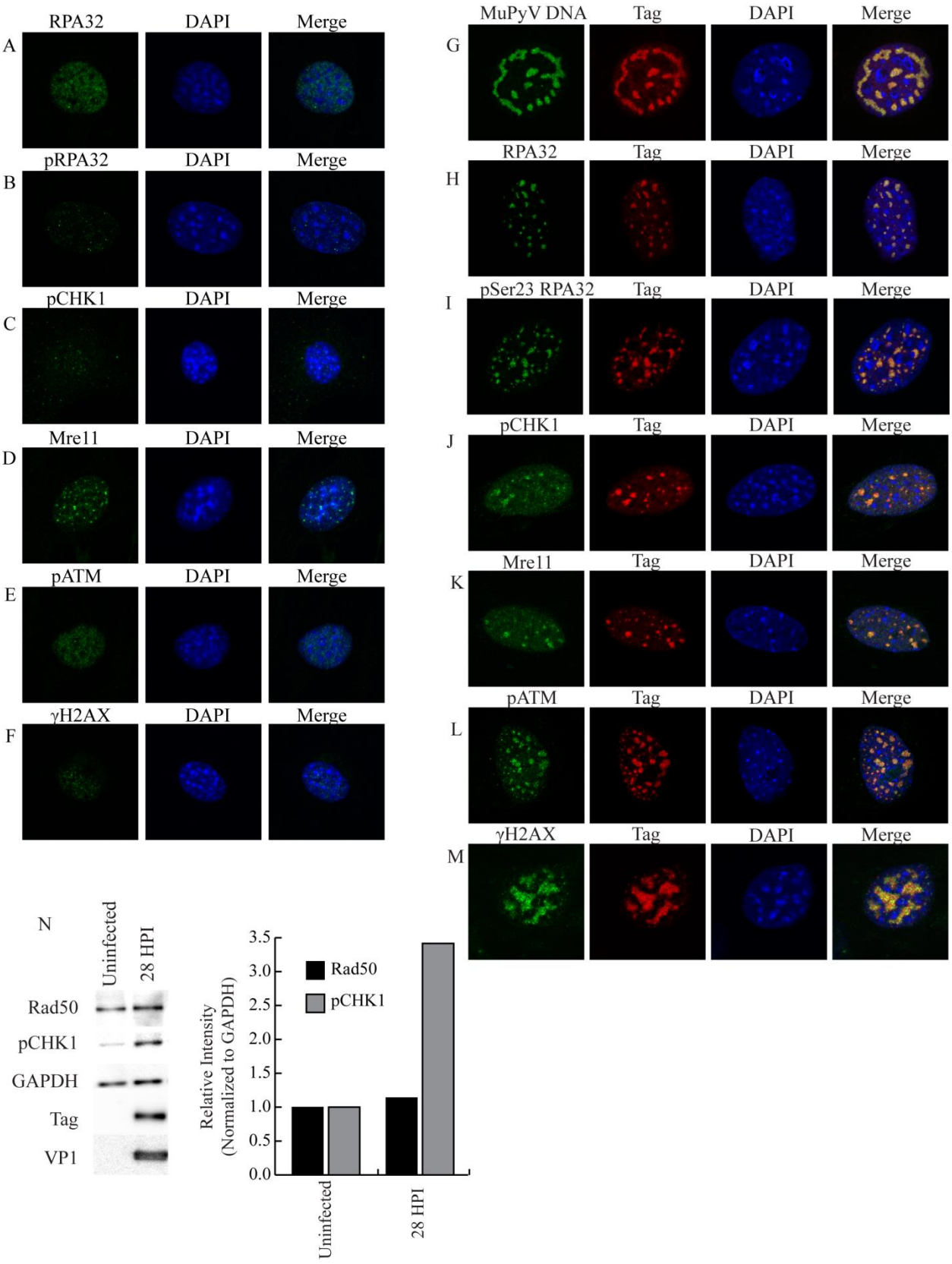
A
RPA32
DAPI
Merge
B
pRPA32
DAPI
Merge
C
pCHK1
DAPI
Merge
D
Mre11
DAPI
Merge
E
pATM
DAPI
Merge
F
γH2AX
DAPI
Merge
G
MuPyV DNA
Tag
DAPI
Merge
H
RPA32
Tag
DAPI
Merge
I
pSer23 RPA32
Tag
DAPI
Merge
J
pCHK1
Tag
DAPI
Merge
K
Mre11
Tag
DAPI
Merge
L
pATM
Tag
DAPI
Merge
M
γH2AX
Tag
DAPI
Merge
N
Uninfected
28 HPI
Rad50
pCHK1
GAPDH
Tag
VP1
Relative Intensity
(Normalized to GAPDH)
3.5
3.0
2.5
2.0
1.5
1.0
0.5
0.0
Rad50
pCHK1
Uninfected
28 HPI

Figure 3.1: MuPyV activates and reorganizes host DDR proteins in the nucleus. A-F) Control, uninfected MEFs were fixed and immunostained for indicated DDR proteins. Single z-plane confocal immunofluorescence images show cells stained for **A**) RPA32 **B**) pSer23 RPA32 **C**) pCHK1 **D**) Mre11 **E**) pATM or **F**) γH2AX.

G-M) MEFs were infected with WT MuPyV (NG59RA), and fixed, permeabilized, and immunostained at 28 hrs post infection (HPI). Single z-plane confocal immunofluorescence images show cells stained for Tag and **G**) MuPyV DNA (FISH) **H**) RPA32 **I**) pSer23 RPA32 **J**) pCHK1 **K**) Mre11 **L**) pATM or **M**) γH2AX.

N) MEFs were mock infected or infected with NG59RA. Total proteins were harvested at 28 HPI and analyzed by western blot for pCHK1 and Rad50 protein levels. Quantification of integrated density of pCHK1 and Rad50 levels in control and infected MEFs normalized to GAPDH loading control. All samples were normalized to uninfected control cells.

3.3.2 Recruitment of DDR proteins is not dependent on ST or MT

Recruitment of DDR proteins to sites of SV40 viral DNA replication depends on the viral LT (Zhao, et al. 2008). Thus, we determined whether MuPyV LT was sufficient for DDR protein recruitment to replication centers, by analyzing the formation of viral replication centers in cells infected with MuPyV mutant viruses lacking ST and MT. NG18 is a mutant virus with a deletion that abrogates the expression of both ST and MT, and 808A is a mutant virus with a mutation in the MT splice acceptor, preventing expression of only MT, while allowing ST expression (Benjamin 1982, Garcea and Benjamin 1983, Garcea, et al. 1989). Interestingly, NG18 replication centers (Fig. 3.2 A) were smaller than either 808A (Fig. 3.2 A) or WT virus (Fig. 3.1 G). These data suggest that ST has a role in the expansion of these centers, possibly through activation of other signaling pathways that aid DNA replication. However, recruitment of phosphorylated RPA32 (Fig. 3.2 B) and Mre11 (Fig. 3.2 C) were maintained during infection by 808A and NG18 mutant viruses, demonstrating that LT is the viral protein responsible for recruitment of DDR proteins to viral replication centers.

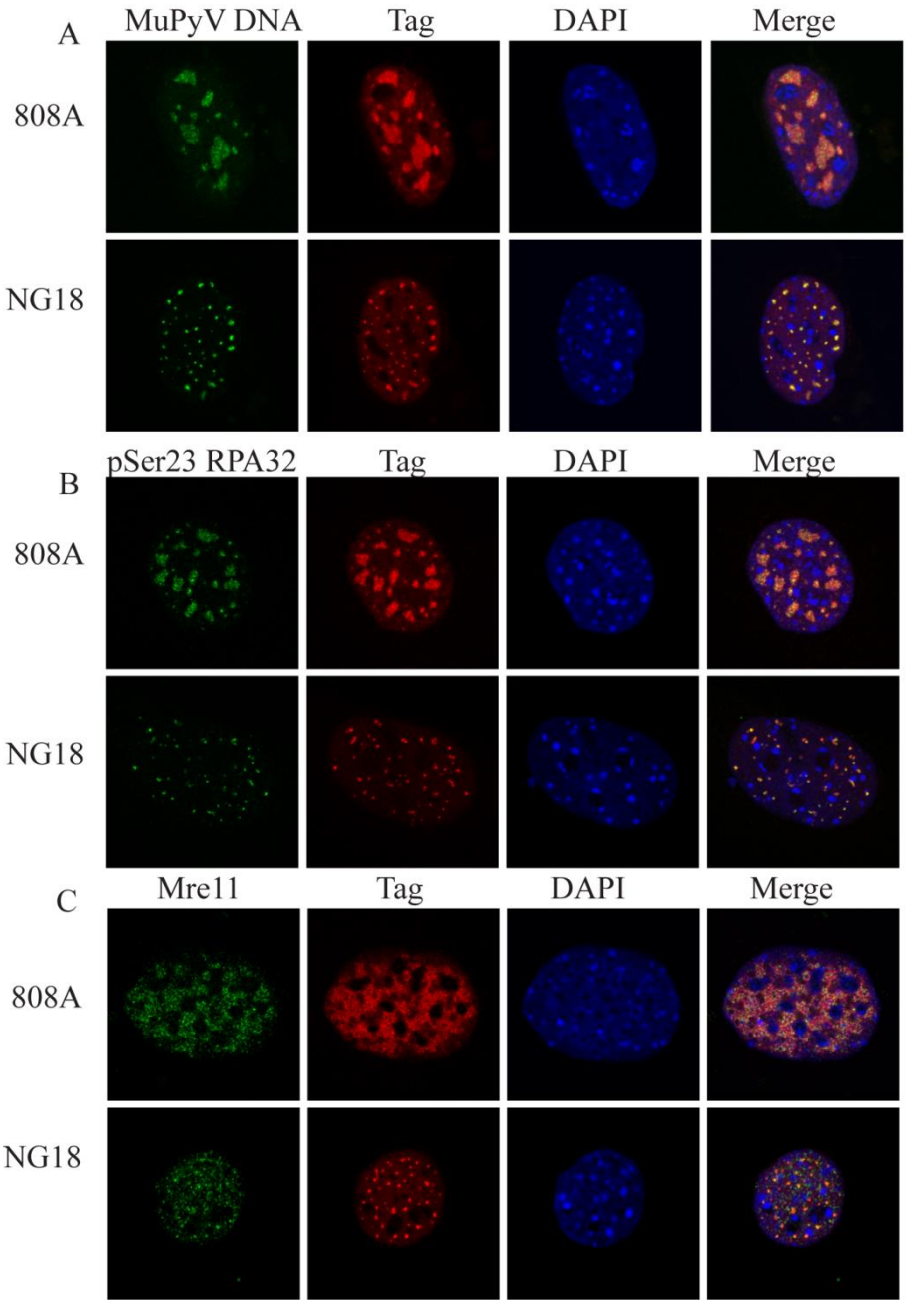

Figure 3.2: ST and MT are not required for localization of DDR proteins to viral replication centers. MEFs were infected with the MT mutant virus (808A) or the ST/MT mutant virus (NG18). At 28 HPI cells were fixed, permeabilized, and immunostained. Single z-plane confocal immunofluorescence images showing cells stained for **A**) Tag and MuPyV DNA (FISH), **B**) Tag and pSer23 RPA32, and **C**) Tag and Mre11.

3.3.3 Mre11 is preferentially recruited to replicating viral DNA

Many DDR proteins, such as the MRN complex, have roles in both the DNA damage response and cellular DNA replication (Stracker and Petrini 2011). The MRN complex normally stabilizes replication forks at sites of cellular DNA replication (Maser, et al. 2001, Tittel-Elmer, et al. 2009). In order to distinguish replicating viral DNA from replicating cellular DNA we labeled replicating DNA in infected cells with EdU, and a fluorescent *in-situ* hybridization (FISH) probe specific to the MuPyV genome (Fig. 3.3 A). To determine whether Mre11 was recruited to all actively replicating DNA, we also immunostained for Mre11 and analyzed its recruitment to replicating host or viral DNA (Fig. 3.3 B). Host cell DNA replicated during early times after infection and could be visualized along with replicating viral DNA. During infection, Mre11 specifically localized to replicating viral DNA and not replicating cellular DNA (Fig 3.3 C, D). Thus, Mre11 is preferentially recruited to viral replication centers.

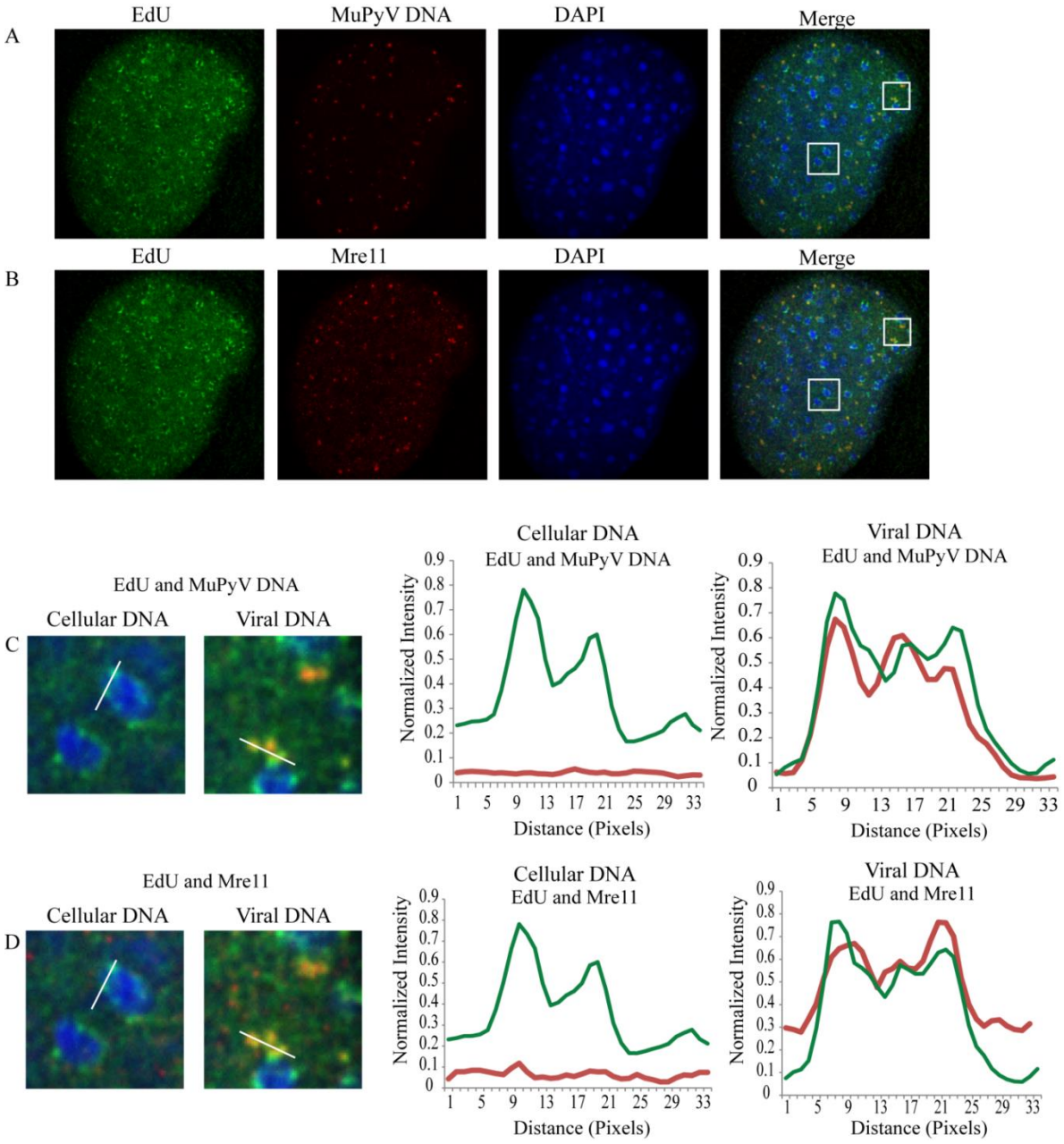

Figure 3.3: Mre11 is preferentially recruited to replicating MuPyV DNA during infection. MEFs were infected with NG59RA, at 28 HPI. 10 μM EdU was added to the media and allowed to incorporate into replicating DNA for 15 mins. Samples were then fixed, permeabilized, and stained for EdU, MuPyV DNA, and Mre11. Single z-plane confocal image shows **A**) EdU and MuPyV DNA or **B**) EdU and Mre11 (same cell, pseudo-colored for clarity) **C**) Insets show EdU-labeled cellular DNA (left) or EdU-labeled viral DNA (right) with corresponding line scan intensity plots, indicated in each panel. **D**) Insets show Mre11 localization with cellular DNA (left) and viral DNA (right), with corresponding line scan intensity plots, indicated in each panel. Intensity plots were normalized to image maximum for each label.

3.3.4 Checkpoint Kinases, CHK1 and CHK2, are not required for MuPyV replication

Activation of CHK1 and CHK2 occurs during JCPyV and SV40 infection (Boichuk, et al. 2010, Orba, et al. 2010). Previous reports suggest that intra S-phase signaling stalls MuPyV-infected cells in S or G2 phase, allowing viral replication to proceed for an extended time (Dahl, et al. 2007, Dahl, et al. 2005). To assess the potential requirement for CHK1 and CHK2 during MuPyV infection, we utilized a CHK1 inhibitor (PF477736) or CHK2-null fibroblasts. Inhibition of CHK1 using PF477736 did not affect viral titers (Fig. 3.4 A) or viral DNA replication (Fig. 3.4 B). Additionally, CHK2-null fibroblasts produced infectious viral progeny (Fig. 3.4 A) and replicated viral DNA at similar levels to syngeneic WT cells (Fig. 3.4 B). These results suggest that, despite robust CHK1 activation during infection, neither CHK1 nor CHK2 kinases are required for efficient MuPyV replication and assembly.

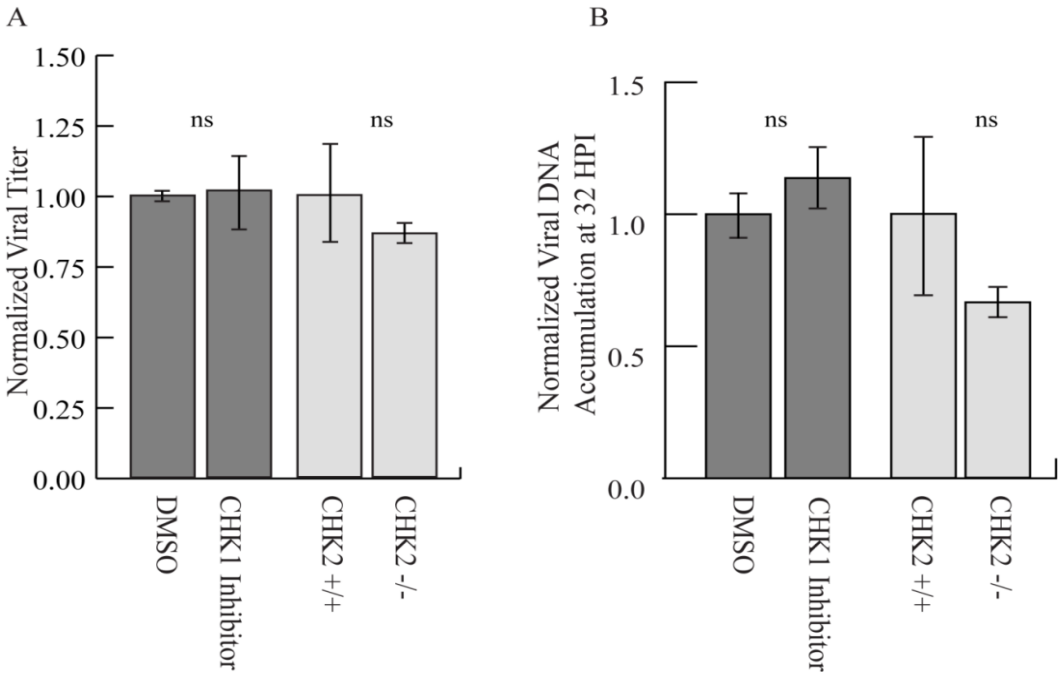

Figure 3.4: CHK2 and CHK1 are not required for MuPyV virus production or viral DNA accumulation. Cells were infected with NG59RA. CHK1 inhibitor or DMSO control was added to media for indicated samples at 2 HPI. **A**) Viral titers at 48 HPI quantified by immunoplaque assay from DMSO or CHK1 inhibitor (PF477736) treated MEFs and CHK2 WT (CHK2 $^{+/+}$) or null (CHK2 $^{-/-}$) fibroblasts, normalized to control. **B**) Viral DNA accumulation at 32 HPI quantified by qPCR, in DMSO or CHK1 inhibitor (PF477736) treated MEFs and CHK2 WT (CHK2 $^{+/+}$) or null (CHK2 $^{-/-}$) fibroblasts, normalized to control.

3.3.5 H2AX is not required for MuPyV Replication

The histone marker γH2AX is required for maintenance of DDR proteins at sites of cellular DNA damage and for full activation of downstream signaling (Bassing, et al. 2002, Celeste, et al. 2002, Rogakou, et al. 1999). Since γH2AX is present at viral replication centers (Fig. 3.1 M), we used H2AX-null fibroblasts to determine whether H2AX is required for viral DNA replication, virus assembly, or DDR signaling during MuPyV infection (Celeste, et al. 2002). We found that viral replication centers that formed in H2AX-null fibroblasts were similar to those observed in WT cells (Fig. 3.5 A). Additionally, H2AX was dispensable for recruitment of Mre11 and pCHK1 to viral replication centers (Fig. 3.5 B, C). Interestingly, H2AX-null fibroblasts produced similar outputs of virus to syngeneic WT cells (Fig. 3.5 D), but replicated approximately two-fold more viral DNA than WT (Fig. 3.5 E). These data suggest that although H2AX may affect accumulation of viral DNA, overall it is not required for MuPyV genome replication and virus assembly.

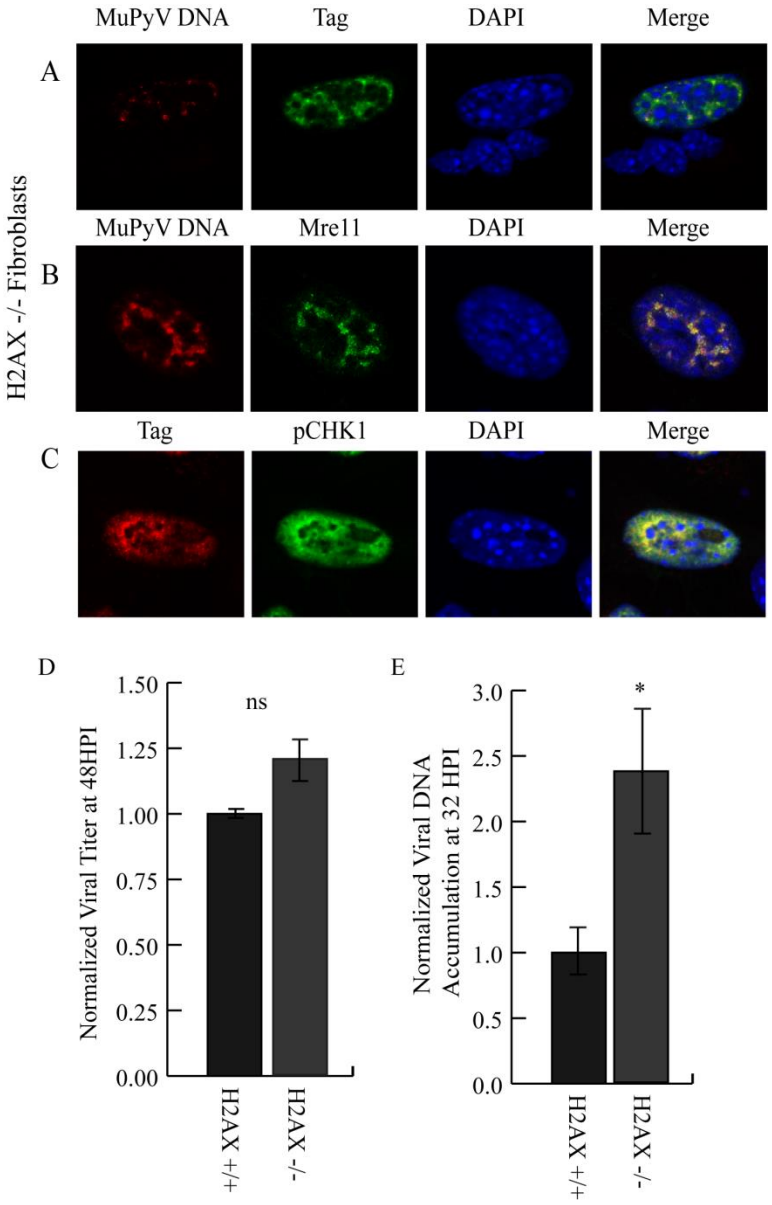

Figure 3.5: H2AX is not required for recruitment of DDR proteins, virus production, or viral DNA accumulation during MuPyV infection. H2AX-null ($H2AX^{-/-}$) fibroblasts were infected with NG59RA, and at 28 HPI cells were fixed and immunostained. Single z-plane confocal images of cells stained for **A**) Viral DNA and Tag, **B**) Viral DNA and Mre11, or **C**) Tag and pCHK1. **D**) H2AX WT ($H2AX^{+/+}$) and null ($H2AX^{-/-}$) cells were infected with NG59RA. Virus supernatants were harvested at 48 HPI and viral titers were quantified by immunoplaque assay, normalized to control or **E**) viral DNA was harvested at 32 HPI and viral DNA accumulation was quantified by qPCR, normalized to control.

3.3.6 ATR signaling is required for MuPyV assembly, but not viral DNA replication

During SV40 infection, ATR kinase activity stabilizes and resolves viral DNA replication intermediates (Sowd, et al. 2013). Following DNA damage, ATR directly phosphorylates CHK1, which can activate checkpoint signaling (Zhao and Piwnica-Worms 2001). In contrast, DNA-PK, the DDR kinase associated with non-homologous end-joining (NHEJ), is not required during SV40 DNA replication (Sowd, et al. 2013). To determine whether ATR activity or DNA-PK activity are required for MuPyV replication, we utilized small molecule inhibitors of ATR (VE-821) and DNA-PKcs (NU7441). As expected, inhibition of ATR resulted in a small (20-30%) decrease in CHK1 phosphorylation in both control and infected MEFs (Fig. 3.6 A, B). However, ATR inhibitor treatment did not affect the recruitment of DDR proteins such as RPA32, Mre11, and pCHK1, to viral replication centers (Fig. 3.6 C). Interestingly, ATR inhibition reduced virus production (Fig. 3.6 D), but did not affect replication of viral DNA (Fig. 3.6 E). In contrast, inhibition of DNA-PK during MuPyV infection did not affect either viral titer (Fig. 3.6 D) or viral DNA accumulation (Fig, 3.6 E), similar to observations for SV40.These results suggest that ATR signaling, but not DNA-PK activity, aids MuPyV in resolving viral DNA replication intermediates, similar to its role in SV40 DNA replication.

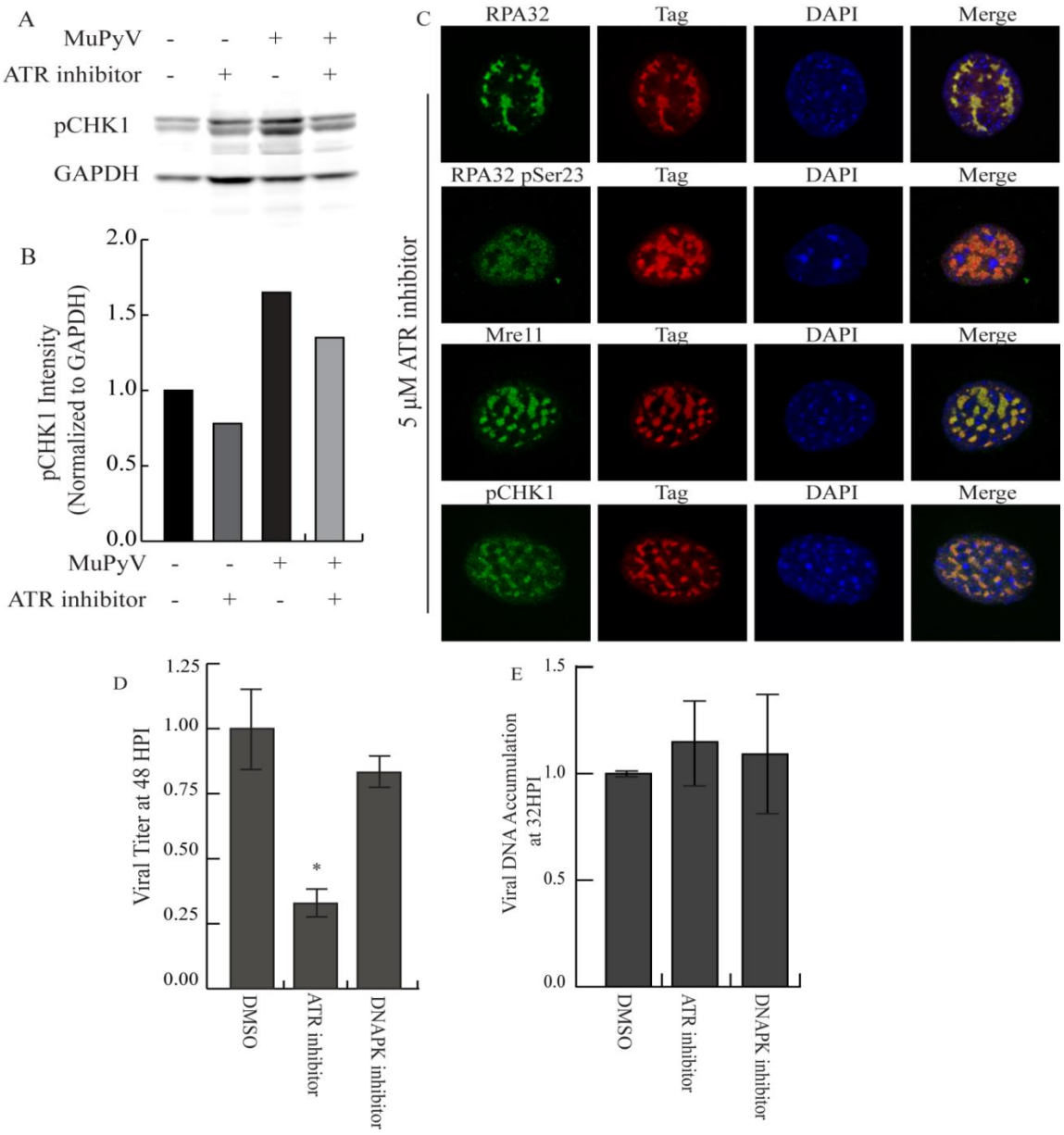

Figure 3.6: ATR signaling is required for virus production, but not viral DNA replication. MEFs were infected with NG59RA. At 16 HPI DMSO control or inhibitors were added and the infection proceeded until analysis. **A**) At 28 HPI total protein from DMSO or ATR inhibitor-treated cells was harvested and analyzed. Immunoblot of pCHK1 (S317) and GAPDH in infected and control MEFs. **B**) Quantification of integrated density of pCHK1 immunoblot, normalized to GAPDH loading control. All samples were normalized to untreated control cells. **C**) Single z-plane confocal immunofluorescence images showing cells stained for Tag and RPA32, pSer23 RPA32, Mre11 or pCHK1. **D**) Viral titers from MEFs treated with DMSO, 2 μM DNA-PK inhibitor (NU7441), or 5 μM ATR inhibitor, quantified by immunoplaque assay. **E**) Viral DNA accumulation from MEFs treated with DMSO, 2 μM DNA-PK inhibitor (NU7441), or 5 μM ATR inhibitor, quantified by qPCR.

3.4 Conclusions:

Viruses and host DDR signaling have a complex relationship that varies significantly between different viruses. PyVs inhibit or degrade members of DDR pathways, such as components of the MRN complex (Wu, et al. 2004, Zhao, et al. 2008). Conversely, DDR signaling through the ATM pathway seems to be ubiquitously required for PyV replication and assembly (Dahl, et al. 2005, Jiang, et al. 2012, Shi, et al. 2005, Sowd, et al. 2013, Tsang, et al. 2014, Zhao, et al. 2008). In order to interrogate the relationship between MuPyV and DDR pathways we utilized knockout cell lines, small molecule inhibitors, and confocal microscopy to visualize viral replication centers. We found that MuPyV LT recruits DDR proteins to replication centers, and that efficient MuPyV assembly requires ATR signaling. Several roles for DDR pathways during PyV infection have been suggested, including maintenance of the S-phase of the cell cycle, repair of damaged viral DNA, resolution of replication intermediates, or a host defense (Dahl, et al. 2005, Jiang, et al. 2012, Orba, et al. 2010, Sowd, et al. 2013, Zhao, et al. 2008). Our results suggest that checkpoint kinase signaling and H2AX phosphorylation may be dispensable for MuPyV replication, but ATR activity is required.

3.5 Discussion:

MuPyV ST and MT interact with PP2A and other host proteins to activate cellular signaling pathways. Mutant viruses lacking ST and MT have significant defects in viral DNA replication and associated reductions in virus outputs. However, viruses with mutations in MT alone have close to WT levels of DNA accumulation, but substantially reduced viral titers (Chen, et al. 2006, Garcea and Benjamin 1983, Garcea, et al. 1989). Cells infected by the ST and MT mutant virus, NG18, had smaller viral replication centers than cells infected by either WT virus

or the MT mutant virus, 808A. Despite the smaller size, DDR proteins, such as Mre11 and RPA32, were recruited to WT and mutant virus replication centers. This observation suggests that recruitment of DDR proteins to replication centers is mediated through LT. The MuPyV LT may facilitate recruitment and activation of DDR protein through an interaction with the RPA complex or NBS1 (Banerjee, et al. 2013, Wu, et al. 2004). However, the increased viral DNA accumulation and the expansion of viral replication centers observed in WT and 808A infected cells is likely dependent on signaling pathways regulated by ST, including AKT or MAPK.

Biochemical analysis of SV40 infected cells revealed that inhibition of either ATM or ATR increased the accumulation of incorrectly resolved viral genomes (Sowd, et al. 2013). Specifically, inhibition of ATM was observed to increase unidirectional fork and rolling circle replication, while inhibition of ATR showed a slight increase in these aberrant replication products along with an increase in broken and unrepaired viral genomes (Sowd, et al. 2013, Sowd, et al. 2014). Previous reports have shown a requirement for ATM kinase in MuPyV replication (Dahl, et al. 2005). We found an additional requirement for ATR signaling during MuPyV infection. ATR inhibition significantly reduced viral titers, but not total viral DNA accumulation, suggesting a defect in assembly. It is likely that ATR inhibitor treatment leads to the formation of viral DNA concatemers or other viral DNA intermediates that cannot be packaged into virions, similar to observations for SV40. However, inhibition of CHK1, a downstream target of ATR, did not affect viral titers or DNA accumulation indicating that checkpoint signaling from the ATR pathway is not required for MuPyV replication and assembly. The defects in viral packaging we observed are therefore due to another function of ATR, such as recruitment or activation of repair proteins. SV40 LT induces the degradation of the MRN complex during infection; however, levels of the MRN complex remained constant

during MuPyV infection. This finding suggests that although SV40 and MuPyV require ATM and ATR signaling, there are differences in their interaction with DDR proteins.

MuPyV may utilize signaling through ATM to induce a prolonged S-phase in order to efficiently replicate (Dahl, et al. 2005). CHK2 is a direct target of ATM kinase and can activate checkpoint signaling following DNA damage (Ahn, et al. 2004). To determine if activation of checkpoint signaling by CHK2 was required for MuPyV infection, we analyzed CHK2-null MEFs (Hirao, et al. 2000) and found that MuPyV did not require CHK2 in order to efficiently replicate. Additionally, we found that CHK1, a downstream target of ATR kinase, was not necessary for efficient MuPyV virus production. Although we did not observe a requirement for either CHK1 or CHK2 signaling during infection, it is possible that either kinase is sufficient to compensate for the other and a combinatorial inhibition or knockdown would be necessary to observe a phenotype.

H2AX is a histone variant present in a subset of nucleosomes and acts as a signal of DNA damage and chromatin abnormalities. Phosphorylation of H2AX at serine 139 generates γH2AX, which activates and recruits downstream DDR proteins. The loss of H2AX during cellular DNA damage results in reduced DDR mediated checkpoint signaling and reduced retention of DDR proteins at DNA break sites (Celeste, et al. 2003, Fernandez-Capetillo, et al. 2002). Interestingly, during MuPyV infection, H2AX is not required to activate checkpoint kinase CHK1 or to retain DDR proteins such as Mre11 at viral DNA replication centers. Additionally, we found that while H2AX null fibroblasts accumulated higher levels of viral DNA, there was not a significant increase in viral titer produced by these cells. Interestingly, when extreme levels of cellular DNA damage occur, H2AX is not required to maintain downstream signaling (Fernandez-Capetillo, et al. 2002). Therefore, it is possible viral replication induces an "extreme" level of DNA damage,

since MuPyV replication activates CHK1 in the absence of H2AX. However, a more intriguing explanation is that a different mechanism of activation or recruitment of DDR proteins occurs during viral infection than during cellular DNA damage.

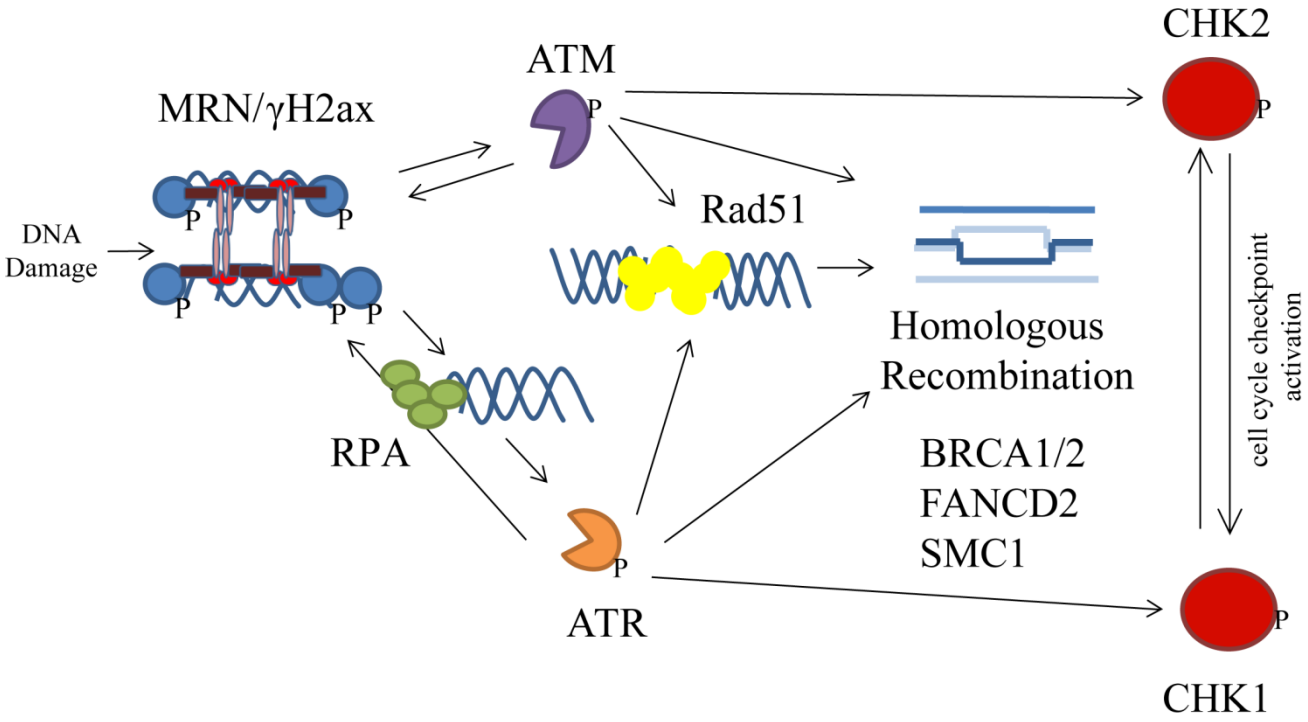

Figure 3.7: A canonical ATM and ATR signaling pathway mediating homologous recombination. Following DNA damage, the MRN complex recognizes and binds to the break site. Exposure of single stranded DNA by Mre11 recruits RPA and activates ATR. A direct interaction between NBS1 and ATM activates ATM. ATM and ATR phosphorylate and recruit downstream effectors including Rad51, FANCD2, BRCA1/2, and SMC1. Finally, CHK1 and CHK2 are activated by ATM and ATR to halt cell cycle progression. This pathway results in homologous recombination mediated repair.

During adenovirus infection, non-canonical DDR pathways are activated in response to viral DNA replication. A “localized” activation of DDR signaling occurs at adenovirus (Ad5) replication centers, which does not induce H2AX phosphorylation (Shah and O'Shea 2015). We

observed a similar activation of DDR signaling that was independent of H2AX. This finding is consistent with models proposing “global” signaling following cellular DNA damage, and “local” DDR signaling at viral replication centers. These varying types of DDR signaling may aid the cell in distinguishing viral DNA from host DNA damage. Our data support the hypothesis that these local signaling events may not require the same signaling molecules as global cellular DDR. Although MuPyV exploits some DDR proteins in order to replicate, it does not require many components of the ATM and ATR pathways, including checkpoint signaling, a hallmark of canonical cellular DDR signaling. A more thorough understanding of the mechanism of activation and recruitment of DDR proteins by viral DNA replication is required to better understand these non-canonical signaling pathways.

Chapter 4
Analysis of the RPA and MRN complexes during MuPyV infection

4.1 Introduction

4.1.1The MRN and RPA complexes are sensors of DNA damage

Three major complexes, the MRN, the Ku70/80, or the RPA complexes identify cellular DNA damage. These three multi-subunit complexes all have DNA binding domains, and an interaction with at least one of the major PIKK family DDR kinases, ATM, ATR, or DNAPK. The MRN and Ku70/80 complexes both primarily bind to double strand breaks and activate downstream signaling of ATM and DNAPK, respectively (Goodarzi and Jeggo 2013, Lee and Paull 2005, Uziel, et al. 2003). The RPA complex recognizes and binds to single stranded DNA lesions, and in concert with ATRIP activates ATR signaling (Zou and Elledge 2003). In addition to their roles in DDR, both RPA and MRN play critical roles in stabilizing cellular DNA during replication.

4.1.2 The MRN Complex and induction of ATM signaling in cellular DDR

The MRN complex, comprised of Mre11, Rad50 and N bs1, has critical roles in cellular DNA damage sensing, signaling, and repair. Following recognition of a break site in cellular DNA, Mre11 directly interacts with DNA and resects a single strand of DNA at the break site (Trujillo, et al. 2003, Trujillo, et al. 1998). Rad50 is an ATPase that facilitates dimerization of the heterotrimeric complex and Nbs1 is the signaling protein of the complex that binds to ATM (Deshpande, et al. 2014, Lee and Paull 2004). The interaction of the MRN complex with ATM activates the kinase by inducing its autophosphorylation (Lee and Paull 2004, Uziel, et al. 2003). Activation of ATM results in the phosphorylation of many DDR substrates, including NBS1,

γH2AX, and RPA 32 (Polo and Jackson 2011).This signaling cascade builds a chromatin domain around the break site that protects it from further damage, and allows repair (Rogakou, et al. 1999). In addition to its role as a damage sensor, the MRN complex is also involved in homologous recombination (HR) mediated repair. Resection of DNA at a break site by MRE11 is required to initiate HR (Langerak, et al. 2011). The MRN complex is involved in several other types of DDR, including NHEJ and micro-homology mediated end joining (MMEJ) (Rass, et al. 2009, Truong, et al. 2013).

4.1.3The MRN complex during viral infection

MRN is a potent antiviral inhibitor of some viral infections such as adenovirus (Stracker, et al. 2002). The MRN complex likely binds to and recognizes broken ends of incoming adenovirus genomes. Recent reports show that this interaction can activate a "local" ATM signal that suppresses replication of adenovirus DNA (Shah and O'Shea 2015). In order to overcome this inhibition, Adenovirus early proteins E4ORF3 and E1B55K induce the degradation of components of the MRN complex (Evans and Hearing 2005, Stracker, et al. 2002). Similarly, SV40 LT binds to NBS1, and facilitates its proteasome dependent degradation (Wu, et al. 2004, Zhao, et al. 2008). Although we did not observe a similar reduction in MRN complex levels (Chapter 3), the role of the MRN complex during MuPyV infection is not well understood.

4.1.4 RPA and ATR signaling

The RPA complex is comprised of RPA 14, RPA 32 and RPA 70. Single stranded DNA binding is primarily mediated through the DNA binding domains of RPA 70, but RPA 32 and 14 each have a DNA binding domain that also contribute to DNA binding (Bastin-Shanower and Brill 2001). Single-stranded DNA binding by RPA is the activating step required for ATR

signaling (Zou and Elledge 2003). Following DNA damage, RPA 32 can be phosphorylated by any of the DDR kinases, ATM, ATR, or DNAPK (Oakley and Patrick 2010, Olson, et al. 2006). The role of this phosphorylation event is not well understood, but may act to regulate the association of the RPA complex with DDR or DNA replication (Olson, et al. 2006, Vassin, et al. 2004). RPA binding to single-stranded DNA activates ATR kinase, which locally recruits proteins to repair lesions and can activate global checkpoint signaling through CHK1 (Zou and Elledge 2003). The RPA complex plays a vital role in several types of DDR, including HR, base excision repair (BER) and nucleotide excision repair (NER) (Krejci, et al. 2012, Li 2008).

4.1.5 RPA during PyV infection

The RPA complex was originally described as an essential cofactor during *in vitro* replication of SV40 DNA (Fairman and Stillman 1988, Matsumoto, et al. 1990, Wold and Kelly 1988). In the absence of the RPA complex, SV40 DNA replication stalls at very early steps of origin unwinding and primer synthesis (Wang, et al. 2000, Weisshart, et al. 1998). There is an RPA binding site on SV40 LT and loss of that binding interaction results in a similar stall at early replication. However, the role of this interaction is not well described during MuPyV infection.

A direct interaction between RPA and MuPyV LT is sufficient to inhibit cellular DNA damage repair and recruitment of downstream proteins to nuclear foci (Banerjee, et al. 2013). Multiple sites on LT are required for the RPA-LT interaction. Mutation of K308, E320, or K381 resulted in a loss of LT binding to RPA and associated loss of cellular DDR inhibition. None of the described mutations had significant effects on other functions of LT, such as Jun/Fos activation or E2F activation (unpublished data, Banerjee and Schaffhausen).

I utilized stable knockdown cell lines to analyze the role of the MRN complex during infection. Additionally, I transiently knocked down subunits of the RPA complex to show their requirement during infection. Finally, I created a mutant MuPyV that expresses a LT that does not bind to RPA by introducing the E320A mutation into the WT NG59RA genome.

4.2 Methods

Cells and Viruses: Similar to Chapter 3. Creation of stable knockdown cell lines is described below. Following selection, KD cell lines were cultured under the same conditions as WT MEFs, described in Chapter 3. Infections were completed using the same methods as those described in Chapter 3.

Creation of E320A Mutant Virus: MuPyV (NG59RA) genome was cloned into a PuC18 vector at the BamHI cloning site. The E320A mutation was created using site directed mutagenesis of Puc-MuPyV. In order to isolate the viral genome, both RA and RA-E320A were digested overnight with BamHI-HF, and then enzyme was inactivated according to manufacturer's instructions. Digests were electrophoresed on 1% agarose gel and 5kb band was gel extracted and purified (Qiagen, Gel Extraction Kit). Finally, genomes were religated with T4 ligase at a DNA concentration of 10 μg/mL and purified using Qiagen PCR clean-up kit. The religated genomes were transfected according to manufacturer's instructions with Lipofectamine 2000 into WT MEFs in six well dishes. 48 hrs after transfection, supernatant containing virus was transferred to fresh WT MEFs in a six well dish, and then the viruses were passaged into larger dishes until a sufficient viral stock accumulated. In experiments with E320A, RA control is always from virus stock created using this method.

Immunofluorescence: See Chapter 3. All antibody dilutions are the same as those listed in Chapter 3.

EdU labeling: Similar to Chapter 3, with 10 min incorporation time.

Fluorescence *in situ* Hybridization: See Chapter 3.

Confocal Microscopy: See Chapter 3.

Virus Supernatant Harvest: See Chapter 3.

Immunoplaque Assay: See Chapter 3.

Cell Line Normalization: See Chapter 3.

Creation of stable knockdown lines: Knockdown cell lines for NBS1 and ATM were created using lentivirus transduction of WT C57 MEFs. Lentiviruses encoding shRNAs targeting NBS1or ATM and non-target controls were purchased from the CU Boulder Functional Genomics Facility. Briefly, knockdown and control lentiviruses were added to WT MEFs ($4x10^4$ per well) seeded on a six well dish. 48 hours after transduction, media with final concentration of 5 ug/mL puromycin was added to all cell lines, including non-transduced control cells. At this concentration, all non-transduced controls were killed within 48 hrs. Non-target and knockdown cell lines were selected for one week at this concentration. The best knockdown for each target was selected using mRNA transcript level normalized to GAPDH level, measured by qPCR.

siRNA Knockdown: MEFs ($4x10^4$ per well) were seeded on a six well dish and siRNAs were transfected with RNAiMAX Lipofectamine at times indicated. Cell death was measured by high throughput imaging of Hoechst dye stained nuclei at 30 HPI. Knockdown was measured by mRNA transcript level at 30 HPI.

Small molecule inhibitors: See Chapter 2 and 3.

DNA Isolation: See Chapter 3.

qPCR for viral DNA: See Chapter 3.

Southern Blot: Viral DNA was extracted using Hirt method, with modifications (Chapter 3), and electrophoresed on a 0.6-0.7% agarose gel for approximately 4 hrs. Gel was then soaked in 500 μg/mL ethidium bromide (EtBr) for 15 min and imaged with UV light to determine the position of the molecular weight markers. To break down larger DNA, gel was UV irradiated in Stratalinker at 1000μJ x100, then soaked for 10 mins in 0.25 N HCl, followed by three washes in dH_20. DNA was denatured in denaturation buffer (0.5 M NaOH, 1.5 M NaCl) for 5 mins, and then fresh denaturation buffer was added and incubated for an additional 25 mins. The gel was briefly rinsed in $dH_20$and neutralized in neutralization buffer (0.5 M Tris, pH 7.5, 1.5 M NaCl) twice for 15 min. Following three washes in dH_20, the gel was equilibrated in 20X SSC. The positively charged nylon membrane was washed once in dH_20, then soaked in 20X SSC for 2 min. DNA was transferred overnight to the membrane, using an upward capillary transfer in 20X SSC. Following transfer, the membrane was UV crosslinked in a Stratalinker at 1500 μJ x100, and then baked at 80°C for 2 hrs.

Prior to hybridization, membrane was rinsed in 5X SSC, then blocked for 1 hr at 45°C in hybridization buffer (5X SSC, 5X Denhardt's Solution, 0.1% SDS, 200μg/mL sonicated salmon sperm DNA). DIG- labeled probe was diluted 1μl in 50 μl of milli-Q H_20 and heated to 95°C for 5 min, and then snap cooled on ice. Probe was then immediately added to prewarmed (45°C) fresh hybridization buffer, and incubated with membrane at 45°C overnight. Blot was washed twice for 15 min in 2X wash buffer (2X SSC, 0.1% SDS) at 55°C, followed by two 15 min

washes in 0.5X wash buffer (0.5X SSC, 0.1% SDS) at 55°C. Membrane was equilibrated to RT in 2X SSC, and then blocked in blocking solution (10% powdered milk, 1x maleic acid buffer) for 1 hr at RT. Primary mouse anti-DIG antibody (Abcam) diluted 1:2000 in blocking buffer and incubated with blot for 1 hr at RT. Following three washes in 1x maleic acid buffer, secondary anti-mouse HRP conjugated antibody was diluted 1:10,000 in blocking buffer and incubated for 1 hr at RT with blot. Blot was washed three times in 1X maleic acid buffer, and then exposed to Enhanced Chemiluminescent detection (SuperSignal West Extended Duration Substrate, Fisher, 34076) following manufacturer's protocol. Image processing and integrated density analysis were completed using ImageJ analysis software (NIH).

Statistical analysis: See Chapter 3.

4.3 Results

4.3.1 ATM inhibitor, KU55933 affects MuPyV entry and Tag expression

KU99533 is described as a specific and potent inhibitor of ATM that is widely used to interrogate the role for ATM kinase activity (Hickson, et al. 2004). It was used to study the effects of ATM signaling in a variety of viruses including HIV-1, SV40, and adenovirus (Lau, et al. 2005, Shah and O'Shea 2015, Sowd, et al. 2013). Reports show ATM signaling is required by PyVs to control the cell cycle and replicate monomeric viral DNA (Dahl, et al. 2005, Sowd, et al. 2013). My initial results with this inhibitor showed a similar phenotype that reduced viral titers without reducing viral DNA replication (Chapter 2). However, I more critically analyzed these results using an immunoplaque assay and found that KU55933 affected early steps in MuPyV infection as well.

In order to assess how treatment with KU55933 affected cell viability, I utilized high throughput imaging to quantify the number of cells under varying treatment times and conditions (Fig. 4.1 A). I found that KU55933 treatment did not affect cell viability. To determine if early steps during infection were affected by KU55933 treatment, I utilized high throughput imaging to quantify the number of infected cells in each sample (Fig. 4.1 B). Treatment with KU55933 for the entire duration of the experiment (2-30 HPI) resulted in an 80% reduction in the number of cells expressing Tag (Fig 4.1 B). Treatment with KU55933 between 2 and 10 HPI resulted in a 50% reduction in the number of cells expressing Tag and treatment from 10-30 HPI also resulted in a similar reduction in Tag expression (Fig 4.1 B). These results taken together suggest that KU55933 affects very early steps in MuPyV infection (2-10 HPI) and may also affect later stages in infection (10-30 HPI). The viral titers produced by these treatments scaled with number of cells expressing Tag (Fig 4.1 C, B). To better understand the effect of Tag expression on viral outputs, I normalized viral titers for number of cells expression Tag (Fig 4.1 D). In conclusion, the primary effect of KU55933 was to reduce the number of cells expressing Tag and did not reduce the amount of virus produced by those cells.

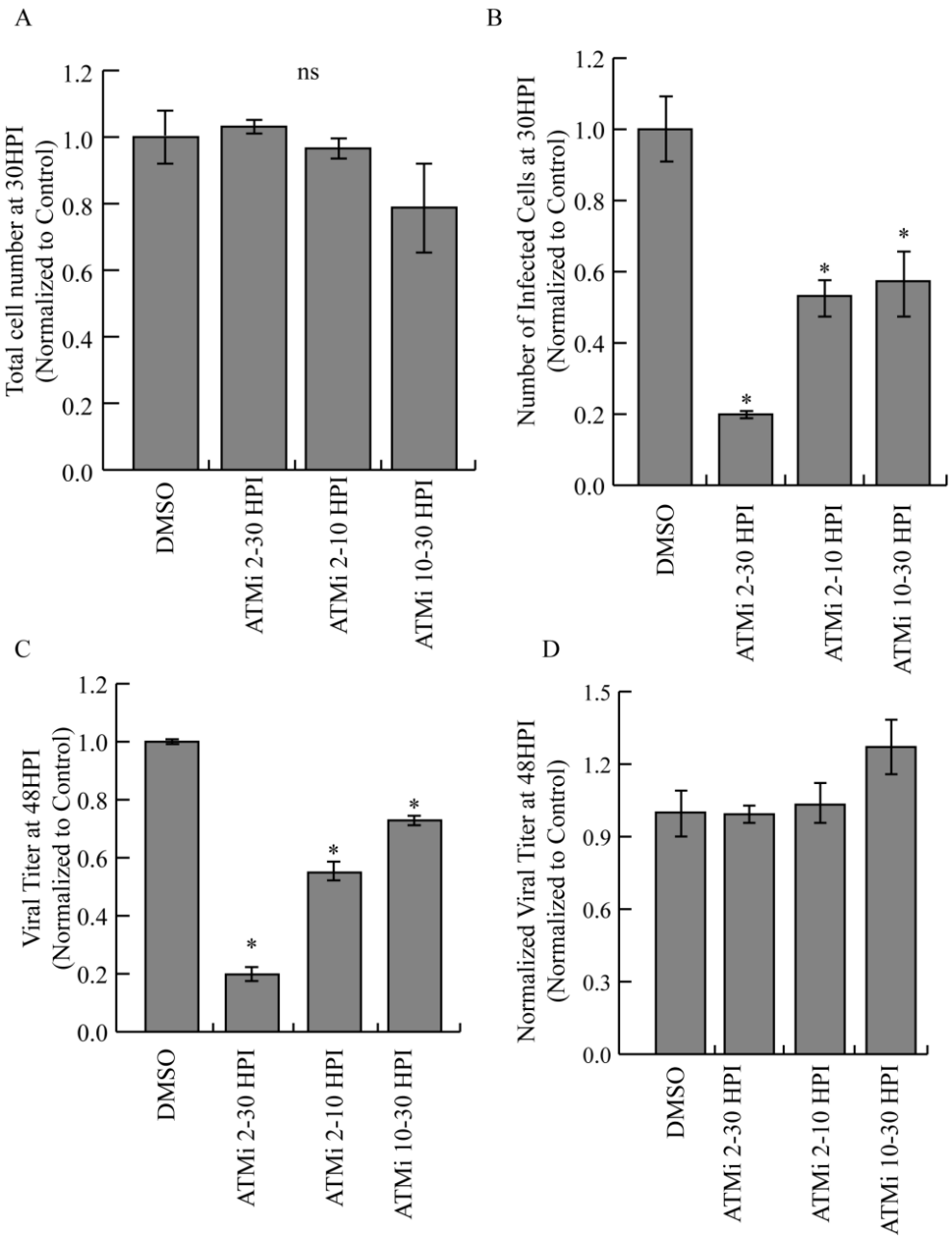

Figure 4.1: ATM inhibitor treatment affects multiple steps during MuPyV infection. MEFs were infected in the presence of ATM inhibitor (KU55933) for the indicated times. **A**) Total cell number for various inhibitor treatments. **B**) Number of cells that were infected at 30 HPI during inhibitor treatments. **C**) Infectious viral titers from various inhibitor treatments. **D**) Viral titer at 48 HPI normalized for number of infected cells at 30 HPI (values from C, divided by values from B).

4.3.2 Knockdown of NBS1 and ATM do not recapitulate inhibitor results

The initial screen of small molecule inhibitors suggested that Mre11 activity and ATM activity were required for MuPyV production (described in Chapter 2). To genetically test the requirement for the MRN complex and ATM kinase I created knockdown cell lines using lentiviruses encoding a shRNA to the target gene. Knockdown of either Mre11 or Rad50 was lethal, but I was able to create two NBS1 knockdown cell lines and one ATM knockdown cell line. NBS1 is required for trafficking of Mre11 and Rad50 to the nucleus, therefore it is unlikely that Mre11 or Rad50 had any relevant function in the absence of NBS1 (Carney, et al. 1998). NBS1 was reduced to less than 1% of control in NBS1 KD1 and less than 10% of control in NBS1 KD2 by mRNA level (Fig. 4.2 A). The expression level of the ATM KD cell line was approximately 10% of the control (Fig. 4.2 A). I initially analyzed viral titers from NBS1 KD1 and the ATM KD cell lines, compared to a non-target shRNA control (Fig. 4.2 B). I found an increase in viral titers produced by NBS1 KD1 compared to control. I also assessed the "infection efficiency" (number of infected cells, quantified by Tag staining) of these cell lines and normalized viral titers for infection efficiency (Fig 4.2 C). These initial results showed no significant difference between control and ATM KD, but an increase in viral titers from NBS1 KD1. This increase is even more apparent when cell lines are normalized for their infection efficiency (Fig 4.2 C).

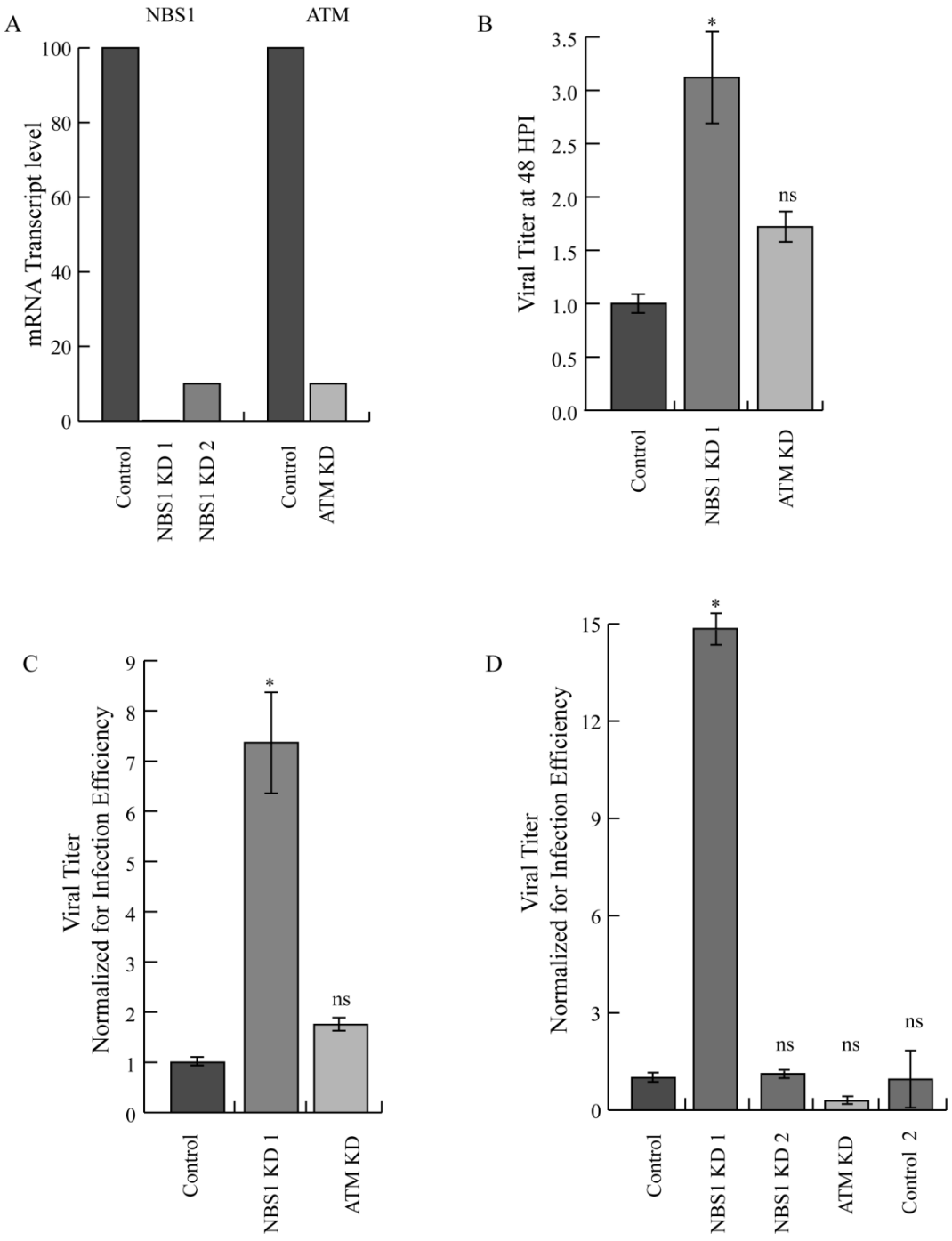

Figure 4.2: NBS1 knockdown may increase viral titer. A) Raw viral titers from NBS1, ATM or control knockdown cell lines at 48 HPI, quantified by immunoplaque assay. **B**) Viral titers from knockdown cells and control, normalized for number of infected cells (infection efficiency), same experiment as "A". **C**) Viral titers from knockdown and control cell lines, with second NBS1 knockdown cell line and control cell line, normalized for infection efficiency.

In order to confirm these results, I again analyzed viral titers and infection efficiency for control, NBS1 KD 1 and ATM KD. However, I included NBS1 KD2 and an additional WT cell line control (untransduced C57 MEFs) in further experiments (Fig. 4.2 D). Viral titers from NBS1 KD2 did not recapitulate the phenotype of NBS1 KD1. Additionally, ATM KD and the second control cell line did not show significant differences from the non-target control (Fig. 4.2 D). It is possible that the ATM KD and NBS1 KD2 cell lines did not show significant differences due to the poor knockdown of the transcript (~10% still expressed). In conclusion, the NBS1 KD cell lines did not show the same phenotype with respect the viral outputs and neither recapitulated the initial phenotype seen with drug targeting the MRN complex (Mirin).

4.3.3 SiRNA knockdown of RPA subunits reduces MuPyV titers

RPA is required for replication of cellular DNA and for *in vitro* replication of SV40. To determine if RPA was similarly required for MuPyV, I used siRNAs to knockdown the three subunits of the RPA complex. Knockdown of any RPA subunit was lethal after approximately 48 hrs, therefore I transfected the siRNAs after the start of the infection to minimize the effects of cell health on the experiment. This short knockdown reduced RPA14, 32, and 70 levels to about 20-30% of the control by mRNA transcript level (Fig. 4.3 A). By 32 HPI, knockdown and control cells had similar cell viability and infection levels (Fig. 4.4 B). However, at 48 HPI the viral titers produced by all three knockdown cell lines were reduced about 2-5 fold compared to the control. Importantly, this experiment serves as a proof of concept that siRNA mediated knockdown after the initial steps of infection can produce significant difference in viral titers.

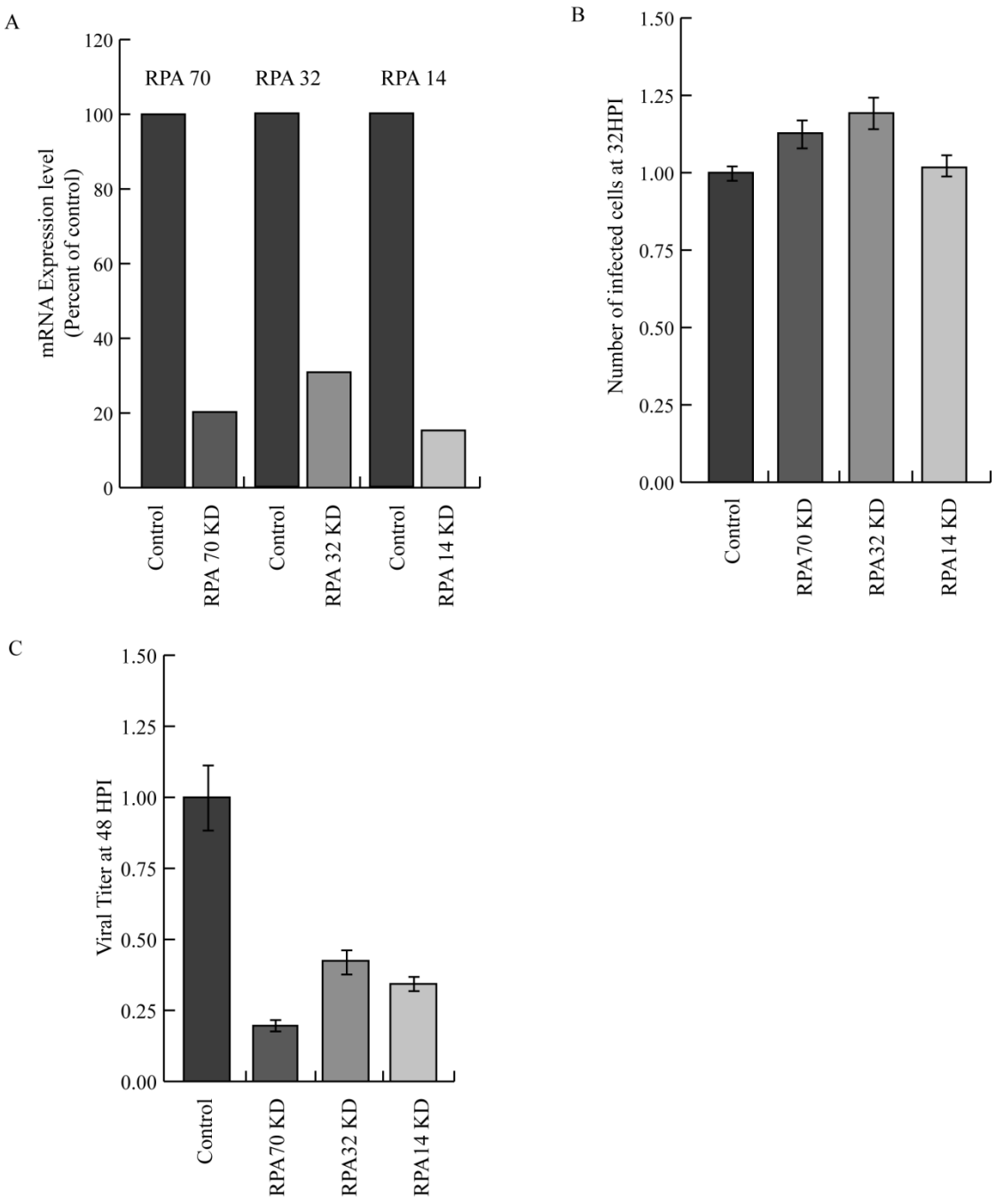

Figure 4.3: RPA is required for efficient production of MuPyV. MEFs were infected with NG59RA and at 6 HPI transfected with control siRNA or siRNA targeting the RPA complex. **A**) Expression level of RPA70, RPA32, or RPA14 by mRNA expression level, for each respective knockdown, normalized to control. **B**) Number of infected cells for control and knockdown conditions, quantified by high throughput imaging of Tag positive cells. **C**) Viral titers at 48 HPI from control and knockdown cell lines, quantified by immunoplaque assay.

4.3.4 RPA binding by LT is required for MuPyV production, but not DNA accumulation or DDR recruitment

SV40 and MuPyV LT bind to the 32 and 70kD subunits of the RPA complex (Arunkumar, et al. 2005, Banerjee, et al. 2013, Jiang, et al. 2006). This interaction aids loading of RPA onto viral DNA and allow full unwinding of the origin during DNA replication. In order to test the requirement for this RPA-LT interaction I made a mutant MuPyV virus, E320A, which is deficient at binding RPA. Although the direct interaction between Tag and RPA is abrogated in E320A, DDR proteins were still recruited to viral replication centers (Fig. 4.4 A-E). RPA 32 and downstream checkpoint kinase CHK1 were recruited to and phosphorylated at E320A replication centers (Fig. 4.4 A-C). Additionally, members of the ATM signaling pathway were recruited to E320A replication centers, including Mre11 and pATM (Fig. 4.4 D, E).

Despite robust recruitment of DDR proteins to replication centers, viral titers produced by E320A infection were 5-fold lower than the WT virus (Fig. 4.4 F). Although, SV40 DNA replication *in vitro* requires Tag binding to RPA, DNA replication was similar at E320A and WT viral replication centers (Fig 4.4 H). Interestingly, viral DNA accumulation was slightly increased in E320A infected cells (Fig. 4.4 G). Taken together these results suggest that the LT interaction with RPA is required for efficient assembly of MuPyV.

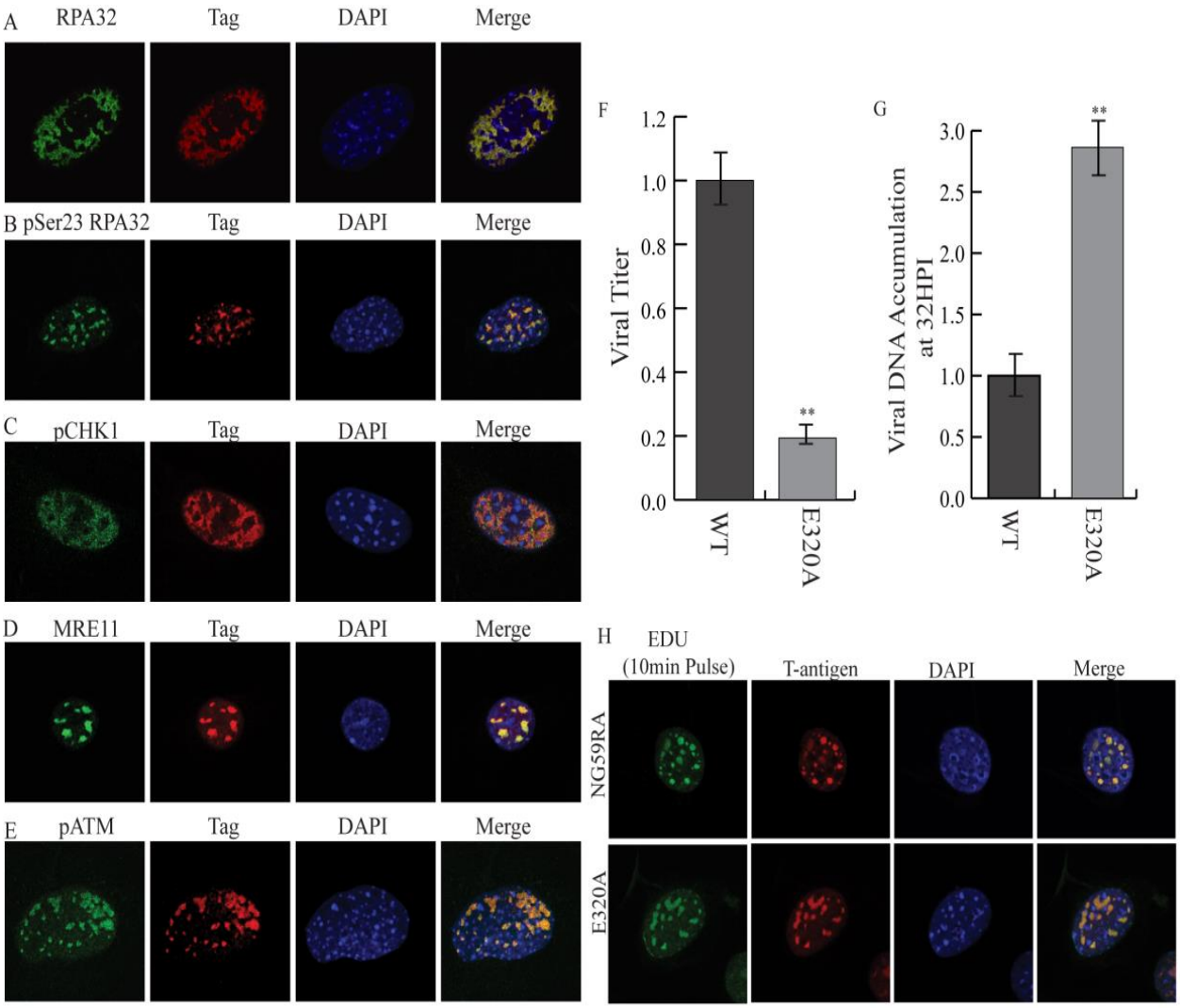

Figure 4: RPA Binding by LT is required for efficient production virus, but not viral DNA replication or recruitment of DDR proteins: MEFs were infected with mutant (NG59RA-E320A) virus for 28 hrs and immunostained for Tag and **A**) RPA32 **B**) pSer23 RPA32 **C**) pCHK1 **D**) MRE11 or **E**) pATM. **F**) Infectious viral titer by immunoplaque assay from MEFs infected with WT (NG59RA) or mutant (NG59RA-E320A) virus for 48 hrs. **G**) Viral DNA accumulation in cells infected with WT or E320A at 30 HPI by qPCR for viral genome. **H**) WT MEFs were infected with either WT (NG59RA) or mutant (NG59RA-E320A) for 28 hrs, EdU was added to media for a 10 minute pulse label, and then slides were immediately fixed and labeled.

4.3.5 E320A mutant virus replicates more viral DNA and expresses VP1 faster than WT virus

Since E320A mutant virus infected cells accumulated more viral DNA than WT, I analyzed viral DNA accumulation over the course of the infection. E320A infected cells accumulated more viral DNA at every time point from 18 to 32 HPI (Fig. 4.5 A). If E320A infected cells were accumulating viral DNA earlier than WT virus infected cells, it seemed possible that the transition from early to late stages of infection might be altered between the viruses. To analyze this possibility, I quantified the percent of Tag positive cells expressing VP1 during E320A infection and NG59RA infection. I found that E320A infected cells had a higher percentage of cells expressing VP1 at 30 HPI when compared to WT virus (Fig 4.5 B). Therefore, E320A viral DNA replication may occur faster than WT, which decreases the amount of time before the transition into later phases of the infection.

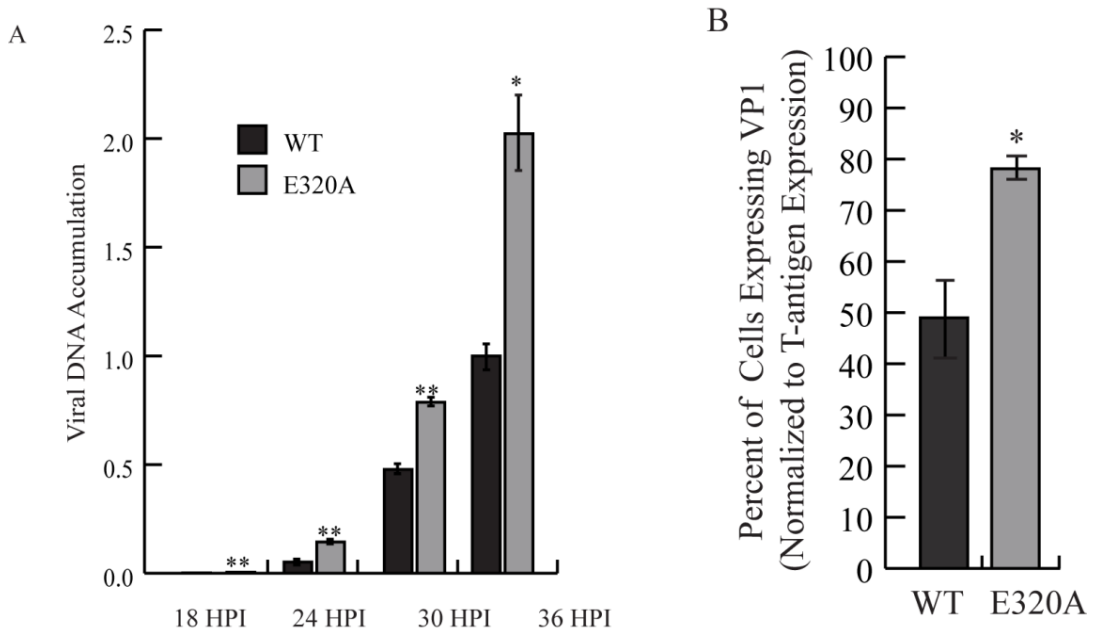

Figure 5: E320A mutant virus replicates more viral DNA and expresses VP1 earlier than WT virus. **A**) MEFs were infected with either NG59RA or NG59RA-E320A mutant virus and viral DNA accumulation was quantified by qPCR at given times. **B**) Infected MEFs were fixed at 30 HPI and stained for VP1 and T-antigen. The graph shows percent of Tag positive cells that also expressed VP1.

4.3.6 LT binding to RPA is required for monomeric viral genome replication

Inhibition of ATM or ATR signaling during SV40 infection resulted in the accumulation of higher-order concatemerized viral DNA. (Sowd, et al. 2013). Since I identified a defect in the E320A mutant virus that did not reduce total viral DNA copy number, but did affect assembly, I analyzed the size of the viral DNA species replicated by the E320A LT using a southern blot. Initial southern blots showed a striking decrease in the quantity of monomeric (~5 kb) viral DNA in E320A infected cells compared to WT infected cells (Fig 4.6 A, B). Additionally, the amount of higher order concatemerized DNA, quantified by integrated density of viral DNA in the well, was increased about 2-fold during E320A infection over WT infection (Fig. 4.6 A, B). However, digestion of the viral DNA with EcoRI to quantify total DNA, showed a second smaller species of the MuPyV genome from E320A infected cells (Fig. 4.6 C). This smaller genome appears to be missing 50-100 bps in the late region of the genome. It is unclear what the biological significance is of the second smaller DNA species.

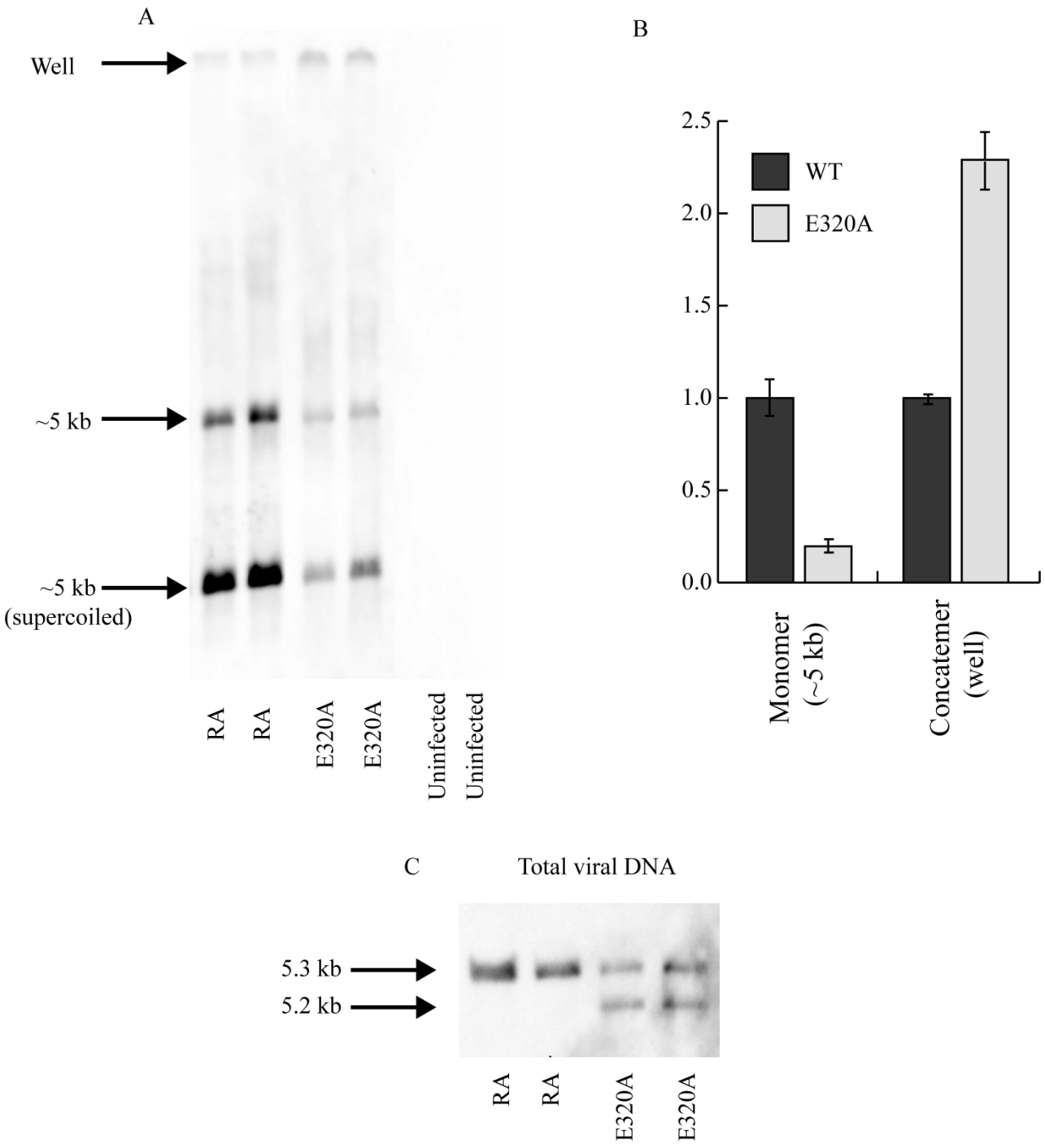

Figure 6: E320A replicates less monomeric and more higher-order viral DNA than WT. Cells were infected with NG59RA or NG59RA-E320A and viral DNA was isolated by Hirt extraction. **A**) Southern Blot of DNA from cells infected with NG59RA, E320A, or control cells. **B**) Monomeric (5kb) or concatermized viral DNA, quantified by integrated density analysis of indicated bands or well. **C**) Viral DNA from NG59RA or E320A infected cells, digested with EcoRI to linearize the genome.

4.4 Conclusions

I better characterized the role for DDR proteins in the RPA and MRN complexes. I also found that ATM inhibitor, KU55933, affected multiple stages of infection, making the interpretation of experiments using this drug difficult. I also attempted to confirm results from Mirin, an inhibitor of Mre11, by analyzing viral titers from NBS1 knockdown cell lines. These results were unfortunately inconclusive, but highlight the need to genetically confirm drug and shRNA results. To circumvent the extreme effect of RPA knockdown on cell health I developed a protocol that allowed for knockdown of the target gene only during later stages of infection. Although the results from this experiment likely only highlight the requirement for RPA during DNA replication, the assay itself presents an interesting alternative to other methods, such as stable knockdown in cell lines. Finally, I created and characterized a Tag mutant virus (E320A) that does not bind to RPA. This virus had a reduction in monomeric viral genomes replicated and an increase in concatermized viral DNA species accumulated. Additionally, further analysis showed that E320A viral DNA accumulated in a WT (5.3kb) size and a slightly smaller (~5.2kb) size. These data highlight the complex role for DDR proteins in viral infection, DNA replication and cell health.

4.5 Discussion

There is a described requirement for ATM signaling during SV40 and MuPyV replication, but I was unable to replicate these results using a small molecule inhibitor (KU55933). I found that KU55933 inhibited MuPyV at multiple steps on infection, including entry. It is possible that ATM activity is required during MuPyV entry steps; however, it is difficult to hypothesize why this might be the case. The other alternative is that an off target

effect of the drug interferes with early steps in the MuPyV infection. I believe that an off target effect is more likely because a requirement for ATM during entry is not described nor suggested by previous studies. These possibilities should be tested using siRNA against ATM at different times of infection.

The initial results from a small screen of DDR inhibitors (Chapter 2), showed a reduction in viral titer following treatment with an Mre11 inhibitor, mirin. Although I was unable to create stable Mre11 knockdown cell lines, I was able to knock down NBS1, another component of the MRN complex. It is unlikely that Mre11 functioned in these cells since knockdown of NBS1 resulted in delocalization of Mre11 from the nucleus. Unfortunately, NBS1 KD lines 1 and 2 did not recapitulate the inhibitor results, suggesting that either Mre11 inhibition results in a different effect than knockdown, or an off target effect of the drug is responsible for the observed phenotype. Interestingly, NBS1 KD1 produced significantly more virus than either control cells or NBS1 KD2. Likely, the best way to elucidate the real role for MRN complex proteins during MuPyV replication and assembly is through transient knockdown.

Using transient siRNA mediated knockdown of subunits of the RPA complex, I showed that RPA is required for efficient MuPyV production. Although this phenotype likely only highlights the requirement for RPA during DNA replication, the method presents promising alternative to stable knockdowns. Knockdown of essential proteins such as members of the MRN complex or ATR during infection might be possible using this transient knockdown protocol. Although RPA is a vital protein in DNA replication, I was able to elucidate a more subtle role for it during MuPyV infection, using a mutant virus, E320A.

There is a direct interaction between MuPyV LT and the 32 and 70kD subunits of RPA. There are several point mutations that abrogate the interaction between RPA and LT including, E320A and K308E (Banerjee, et al. 2013). Since mutating K308 in the NG59RA genome would also mutate the open reading frame for MT, I created a mutant virus encoding the E320A mutation. I created the virus by extracting the genome from a plasmid encoding the entire MuPyV genome, religating it and transfecting it into MEFs. From there, I determined the RA-E320A produced 5-10X reduced viral titers compared to NG59RA and 2-3X more viral DNA accumulated in E320A infected cells. Additionally southern blot analysis showed that E320A produced more higher-order concatermized viral DNA and 5x less monomeric viral DNA than NG59RA. These data suggest that RPA binding by LT is required to resolve viral genomes correctly (Fig 4.7). It is possible that RPA recruits proteins required for a specific mechanism of repair, such as HR, or RPA binding by LT may regulate the mechanism of replication and prevent rolling circle replication from occurring during WT infection.

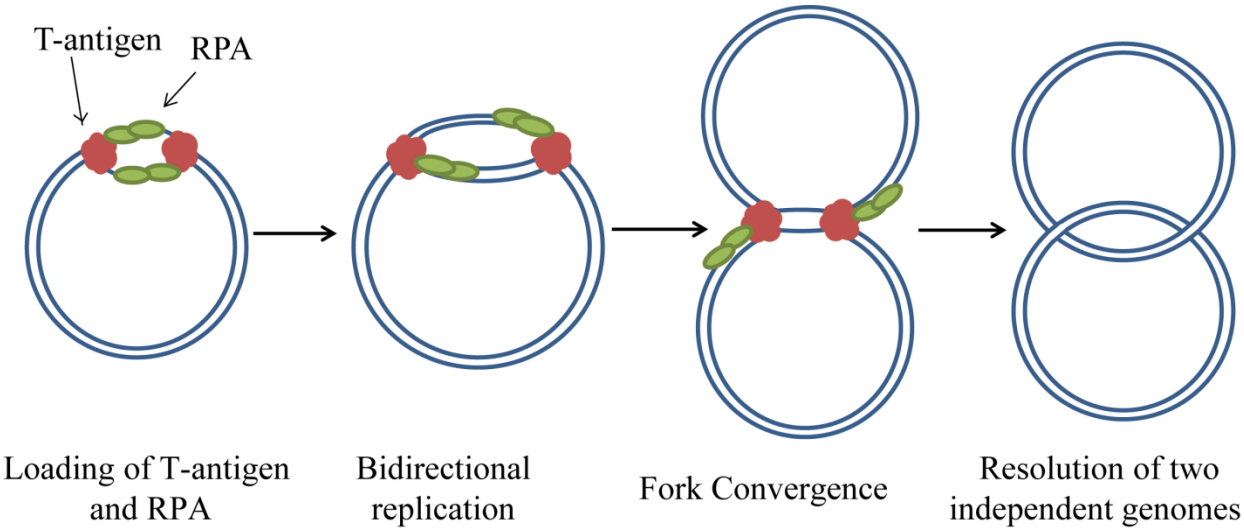

Figure 4.7: Model of WT bidirectional MuPyV replication. LT binds to the viral origin of replication, unwinds a stretch of DNA and loads RPA onto single stranded DNA. Viral DNA replication proceeds bidirectionally around the viral genome, until the forks converge and a high stress intermediate is formed. Eventually two fully formed interlocked daughter genomes are completed.

Inhibition of ATM or ATR during SV40 DNA replication resulted in increased formation of higher order concatemers of viral DNA (Sowd, et al. 2013). A current model suggests that SV40 utilizes HR proteins to correctly resolve replication intermediates and prevent NHEJ of viral DNA (Sowd, et al. 2014). During MuPyV infection, it is possible that the LT interaction with RPA is required to recruit downstream HR proteins or activate ATM and ATR signaling during DNA replication. In the absence of ATM and ATR, signaling, viral genomes could be incorrectly resolved into higher order concatemers that undergo rolling circle or unidirectional replication. Alternatively, RPA loading on to viral DNA by LT may be required for bidirectional replication of the viral genome. Inefficient loading of RPA onto the viral origin could result in rolling circle replication of a subset of viral genomes (Fig 4.8). These rolling circle replication products could replicate faster than correctly resolved monomeric viral genomes and would be too large to be packaged into a single virion.

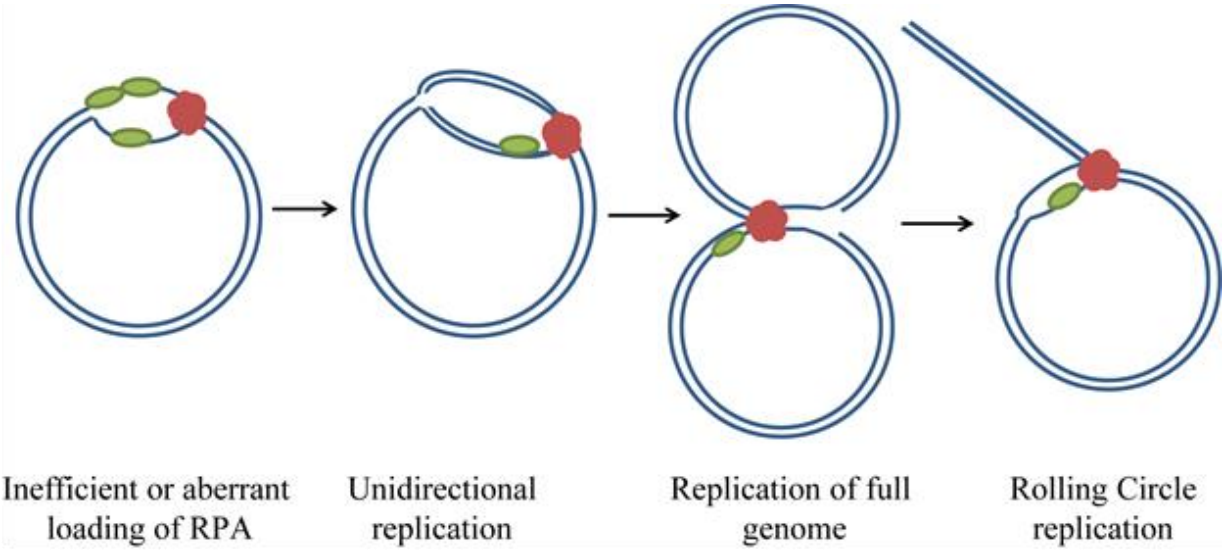

Figure 4.8: Model of rolling circle replication in the absence of RPA-LT binding. In the absence of LT (pink) binding to RPA (green), replication fork collapse or inappropriate loading of the replisome could result in unidirectional progression of replication. Once unidirectional replication begins no high stress intermediate forms and the LT driven complex continues around the viral genome into rolling circle replication. Rolling circle replication creates end to end linked concatemers of viral DNA that are not able to be packaged into virions.

The presence of a second species of viral DNA in the E320A infected cells complicates the interpretation of the E320A mutant virus results. The small viral DNA product could be the product of a cloning artifact or direct result of the E320A mutation. It is possible that the interaction between LT and RPA stabilizes an area of the genome that was lost during E320A viral DNA replication. In order to distinguish these possibilities, I will clone the E320A, K381E, and WT viruses using a different restriction site. These experiments will clarify the role of the RPA-LT interaction during MuPyV infection.

Chapter 5
Stochastic Optical Reconstruction Microscopy (STORM) of MuPyV Infected Nuclei

5.1 Introduction:

5.1.1 Viruses reorganize the host cell to facilitate viral replication and assembly

Viruses tightly couple replication of the viral genome with assembly of progeny virions in structures called "virus factories". These replication factories may increase the efficiency of virus assembly by concentrating viral proteins and genomes in one location (Novoa, et al. 2005). Some RNA viruses, such as poliovirus, reorganize the membranes of the ER to create viral replication factories in the cytoplasm (Suhy, et al. 2000). The reorganized ER membranes may act as a scaffold on which viruses assemble. Most DNA viruses form replication centers in the nucleus of host cells where they replicate viral DNA and assembly progeny virions (Schmid, et al. 2014). Many larger DNA viruses, such as adenoviruses or herpesviruses, form progeny virions by injecting the viral genome into a preformed capsid (Brown and Newcomb 2011, Ostapchuk and Hearing 2005). Current evidence suggests that smaller DNA viruses such as PyVs utilize a different mechanism. A polymerization based model for the assembly of PyVs was proposed in the 1980s, but until recently, very little progress was made in discerning the mechanism of PyV assembly (Garber, et al. 1980).

5.1.2 Reorganization of cellular proteins by PyV infection

PyVs express early T-antigen (Tag) proteins that manipulate the host cell to aid viral replication and late proteins VP1, VP2 and VP3 that comprise the viral capsid (Treisman, et al. 1981). PyV infection re-organizes DNA replication and repair proteins into replication centers in

the nucleus (Zhao, et al. 2008). In several PyVs these replication centers form at or adjacent to PML nuclear bodies (PML-NBs) (Erickson, et al. 2012, Jul-Larsen, et al. 2004).

PML-NBs are highly multi-functional nuclear structures associated with transcriptional regulation, apoptosis, DNA repair, and the interferon response (Takahashi, et al. 2004). PML-NBs are implicated in conflicting roles in different viral infections (Ishov and Maul 1996). PML-NBs have potent antiviral effects during some infections, such as adenovirus (Stracker, et al. 2002). In contrast PML-NBs serve as a scaffold or recruitment center for viral proteins during papillomaviruses infection (Day, et al. 1998). It was hypothesized that PML-NBs may serve as scaffolds or sites for PyV assembly in the nucleus, however a recent report showed that PML protein is not required for MuPyV infection (Jul-Larsen, et al. 2004). In contrast, recent reports suggest that PML and LT may have an antagonistic relationship (Jiang, et al. 2011). PyVs also recruit DNA damage repair proteins to viral DNA replication centers in the nucleus of cells (Jiang, et al. 2012, Orba, et al. 2010, Zhao, et al. 2008). These replication centers are well described by confocal microscopy, but the nanoscale organization of these DNA replication centers is not well understood.

5.1.3 Ultrastructure of PyV replication factories

The ultrastructure of PyV assembly was described using electron microscopy. The MuPyV major capsid protein, VP1 forms filamentous structures in the nucleus of infected cells. These structures are associated with progeny virions and are termed “virus factories” (Erickson, et al. 2012). These filamentous structures were observed in JCV infected brain tissues and very early studies of MuPyV infected cells (Mattern, et al. 1966, Silverman and Rubinstein 1965, Zurhein and Chou 1965). The description of these structures led to the hypothesis that PyV VP1

forms tubes filled with viral DNA that bud off newly formed virions. However, it is unclear whether proteins other than VP1 are associated with these tubes.

Electron dense cellular structures or those that stain with an electron dense dye are easily imaged by electron microscopy. Additionally, cellular proteins labeled with gold conjugated antibodies are identifiable by immuno-EM (Ou, et al. 2015, Tokuyasu 1973). However, far fewer antibodies and epitopes are compatible with EM sample preparation methods, than immunofluorescence protocols. Due to the antibody epitope limitations of electron microscopy, little is known about how these virus factories are spatially organized with respect to other viral and cellular components. The resolution limit of light microscopy prevents imaging of these nanoscale virus factories with immunofluorescence-based techniques.

5.1.4 Super resolution imaging bridges resolution gap

Recent advances in super resolution imaging reduced the resolution gap between EM and light microscopy. STochastic Optical Reconstruction Microscopy (STORM) is a type of single molecule localization microscopy that depends on imaging of single molecules to reconstruct images above the resolution of light microscopy (Rust, et al. 2006). The resolution of traditional light microscopy is limited by diffraction to a lateral resolution of about 200 nm. STORM can improve this resolution by an order of magnitude or more to approximately 10-20 nm (Han, et al. 2013). Additionally, STORM utilizes synthetic fluorophores that can be easily conjugated to antibodies or other biomolecules, which enables imaging of a wide range of targets.

STORM imaging requires synthetic fluorophore blinking that allows for the imaging of a subset of single molecules (Rust, et al. 2006). There are two primary types of multicolor STORM imaging, direct (dSTORM) or activator-reporter dye pairs (Huang, et al. 2008, van de Linde, et

al. 2011). Using activator-reporter pairs enables the use of an optimal fluorophore, such as Alexa Fluor 647 as the reporter for all labels. Although this greatly benefits the localization precision, stochastic reactivation of the reporter results in cross-talk that must be mathematically subtracted from the dataset (Huang, et al. 2008). dSTORM does not suffer from similar fluorophore cross-talk, however the optimal STORM fluorophores are all in the Cy5 family of dyes. One of the major challenges of two-color dSTORM is optimization of a second fluorophore.

A major limitation of STORM is the ability to image thick or densely labeled samples, because of this requirement for single fluorophore visualization. High background from out of focus fluorophores and cross activation of fluorophores reduces the accuracy of single molecule localizations. We utilized optical, computational, and biochemical methods to overcome these limitations to image the sub-nuclear organization of infected cells.

5.2 Methods

Cell Lines and Infections: C57BL/6 mouse embryonic fibroblasts (MEF) were obtained from ATCC (SCRC-1008; Manassas, VA) and served as a wild-type (WT) MEF. MEFs were grown in DMEM (D6429, Sigma) supplemented with 10% fetal bovine calf serum (FBS; F0926, Sigma), and 55 μM β-mercaptoethanol (βME) at 37°C with 5% CO_2. Virus strain NG59RA (Feunteun, et al. 1976) was used for all WT virus infections. Cells were plated on 35mm imaging dishes with 1.5 thickness coverslips (Mattek, P35G-0.170-14) for 24 hrs, then cultured in DMEM supplemented with 0.5% FBS for 24 hrs, before infections were carried out in adsorption buffer (Hanks Balanced Salt Solution (HBSS) with 10 mM HEPES, pH 5.6 and 0.5% BCS) as previously described (Cripe, et al. 1995). Cells were infected for 2 hrs at a multiplicity of

infection of approximately 10-15 pfu/cell, and then cultured in DMEM supplemented with serum for the remainder of the experiment.

Confocal Imaging: See chapter 3.

Immunofluorescence sample preparation for STORM: Following a brief wash in 37°C PBS, cells were fixed in 4% paraformaldehyde (PFA) and 0.1% glutaraldehyde (GA) in PBS at RT for 10minutes, permeabilized in 0.5% Triton-X100 in PBS for 10 min and blocked overnight in 10% BCS/ PBS.

Cells that were pre-extracted were rinsed briefly in ice cold CSK Buffer (10 mM piperazine-1,4-bis(2-ethanesulfonic acid) (PIPES), pH 6.8, 100 mM NaCl, 300 mM sucrose, 1 mM MgCl2, 1 mM EGTA) then permeabilized in 0.5% triton in CSK buffer, on ice for 5 minutes, rinsed twice with 4°C PBS and fixed in 4% PFA and 0.1% GA in PBS at RT for 10minutes, then blocked overnight in 10% BCS/PBS.

Directly labeled primary antibodies, diluted in 10% BCS/PBS were incubated with samples for 1-2 hrs at RT. Samples were washed twice in 10% BCS/ PBS and once in PBS, then antibodies were post-fixed with 4% PFA and 0.1% GA in PBS for 10 min. Samples were washed twice with 10% BCS/ PBS and stored in PBS at 4°C until imaging.

Direct Antibody labeling: Tag was detected using polyclonal rat anti-Tag antibody (E1, gift of Tom Benjamin), VP1 was detected using anti-VP1 monoclonal antibody (FD9), and PML was detected using mouse anti-PML monoclonal antibody (ALX-804-816; Enzo). Antibodies were directly conjugated with either Alexa Fluor 647-NHS ester or ATTO 565-NHS Ester, per manufacturer's instructions with a degree of labeling between 1 and 3 dye molecules per antibody.

Imaging Buffers: STORM imaging was carried out in 100mM Tris, pH 8.0, 10% glucose, 10mM NaCl, 1% βME and 1% GLOX enzyme mix (50mg/ml glucose oxidase, Sigma and 4mg/ml catalase, Sigma in PBS)

Imaging set up: STORM imaging was performed on an N-STORM microscope with 561 and 647 lasers. The 561 and 647 lasers were triggered in alternating 10ms frames. The emission light from the fluorophores was also split using a dichroic mirror and filter on to independent Andor EMCCD cameras. The cameras were simultaneously triggered and at least 30,000 frames for each channel were collected.

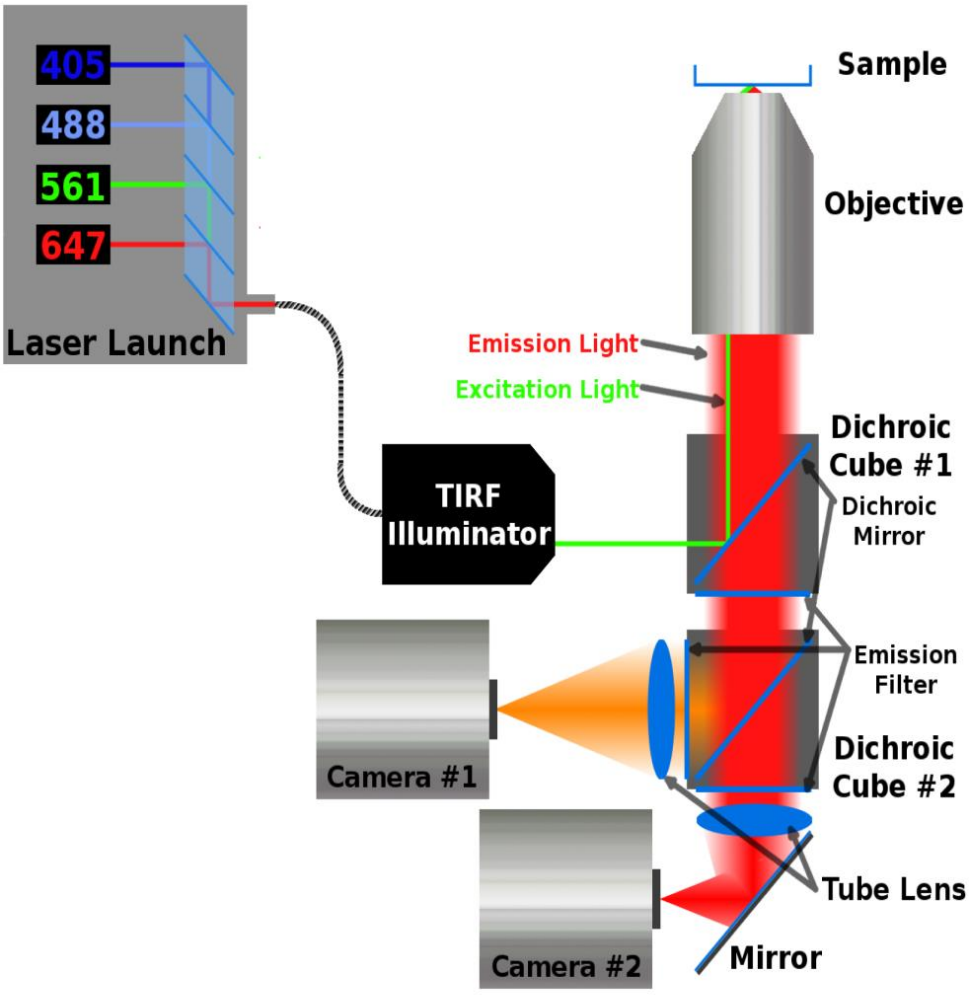

Figure M5.1: Optical configuration of N-STORM for dual color super resolution imaging. Dichroic cube #2 splits the emission light from the two fluorophores onto two independent cameras. This set up prevents bleed through of the Alexa Fluor 647 into the ATTO 565 image. Figure created by Anthony Barsic.

Data analysis and image reconstruction (Anthony Barsic): (Barsic, et al. 2014) The method for resolving and localizing images of single molecules involves a combination of optical and digital techniques: (a) Creating a model of the optical system with a combination of experimental measurements and theoretical calculations; (b) Establishing a dictionary composed of the image of a point source for different locations in a dense grid; (c) Solving the estimation problem of

determining the coefficients of the dictionary elements that best represent the data. Once the non-zero coefficients are known, the number of molecules and their locations and brightnesses can be determined. To solve the coefficient estimation problem, we use Matching Pursuit (MP). In MP, an iteration consists of projecting the image onto the dictionary, finding and storing the largest coefficient, and subtracting that element from the image (Bergeaud and Mallat 1995). Iterations continue until a stopping criterion is met.

5.3 Results

5.3.1 Confocal imaging of infected nuclei

PyV infected nuclei show discrete viral replication centers, marked by Tag, using confocal microscopy. These structures can be readily imaged following a pre-extraction of soluble cytoplasmic and nuclear proteins. Tag forms discrete "tracks" throughout the nucleus which co-localize with DNA replication and repair proteins (Fig 5.1 A). Similar to reports for other PyV infected cells, PML-NBs localize adjacent to viral replication centers (Fig 5.1 A). VP1 appears localized diffusely through the nucleus with a more concentrated ring around the edge of the nucleus (Fig 5.1 B). In order to determine where VP1 was localized with respect to the nuclear lamina we examined the localization of VP1 and lamin B during infection. We found VP1 localized throughout the nucleoplasm and inside the nuclear lamina (Fig 5.1 C). These data show the nuclear localization of these proteins, but little else about the structure or organization of these proteins within the nucleus.

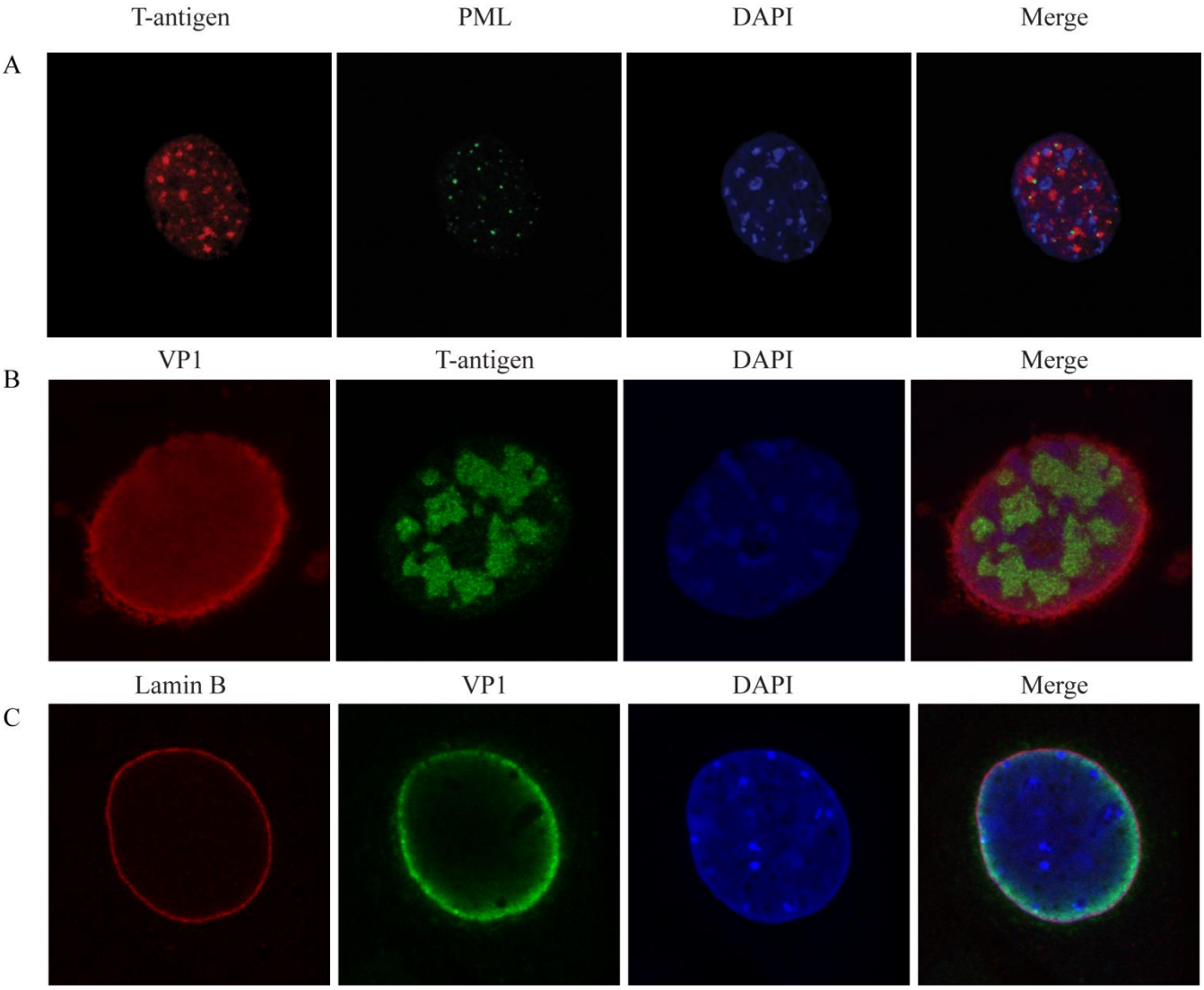

Figure 5.1: Confocal images of VP1 and T-antigen in the nucleus. A) MEFs were infected with NG59RA, at 28 HPI cells were fixed, permeabilized and immunostained for PML and Tag. **B**) MEFs at 32 HPI, immunostained for VP1 and Tag. **C**) MEFs at 32 HPI immunostained for Lamin B and VP1.

5.3.2 Optimization of two color dSTORM imaging of infected nuclei

Here we describe an improved method for 2-color dSTORM imaging in densely labeled biological samples. Alexa Fluor 647 is the best known synthetic fluorophore for STORM imaging and is also the mostly commonly utilized (Jensen and Crossman 2014). We optimized a second dye in the Cy3 family of dyes to accomplish two-color imaging in conjunction with Alexa Fluor 647. We determined the best option to be a non-traditional super resolution fluorophore, ATTO565 (Fig 5.2). Additionally, we used an improved optical set up with two cameras and emission filters. We utilized existing datasets to pick candidate dyes and then we tested those dyes within our system. We calculated and compared the signal to noise ratio of several fluorophores under different buffer conditions and imaging conditions to determine the best option. This optimization is critical in a sample with high background because single molecules must be identified and localized above noise. The localization precision of STORM is directly correlated with the peak intensity of the fluorophore, so reconstruction precision can be reduced in samples with high background. We found that ATTO 565 emitted more photons per localization event, than Alexa Fluor 568, resulting in substantially improved localization precision (Fig. 5.2).

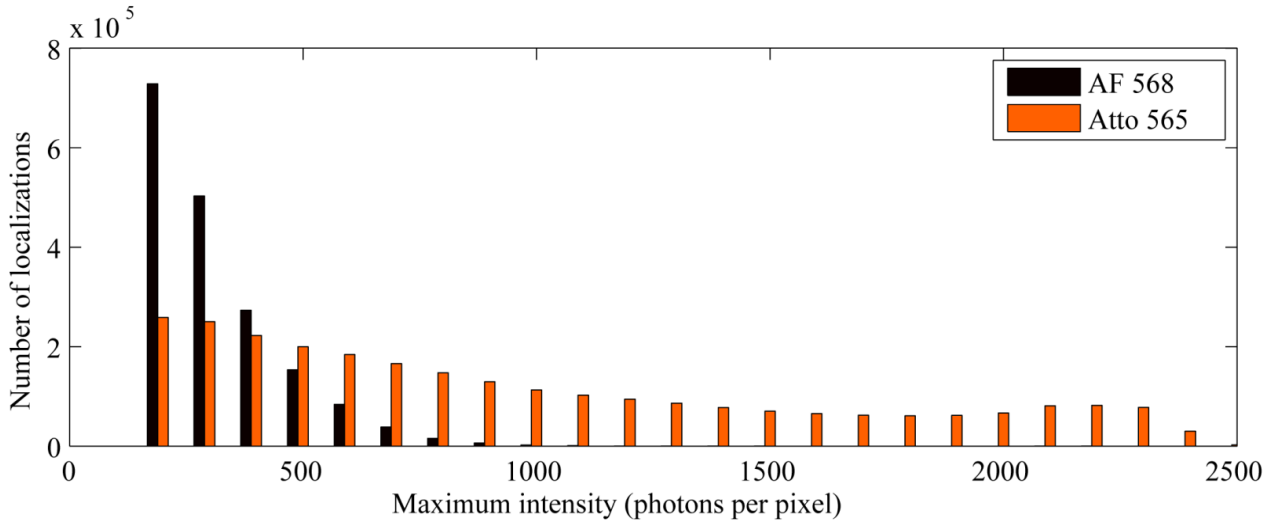

Figure 5.2: ATTO 565 is brighter than Alexa Fluor 568. Histogram showing the maximum intensity of single molecule localizations for ATTO 565 and Alexa Fluor 568, with the number of localizations per bin on the y-axis and max intensity on the x-axis.

5.3.3 PML and viral protein Tag have an exclusionary relationship

PML protein is not required during MuPyV infection, suggesting PML is not a scaffold or recruitment center for PyVs. However, PyVs may functionally inhibit PML-NBs through reorganization. By confocal microscopy, viral replication centers, marked by Tag staining, form adjacent to PML-NBs with small regions of co-localization. Observing this type of localization by confocal microscopy could indicate a small region of overlap between the two structures or as much as 200 nm between them because of the limit of resolution of light microscopy.

Using 2-color dSTORM super resolution imaging, we observed Tag in clusters throughout the infected host cell nucleus, and PML protein in ring shaped PML-NBs (Fig 5.3 A). We also found a subset of Tag that is more closely associated with PML-NBs (Fig 5.3 B). Additionally, we were better able to visualize the ring-like structures formed by PML-NBs. In many instances, the less dense core of the PML-NB would not be visible by confocal microscopy. The variance in the thickness of the PML-NB was also easier to visualize and quantify using super resolution imaging over confocal microscopy.

A

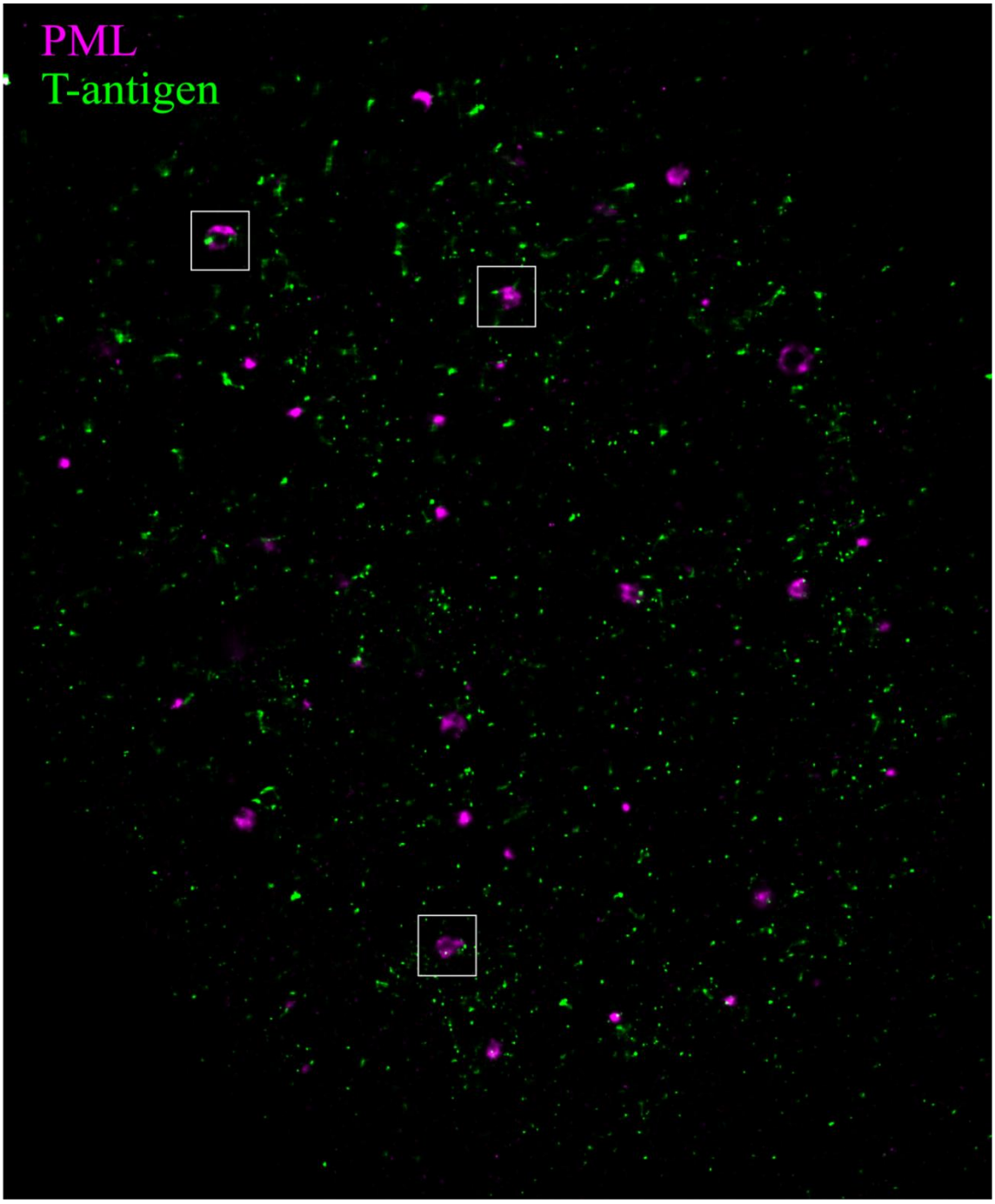

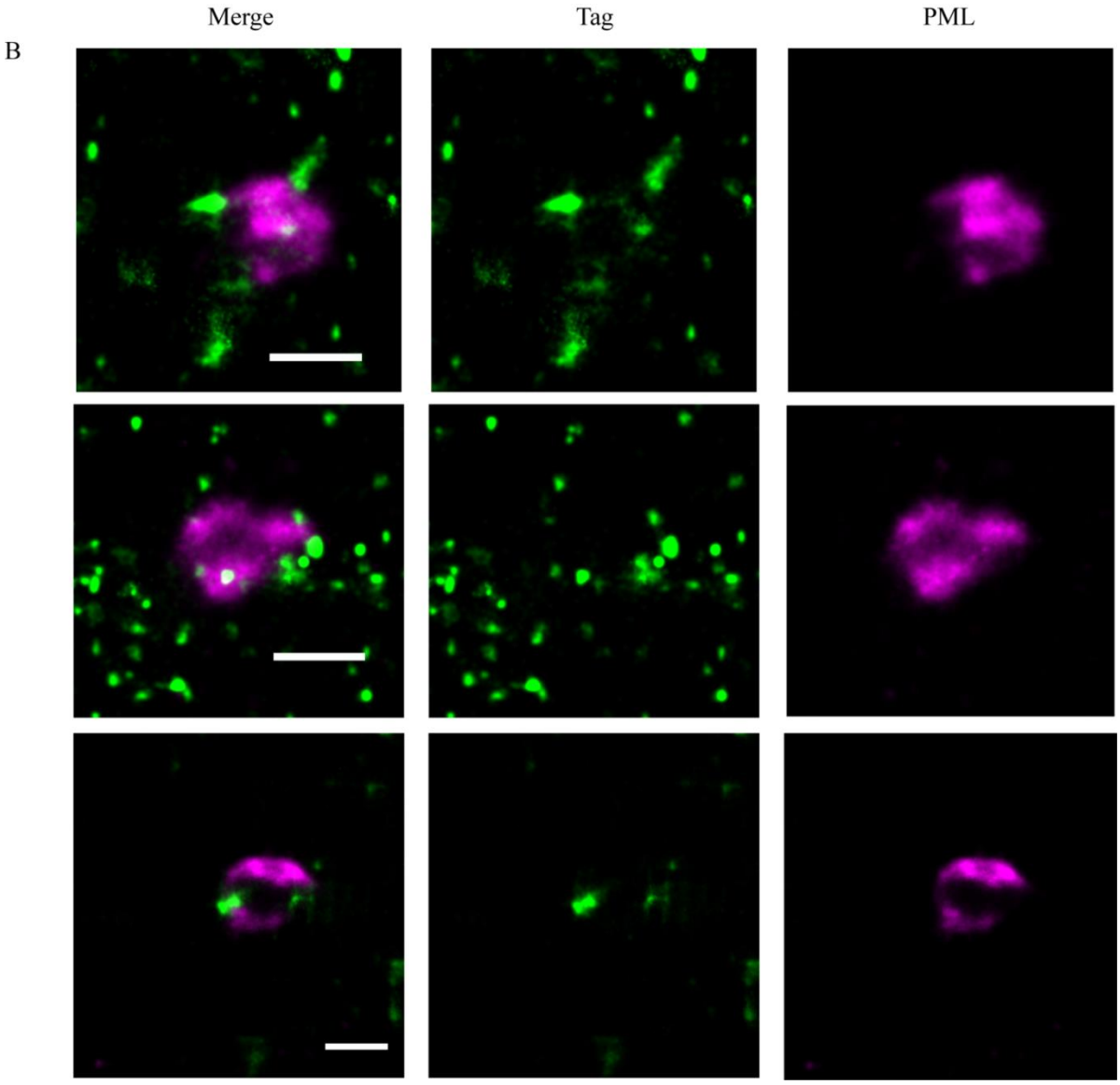

Figure 5.3: PML-NBs and T-antigen have an exclusionary relationship. **A**) MEFs were infected with NG59RA and at 28 HPI cells were pre-extracted, fixed and immunostained for Tag and PML. STORM reconstruction of full nuclei, with PML displayed in purple and Tag displayed in green. **B**) Insets from A, with 500nm scale bar.

5.3.4 VP1 forms tubes and virion clusters in the nucleus of infected cells

MuPyV LT is required for packaging of viral genomes into progeny virions (Peden, et al. 1990). However, the spatial organization of LT and VP1 during the replication and assembly process is unknown. In order to better understand how these proteins interact, we analyzed the localization of VP1 and Tag at 32 HPI. VP1 forms tubes and virions in the nucleus of infected cells at 32 HPI by electron microscopy. These "virus factories" cannot be visualized by traditional light microscopy. Using STORM, we found that VP1 forms higher order structures that cluster around the edge of the nucleus, but also localize throughout the nucleoplasm (Fig 5.4 A, B). These long branching tube-like structures tend to be 100-120 nm in width and 200 nm to 2 μm in length. The width of these structures observed by STORM is greater than the width of tubes observed by EM. It is possible that these larger structures visualized in STORM images are actually bundles or clusters of the VP1 tubes observable by EM. In some cases, smaller 40-50nm tubes are observed by STORM, which are likely the same structures that are observable by EM. Interestingly, in many cases these bundles of VP1 tubes inside the nucleus appear to branch and form networks. These tubular networks appear to extend out from the periphery of the nucleus.

Tag appears to localize throughout the nucleus, with only a small subset of Tag near the tubes and virions formed by VP1 (Fig 5.4). This subset of Tag generally localizes adjacent to virions and tubules. Since LT is the viral protein responsible for viral DNA replication, it seems likely that the majority may be associated with viral DNA replication or other functions and not virion packaging.

During MuPyV infection, the tube-like structures described by EM are less prevalent at very late times of infection (Erickson, et al. 2012). The current model suggests that these tube-

like structures bud off, or break down into fully formed virions as the assembly process progresses. We similarly observed nuclei during late time points that were filled with virions, and very few larger structures (Fig 5.5). In these experiments, to detect VP1 we utilized a directly labeled anti-VP1 antibody, which adds approximately 10-20 nm to the perceived size of the object. PyV virions are 50 nm in size and would therefore appear to be roughly 60-70 nm when labeled with an antibody. The localization precision of these datasets is about 20 nm which introduces additional variance to the perceived size of objects. White arrows mark objects that are consistent with single virions (60-80 nm). It is likely that there are many other objects in these images that are consistent with the size of a single virus particle, however additional analysis is necessary to make that distinction.

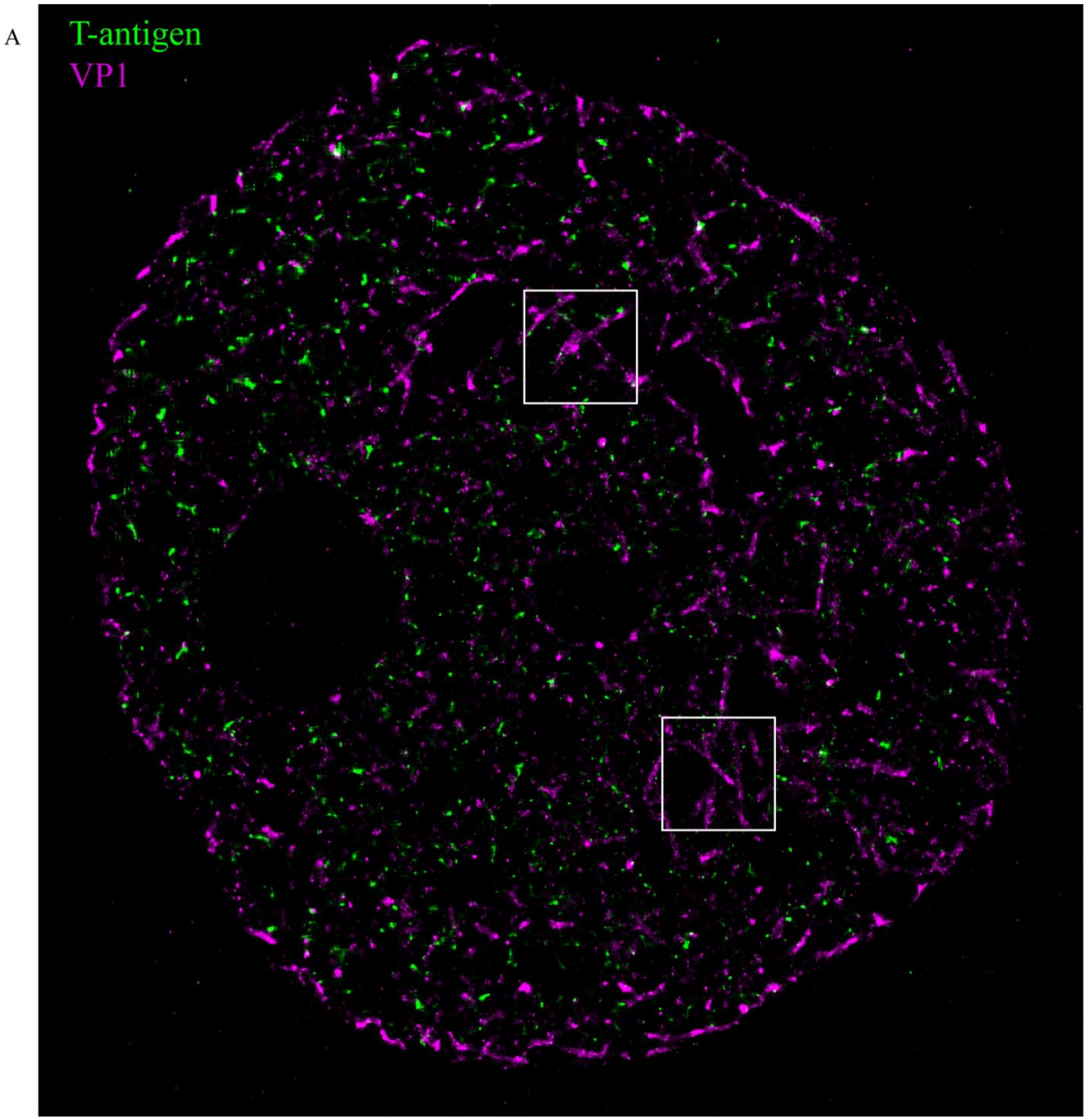

Figure 5.4: VP1 forms a network of tubes in the nucleus during MuPyV infection. A) MEFs were infected with NG59RA and at 32 HPI cells were fixed, permeabilized and immunostained for Tag and VP1. STORM image of full nuclei, with VP1 displayed in purple and Tag displayed in green. **B-C**) Insets from A, with 500nm scale bar. White arrows indicate objects the approximate size of a single virion, yellow arrows indicate objects the size of a single "tube".
B and C on next page

B

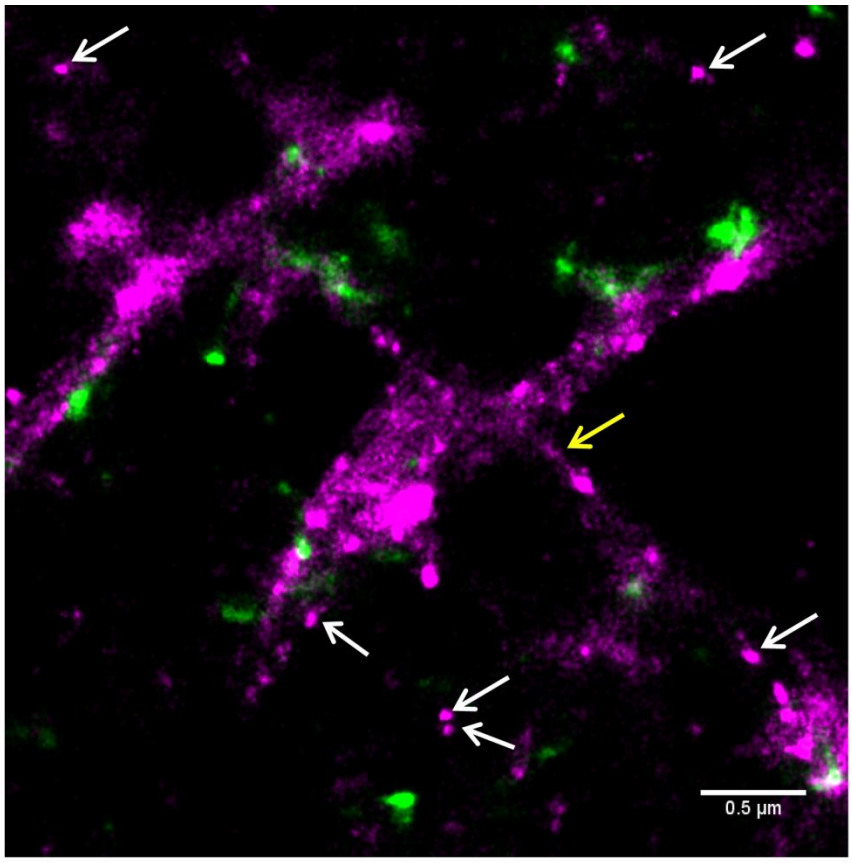

C

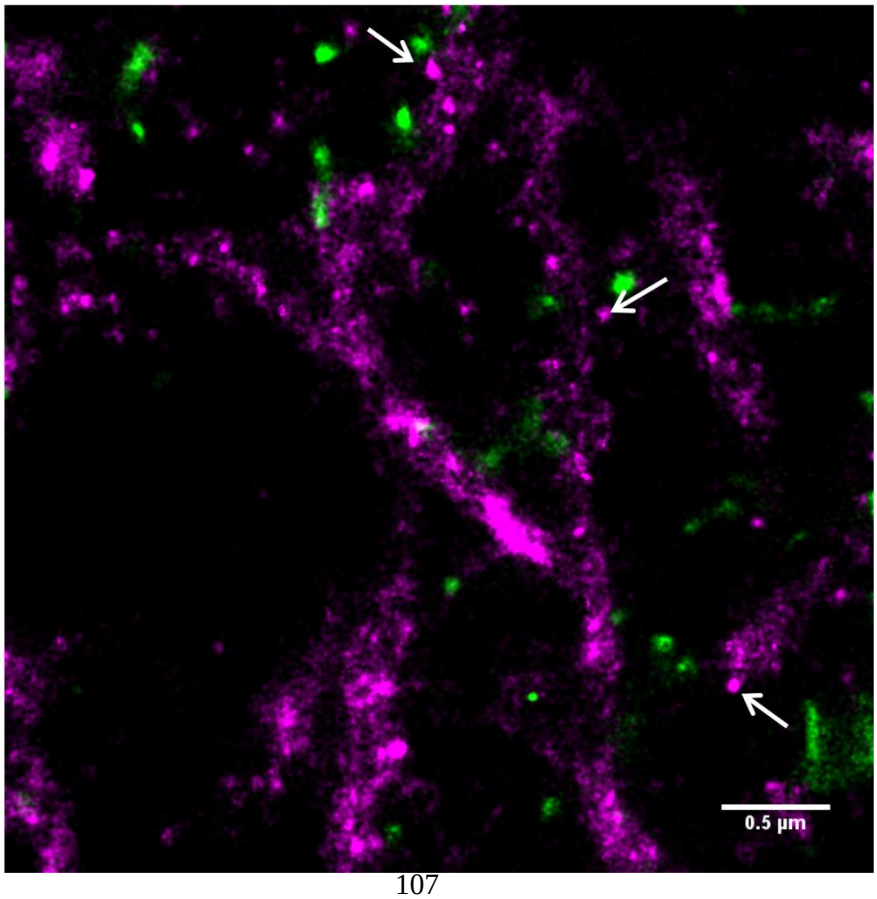

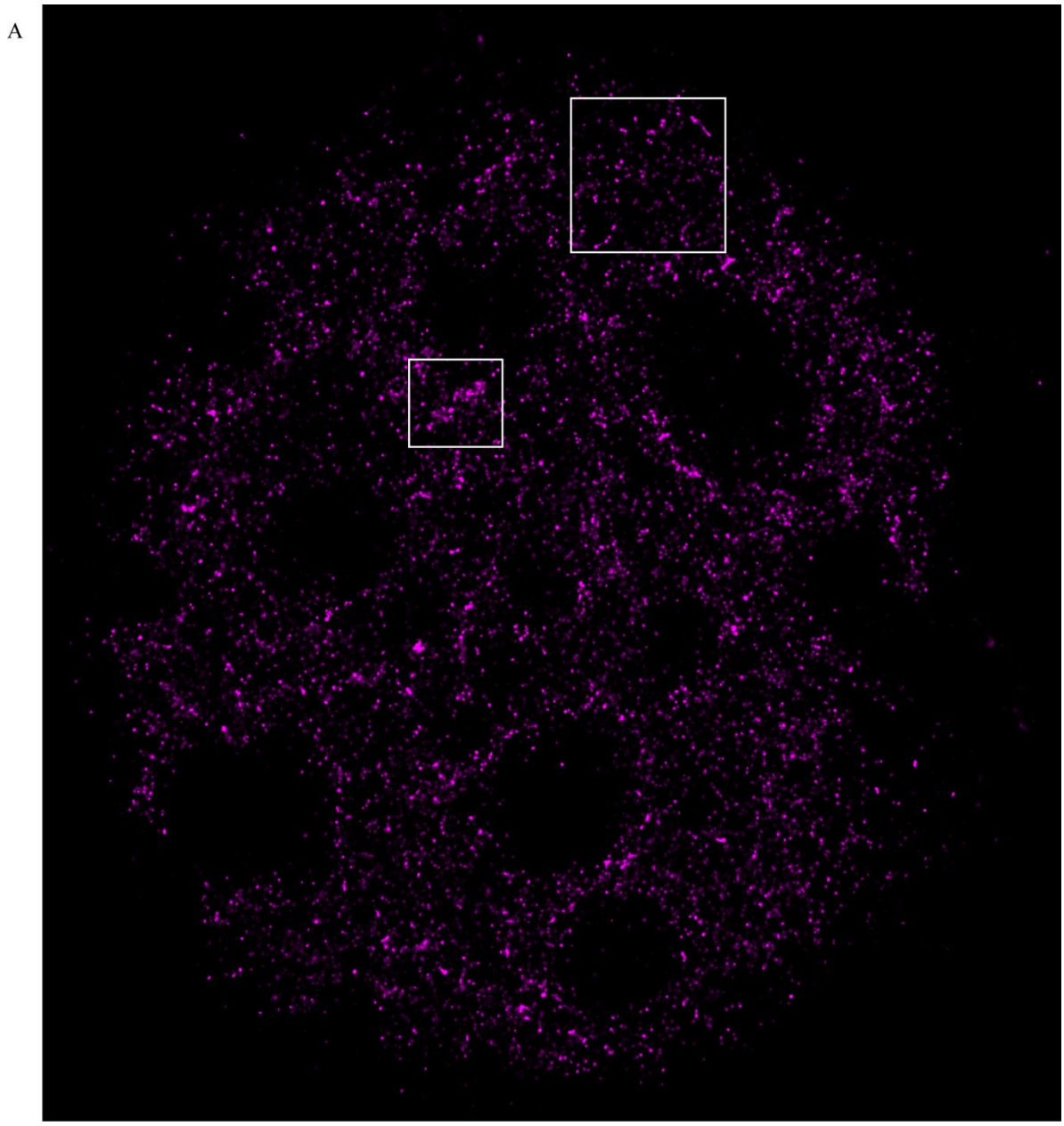

Figure 5.5: VP1 forms clusters of virions in the nucleus of infected cells. A) Full Nuclei of 32 HPI MEF, fixed, permeabilized and immunostained for VP1. **B -C**) Insets from "A", with 500nm scale bar, white arrows indicate objects that are approximately the size of a single virion, yellow arrows indicate objects the size of a single "tube".
B and C on next page

B

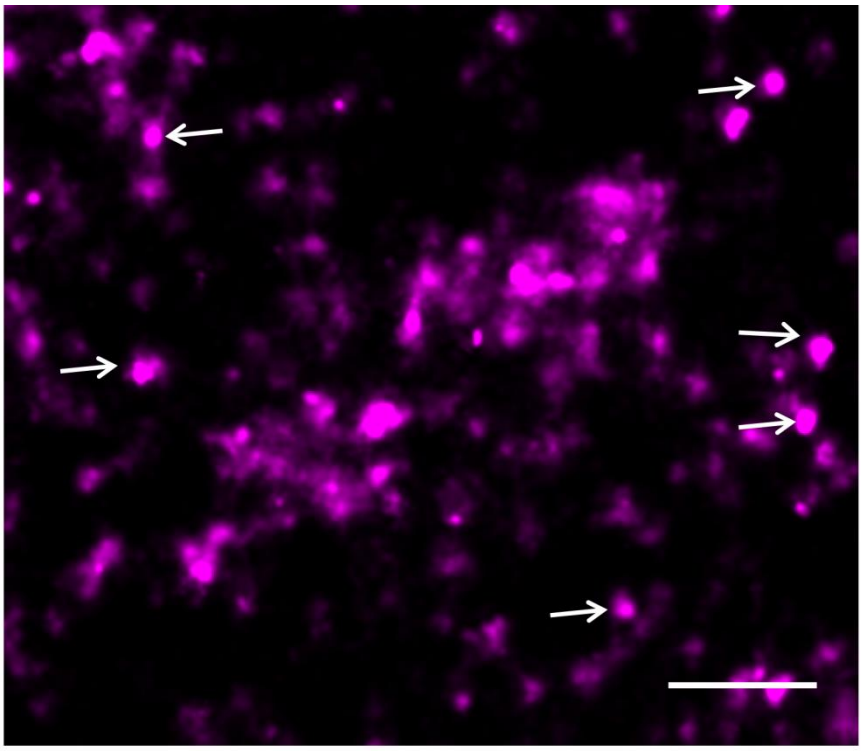

C

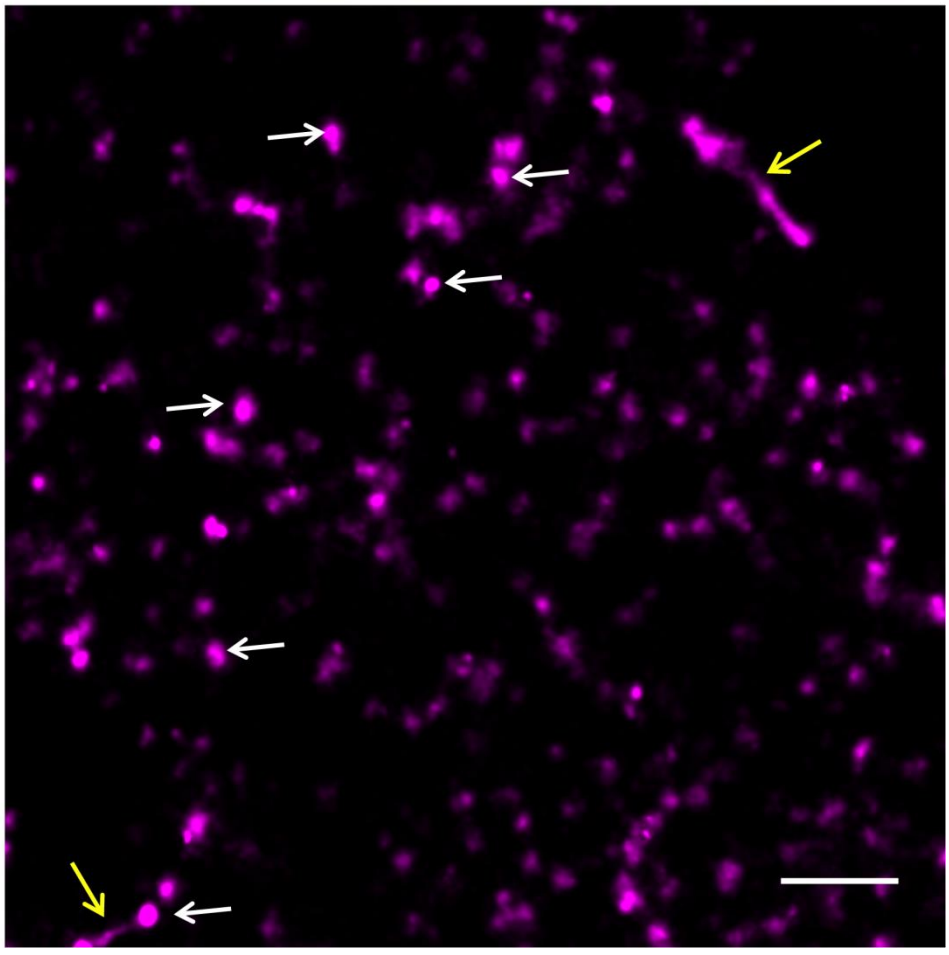

5.4 Conclusions

We were able to optimize two-color STORM imaging for analyzing MuPyV infected nuclei. We utilized a two-camera system and a non-canonical STORM fluorophore, ATTO 565 to improve the signal to noise ratio during image acquisition. With this system, we were able to more closely analyze the relationship between a host protein, PML and a viral protein, Tag. Additionally, we were able to visualize viral proteins Tag and VP1 together, at a resolution above that of traditional light microscopy for the first time. Interestingly we observed higher order structures of VP1 and objects consistent with single virions, inside the nucleus of infected cells.

5.5 Discussion

STORM imaging is difficult in thick, densely labeled samples because single molecules must be visible over background out-of-focus fluorescence. The localization precision of a single molecule is defined by the full width at half the maximum intensity of the point spread function (PSF) of the fluorophore. If the peak fluorescence of single emitters is marginally above background, the localization precision is severely compromised. Viral proteins expressed inside the nucleus represent a thick, densely labeled sample that required further optimization of standard imaging protocols to avoid these problems. We optimized the ATTO 565 fluorophore for two-color STORM imaging of MuPyV proteins.

PyVs reorganize host cell components in order to efficiently replicate viral DNA and assemble new virions. LT is the highly multifunctional viral protein associated with viral DNA replication that is primarily responsible for this reorganization. LT is involved in DNA replication, viral gene transcription, inhibition of cellular pathways, and virion packaging. It is

unclear how these various processes spatially segregate. In order to better understand this process, we visualized Tag in conjunction with other viral and cellular proteins.

Tag localized to clusters throughout the nucleus, with a subset of Tag more closely associated with PML-NBs. Additionally we observed a small subset of Tag associated with VP1 tubes throughout the nucleus. The subset of Tag associated with PML-NBs appears to be largely excluded from the nuclear bodies. This exclusion may be related to the MuPyV induced reorganization of PML into ring-like structures. It is also possible that the dense PML-NB simply acts as a barrier to the expansion of Tag tracks through the nucleus. The nucleus is packed densely with proteins and nucleic acids; therefore, an alternative explanation is that this exclusionary relationship is simply due to spatial constraints. The subset of Tag associated with VP1 was localized adjacent to tube-like structures in the nucleus. However, we did not observe a consistent association of Tag with VP1 tubes. It is unclear whether this is due to sampling bias in STORM imaging, or a real biological phenomenon.

Recently PyV "factories" were described using EM and tomographic reconstruction. These factories are comprised of long tube-like structures adjacent to progeny virions. Additionally, viral replication centers are well described using confocal microscopy. The intersection of these two structures was not evaluated, because of the constraints of immuno-EM and the limit of light microscopy. Here we show the first images of these PyV factories using a light microscopy based technique, STORM. We show a network of tube like structures extending from the nuclear periphery. This localization could suggest a mechanism of tube "nucleation" near the nuclear lamina that builds a lattice of VP1 tubes throughout the nucleus. These data could suggest the interesting possibility that VP1 scaffolds on an existing cellular protein or structure in order to build these tubes. The ability to image these structures using light

microscopy greatly expands the number of candidate proteins that can be visualized alongside VP1. Our ability to characterize these structures will no longer be limited by electron density or the availability of immuno-EM compatible antibodies.

Three-dimensional STORM imaging is required to distinguish whether these large tube-like structures observable by STORM are clusters of tubes visible by EM. Since the axial space sampled in 2D STORM could be as much as a micron, it is impossible to distinguish the 3D size of these objects. Double-Helix (DH) microscopy is a point spread function engineering technique that encodes the z-position of the molecule into the image (Pavani and Piestun 2008, Pavani, et al. 2009). DH can improve the z-resolution for single molecule imaging to approximately 20nm. Combining the techniques we developed with DH will enable us to visualize these structures in even greater detail.

Chapter 6

Conclusions, Discussion, and Future Directions

6.1 Conclusions and Discussion

Viruses manipulate the host cell environment in order to efficiently replicate the viral genome and assemble progeny virions. DNA viruses have diverse mechanisms of DNA replication and may utilize different pathways to replicate their genomes. For example, PML-NBs appear to serve as sites for papillomavirus assembly, whereas we showed that MuPyV does not require PML-NBs to replicate or assemble (Day, et al. 1998, Erickson, et al. 2012). Adenovirus replication is inhibited by MRN dependent ATM signaling during early steps of viral replication, but PyVs seem to require ATM for efficient replication (Dahl, et al. 2005, Shah and O'Shea 2015). These variations may be due to difference in viral genome shape, phase of the cell cycle or cell type in which these viruses replicate.

6.1.1 Requirement for DDR proteins during MuPyV infection

I extensively analyzed the requirement for DDR proteins during MuPyV replication and assembly. I found CHK1, CHK2, H2AX and DNA-PK signaling were not necessary, but ATR activity was required during MuPyV infection. I found conflicting outcomes when I attempted to assay the requirement for ATM or the MRN complex during infection. I was not able to recapitulate previous reports showing a requirement for ATM during PyV infection and NBS1 knockdown cell lines showed either no change in viral titers or an increase in viral titers. This suggests that NBS1 is not required for MuPyV infection, but may in fact act as an antiviral agent. Finally, I identified a more subtle role for the RPA interaction with LT in viral genome resolution. Abrogation of the RPA-LT interaction resulted in an accumulation of concatemerized

viral DNA that is unable to be packaged into virions. These data highlight the complex relationship between DDR proteins, DNA replication, and MuPyV. An interesting possibility is that MuPyV activates and utilizes non-canonical DDR pathways in order to aid replication of the viral genome. However, a better understanding of which proteins are activated during infection and which of those are required for virus production is necessary before that distinction can be made.

SV40 recruits homologous recombination mediated repair proteins to its replication centers through ATM kinase signaling (Sowd, et al. 2014). When ATM signaling was inhibited, DNAPK and NHEJ associated proteins co-localized at replication centers. Current hypotheses suggest that SV40 utilizes homologous recombination to resolve viral genomes appropriately, whereas NHEJ mediated repair results in higher-order concatemers. Although this presents evidence that homologous recombination proteins are associated with correct resolution, their functional requirement during infection was never tested. A more comprehensive study of the requirement for DDR proteins during PyV infection is required before homologous recombination can be implicated in PyV DNA resolution.

SV40 DNA switches from a bidirectional mechanism to rolling circle and uni-directional replication in the presence of an ATM inhibitor (Sowd, et al. 2013). I saw a similar concatermization of viral DNA during E320A compared to WT MuPyV infection. It is likely that these DDR proteins are acting to stabilize viral DNA replication complexes or DNA intermediates. Cairns intermediates are formed during bidirectional replication of viral DNA. Cairns intermediates are high stress intermediates that likely contain nicked and single stranded DNA. Homologous recombination mediated repair proteins could stabilize this intermediate similarly to their role in cellular DDR. In the absence of these stabilizing proteins one replication

fork could collapse, resulting in unidirectional replication of the DNA. Alternatively, incorrect resolution of this intermediate could result in ligation of the daughter viral genomes, into a 10 kb dimer.

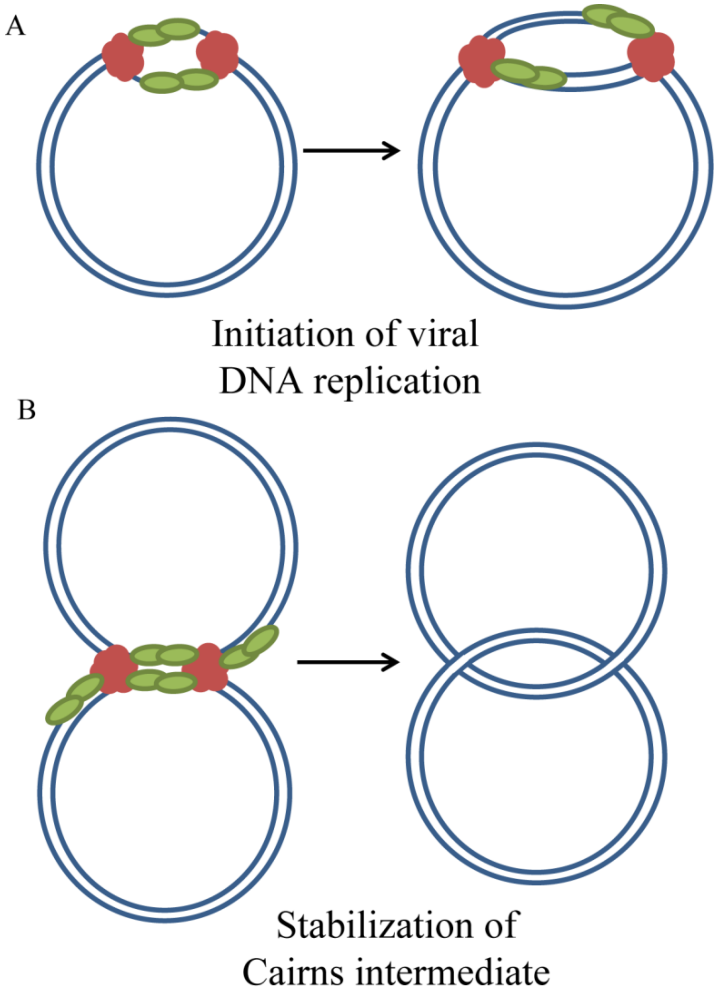

Figure 6.1: Candidate steps for DDR protein activity during MuPyV DNA replication. A) DDR proteins may act to stabilize the formation of the Tag driven replisome at the viral origin of replication. B) DDR proteins may stabilize the Cairns intermediate that forms during bidirectional replication, to prevent breakage or incorrect resolution.

SV40 LT requires an interaction with RPA in order to replicate viral DNA *in vitro*. Abrogation of the interaction between LT and RPA results in a very early failure of viral DNA replication. MuPyV LT still replicated viral DNA in the absence of an interaction with RPA, however the viral DNA was concatemerized. This finding suggests a difference in either the SV40 and MuPyV LTs or the viral origins of replication. It is possible that MuPyV LT unwinds DNA more efficiently than the SV40 LT and therefore does not require RPA to hold the origin of replication open. Alternatively, the MuPyV DNA origin may be more easily unwound and therefore does not require additional stabilization by RPA. In either case, the early requirement for an RPA-LT interaction during SV40 DNA replication would obscure any downstream phenotype such as viral DNA concatemerization. It will be important to determine whether similar mutations to the LT of different PyVs results in a phenotype more similar to that of MuPyV or SV40.

Studies of different PyVs have identified varying requirements for DDR proteins, including checkpoint proteins, CHK1 and CHK2. These differences may be partially due to the difficulty in controlling for cell health during inhibition or knockout of DDR proteins. DDR signaling plays a substantial role in regulating the cell cycle and blocking this signaling can alter both cell number and growth rate between conditions. I believe these secondary variables could lead to false positives in assaying the requirement for DDR during infections. However, if these studies correctly control for these variables, it is still possible that cell type or virus type differences account for differential requirements.

6.1.2 The role of DDR and cell type in different PyV lifecycles

In cell culture models, MuPyV infection progresses over the course of approximately 48 hrs, whereas human PyVs such as JCV replicate poorly in culture and infection cycles last days to weeks. Additionally, MuPyV can replicate in tissue culture in endogenous primary cell types, but JC and other human PyVs replicate in transformed or non-native cell types. Therefore, it is unclear how well these phenotypes recapitulate *in vivo* replication strategies of human PyVs; however, there may be substantial differences in the speed of infection progression between the different PyVs. MuPyV likely primarily utilizes E2F activation through pRb to maintain the S-phase of the cell cycle. However, JCPyV and similar PyVs could rely more heavily on an alternate pathway, such as DDR in order to regulate the cell cycle. JC and similar viruses may maintain the infected host cell in S or G2 phase for the duration of the multi-day replication cycle, or more intriguingly, these viruses may replicate in a cycling or pseudo-cycling cell. In either case, an increased reliance on checkpoint signaling seems feasible. In the case of a cycling or pseudo-cycling cell, DDR signaling could increase the length of s-phase allowing for increased accumulation of viral DNA. This may help explain the differences in phenotypes observed during PyV infection when DDR is inhibited. Some reports show a reduction in viral DNA accumulation, whereas others show a reduction in productive viral titers and some show a mix of both phenotypes.

The PyVs all encode a conserved large Tag protein with helicase activity required for replicating viral DNA. This large Tag mediated DNA replication is likely the driving factor for recruitment and activation of DDR proteins. It is difficult to understand how these large Tag proteins could mediate the resolution of viral DNA through substantially different mechanisms. Therefore, I believe that cell type differences would likely to account for some of the varying

DDR requirements during PyV replication. For example, CHK2 and ATM kinases may have overlapping substrates (Smolka, et al. 2007, Stolz, et al. 2011). It seems likely that in cell types in which CHK2 activity contributes to phosphorylation of DDR proteins, it may have a more pronounced role in viral replication. In cell types in which ATM is the primary kinase of many DDR proteins, CHK2 could be unnecessary. These differences in cell type and virus lifecycle between PyV may account for the complex findings in the field of DDR and PyVs.

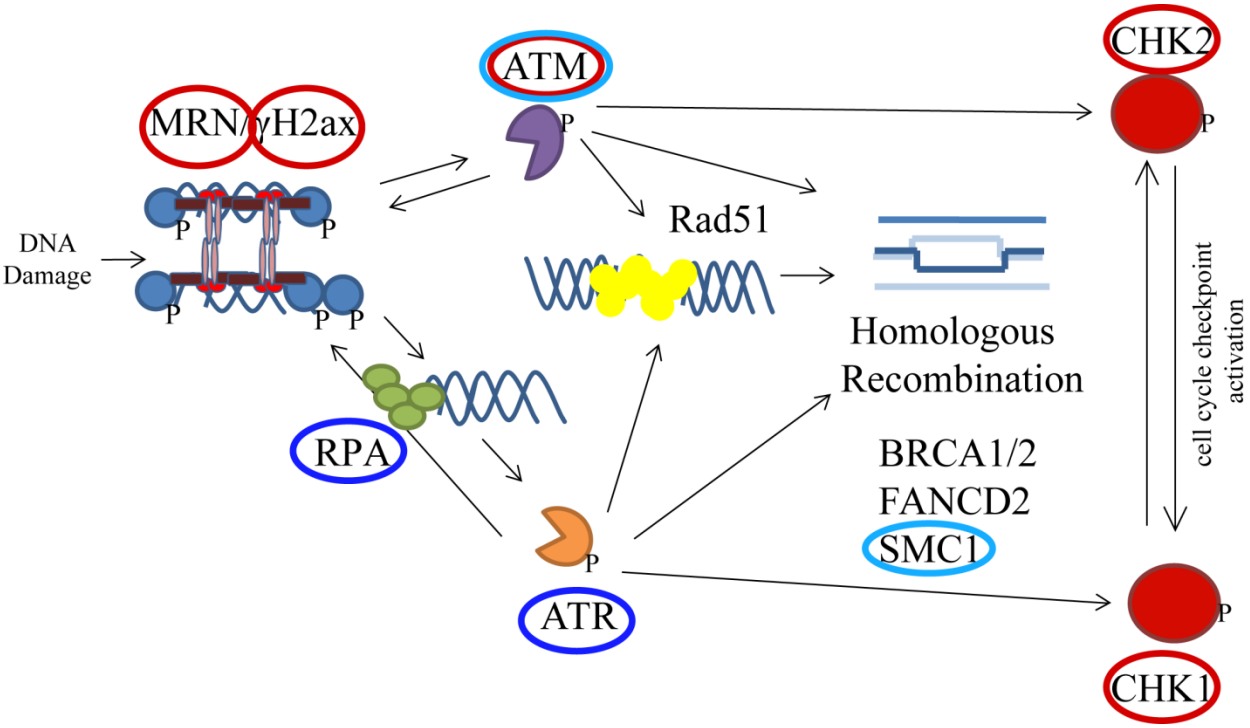

Figure 6.2: Complex requirement for DDR signaling during MuPyV infection. DDR proteins from homologous recombination (ATM and ATR) signaling pathways are shown. Proteins I found to be required for MuPyV replication or assembly are circled in dark blue, those identified in other studies are circled in light blue. Components I did not find a requirement for are circled in red.

The interwoven effects of DDR signaling on host cell viability and viral infection led me to develop more precise methods to interrogate these questions. The improved sensitivity of the immunoplaque assay greatly enhanced my ability to quantify viral titers from different cell lines and inhibitor treatments. This assay in conjunction with simultaneous analysis of infection levels and viral DNA accumulation enabled me to distinguish effects on virus entry, viral DNA replication, or virion assembly during a single experiment. This experimental set up is coupled easily with siRNAs targeting host cell proteins to assess their specific requirement during infection.

6.1.3 The MRN complex during PyV infection

I found that stable knockdown of NBS1 resulted in either no change in viral titers or an increase in viral titers. Interestingly, the later result could suggest that NBS1 has antiviral effects during MuPyV infection. Findings from SV40 infection support an antiviral role for NBS1. SV40 large Tag binds to NBS1 and through this interaction inhibits cellular DNA re-replication control (Wu, et al. 2004). Additionally a previous report shows the SV40 large Tag induced the proteasome dependent degradation of members of the MRN complex, including NBS1 (Zhao, et al. 2008). Although we did not observe a similar degradation during MuPyV infection, it is possible that MuPyV inhibits NBS1 through a different mechanism than SV40. The MRN complex is generally considered to be required for ATM activation during cellular DNA damage events, but recently an MRN independent activation of ATM was reported during adenovirus infection (Lee and Paull 2005, Shah and O'Shea 2015). During adenovirus infection, this non-canonical activation of ATM inhibits viral DNA replication, but PyVs could exploit a similar signaling event to replicate efficiently.

6.1.4 Spatial organization of PyV replication and assembly

As we better understand the requirement for host cell proteins during distinct steps during MuPyV infection, we can better define their functional role. PyV must segregate some of these discrete steps of replication within domains the nucleus. However, our ability to observe sub-nuclear domains was limited previously by the resolution of light microscopy. We demonstrated an improved STORM method that enabled the analysis of MuPyV factories using light microscopy. In conjunction with EdU labeling of DNA, we will be able to determine which host proteins are associated with actively replicating viral DNA. Additionally we will determine whether DDR proteins that are required by MuPyV are spatially segregated from those DDR proteins that are not required. These insights will enable us to better understand the spatial organization of PyV replication and assembly.

PyV "factories" were described using EM as clusters of progeny virions associated with long filamentous structures (Erickson, et al. 2012). I observed higher-order structures of VP1 in the nucleus of infected cells using STORM. If these structures observed by STORM are correlated to ultrastructure observed by EM, this will expand our ability to analyze these structures using light microscopy based techniques. The ability to observe PyV factories using light microscopy will dramatically increase the number of host proteins we are able to analyze as potential components of these factories. These data together could give us unprecedented insight into spatial organization of different functional sub-domains of MuPyV replication and assembly.

6.2. Future directions

6.2.1 E320A mutant MuPyV analysis

The interpretation of the E320A mutant virus experiments requires that I distinguish from where the smaller E320A viral DNA species originated. In order to determine whether the second species of viral DNA observed during infection by E320A was a cloning artifact or a result of the mutation, I will re-clone the E320A mutant virus. Additionally I will create the K381E mutant virus, which also has a defect in RPA-LT binding, to confirm the specificity of the phenotype. Like the E320A mutation, K381E will not overlap the ST or MT open reading frames, making it a good candidate for analysis. Specifically, I will create both of these mutant viruses and the WT control from an EcoRI cloning site in a pUC19 vector to alleviate the possibility of a cloning artifact. The phenotypes shared by the two mutant viruses will better demonstrate the specificity of these mutations for the RPA-LT interaction. A better understanding of the LT-RPA interaction during MuPyV infection is important, especially because I observed a phenotype different from that described for SV40 LT.

The qPCR and southern blot data suggest that rolling circle replication may be the primary reason for the higher-order DNA species that form during E320A infection. The hallmark of rolling circle replication is an increase in the prevalence of unidirectional replication forks and a decrease in the abundance of bidirectional replication intermediates. These DNA species can be detected biochemically using two-dimensional gel electrophoresis. This type of analysis demonstrated the induction of rolling circle replication during SV40 infection in the presence of an ATM inhibitor (Sowd, et al. 2013). Two-dimensional gel analysis of E320A viral DNA would uncover the mechanism of viral DNA concatemerization during E320A replication.

6.2.2 Role of individual DDR proteins during MuPyV infection

In Chapter 4 I demonstrated a protocol that allowed for transient knockdown of RPA during infection without substantially affecting cell viable during the course of the experiment. This method should allow me to target and assess the requirement for other essential host proteins, including Mre11, Rad50, Nbs1, and ATR. I will then target proteins from specific types of DDR, including HR proteins such as FANCD2, Rad51 and Rad52. The HR pathway will be my first target because previous reports suggest that SV40 utilizes HR proteins to resolve the viral genome appropriately (Sowd, et al. 2014). These data will greatly increase our understanding of the requirement for DDR proteins and pathways during MuPyV infection. With this information, we should be able to determine whether MuPyV is utilizing a canonical DDR pathway, or potential a novel subset of proteins involved in DDR. Understanding the requirement for DDR pathways during MuPyV DNA replication may help further elucidate the mechanism of viral genome resolution into monomeric circular DNA.

6.2.3 Super resolution analysis of viral infection

We will continue our studies of MuPyV replication center sub-domains, using three-dimensional super resolution microscopy. Adding a Double Helix module to our optimized STORM set up will enable us to visualize MuPyV factories in three dimensions (Pavani, et al. 2009). This analysis will allow us to better quantify the dimensions of the virus sized objects and tube-like structures observed in STORM reconstructions. Using the assays described above we will be able to identify host proteins required for viral DNA replication, viral DNA resolution, or virion assembly. This information will allow us to define functional domains of replication, repair or assembly by STORM imaging. Combining our better understanding of host proteins'

functional requirements during infection with STORM imaging, we will be able to better elucidate the spatial and temporal segregation of MuPyV replication and assembly.

6.2.4 Extension of studies to other PyVs

The methods I developed using MuPyV should be highly amenable to modification for analysis of other PyVs, including the human PyV, JCPyV. In contrast to MuPyV infection, checkpoint signaling enhances JCPyV DNA replication. Using the system I developed for MuPyV, I could better confirm the specificity of this requirement during JCPyV replication and potentially extend this observation to include other members of DDR pathways. Additionally, there are currently no extensive analyses of the DDR protein requirements during JCPyV infection. It is possible that JCPyV does have substantially different requirements for DDR proteins than MuPyV because of host cell differences or differences in the viral lifecycle. Specifically, JCPyV infection lasts days to weeks longer than MuPyV infection in tissue culture and may therefore have different requirements for cell cycle related proteins. Transitioning these studies into JCPyV would greatly improve our understanding of its replication and assembly. A better understanding of the pathways utilized by JCPyV could identify new drug targets for the treatment of diseases such as Progressive Multifocal Leukoencephalopathy.

References

1. **Aguzzi, A., E. F. Wagner, R. L. Williams, and S. A. Courtneidge.** 1990. Sympathetic hyperplasia and neuroblastomas in transgenic mice expressing polyoma middle T antigen. New Biol **2:**533-543.

2. **Ahn, J., M. Urist, and C. Prives.** 2004. The Chk2 protein kinase. DNA Repair (Amst) **3:**1039-1047.

3. **Andrabi, S., O. V. Gjoerup, J. A. Kean, T. M. Roberts, and B. Schaffhausen.** 2007. Protein phosphatase 2A regulates life and death decisions via Akt in a context-dependent manner. Proc Natl Acad Sci U S A **104:**19011-19016.

4. **Andrews, D. W., J. Gupta, and G. Abisdris.** 1993. Evidence that the middle T antigen of polyomavirus interacts with the membrane skeleton. Mol Cell Biol **13:**4703-4713.

5. **Arroyo, J. D., and W. C. Hahn.** 2005. Involvement of PP2A in viral and cellular transformation. Oncogene **24:**7746-7755.

6. **Arunkumar, A. I., V. Klimovich, X. Jiang, R. D. Ott, L. Mizoue, E. Fanning, and W. J. Chazin.** 2005. Insights into hRPA32 C-terminal domain--mediated assembly of the simian virus 40 replisome. Nat Struct Mol Biol **12:**332-339.

7. **Banerjee, P., R. DeJesus, O. Gjoerup, and B. S. Schaffhausen.** 2013. Viral interference with DNA repair by targeting of the single-stranded DNA binding protein RPA. PLoS Pathog **9:**e1003725.

8. **Barr, S. M., C. G. Leung, E. E. Chang, and K. A. Cimprich.** 2003. ATR kinase activity regulates the intranuclear translocation of ATR and RPA following ionizing radiation. Curr Biol **13:**1047-1051.

9. **Barsic, A., G. Grover, and R. Piestun.** 2014. Three-dimensional super-resolution and localization of dense clusters of single molecules. Sci Rep **4:**5388.

10. **Bassing, C. H., K. F. Chua, J. Sekiguchi, H. Suh, S. R. Whitlow, J. C. Fleming, B. C. Monroe, D. N. Ciccone, C. Yan, K. Vlasakova, D. M. Livingston, D. O. Ferguson, R. Scully, and F. W. Alt.** 2002. Increased ionizing radiation sensitivity and genomic instability in the absence of histone H2AX. Proc Natl Acad Sci U S A **99:**8173-8178.

11. **Bastin-Shanower, S. A., and S. J. Brill.** 2001. Functional analysis of the four DNA binding domains of replication protein A. The role of RPA2 in ssDNA binding. J Biol Chem **276:**36446-36453.

12. **Bautch, V. L., S. Toda, J. A. Hassell, and D. Hanahan.** 1987. Endothelial cell tumors develop in transgenic mice carrying polyoma virus middle T oncogene. Cell **51:**529-537.

13. **Benjamin, T. L.** 1982. The hr-t gene of polyoma virus. Biochim Biophys Acta **695:**69-95.

14. **Bergeaud, F., and S. Mallat.** 1995. Matching Pursuit of Images. Wavelet Applications Ii, Pts 1 and 2 **2491:**2-13.

15. **Bochkareva, E., D. Martynowski, A. Seitova, and A. Bochkarev.** 2006. Structure of the origin-binding domain of simian virus 40 large T antigen bound to DNA. EMBO J **25:**5961-5969.

16. **Boichuk, S., L. Hu, J. Hein, and O. V. Gjoerup.** 2010. Multiple DNA damage signaling and repair pathways deregulated by simian virus 40 large T antigen. J Virol **84:**8007-8020.

17. **Borowiec, J. A., and J. Hurwitz.** 1988. ATP stimulates the binding of simian virus 40 (SV40) large tumor antigen to the SV40 origin of replication. Proc Natl Acad Sci U S A **85:**64-68.

18. **Brady, J., J. B. Bolen, M. Radonovich, N. Salzman, and G. Khoury.** 1984. Stimulation of simian virus 40 late gene expression by simian virus 40 tumor antigen. Proc Natl Acad Sci U S A **81:**2040-2044.

19. **Brown, J. C., and W. W. Newcomb.** 2011. Herpesvirus capsid assembly: insights from structural analysis. Curr Opin Virol **1:**142-149.

20. **Campbell, K. S., K. P. Mullane, I. A. Aksoy, H. Stubdal, J. Zalvide, J. M. Pipas, P. A. Silver, T. M. Roberts, B. S. Schaffhausen, and J. A. DeCaprio.** 1997. DnaJ/hsp40 chaperone domain of SV40 large T antigen promotes efficient viral DNA replication. Genes Dev **11:**1098-1110.

21. **Carney, J. P., R. S. Maser, H. Olivares, E. M. Davis, M. Le Beau, J. R. Yates, 3rd, L. Hays, W. F. Morgan, and J. H. Petrini.** 1998. The hMre11/hRad50 protein complex and Nijmegen breakage syndrome: linkage of double-strand break repair to the cellular DNA damage response. Cell **93:**477-486.

22. **Carson, C. T., R. A. Schwartz, T. H. Stracker, C. E. Lilley, D. V. Lee, and M. D. Weitzman.** 2003. The Mre11 complex is required for ATM activation and the G2/M checkpoint. EMBO J **22:**6610-6620.

23. **Caruso, M., L. Belloni, O. Sthandier, P. Amati, and M. I. Garcia.** 2003. Alpha4beta1 integrin acts as a cell receptor for murine polyomavirus at the postattachment level. J Virol **77:**3913-3921.

24. **Carvalho, T., J. S. Seeler, K. Ohman, P. Jordan, U. Pettersson, G. Akusjarvi, M. Carmo-Fonseca, and A. Dejean.** 1995. Targeting of adenovirus E1A and E4-ORF3 proteins to nuclear matrix-associated PML bodies. J Cell Biol **131:**45-56.

25. **Celeste, A., O. Fernandez-Capetillo, M. J. Kruhlak, D. R. Pilch, D. W. Staudt, A. Lee, R. F. Bonner, W. M. Bonner, and A. Nussenzweig.** 2003. Histone H2AX phosphorylation is dispensable for the initial recognition of DNA breaks. Nature Cell Biology **5:**675-U651.

26. **Celeste, A., S. Petersen, P. J. Romanienko, O. Fernandez-Capetillo, H. T. Chen, O. A. Sedelnikova, B. Reina-San-Martin, V. Coppola, E. Meffre, M. J. Difilippantonio, C. Redon, D. R. Pilch, A. Olaru, M. Eckhaus, R. D. Camerini-Otero, L. Tessarollo, F. Livak, K. Manova, W. M. Bonner, M. C. Nussenzweig, and A. Nussenzweig.** 2002. Genomic instability in mice lacking histone H2AX. Science **296:**922-927.

27. **Chaurushiya, M. S., and M. D. Weitzman.** 2009. Viral manipulation of DNA repair and cell cycle checkpoints. DNA Repair (Amst) **8:**1166-1176.

28. **Chelbi-Alix, M. K., L. Pelicano, F. Quignon, M. H. Koken, L. Venturini, M. Stadler, J. Pavlovic, L. Degos, and H. de The.** 1995. Induction of the PML protein by interferons in normal and APL cells. Leukemia **9:**2027-2033.

29. **Chen, L., X. Wang, and M. M. Fluck.** 2006. Independent contributions of polyomavirus middle T and small T to the regulation of early and late gene expression and DNA replication. J Virol **80:**7295-7307.

30. **Cheng, S. H., R. Harvey, P. C. Espino, K. Semba, T. Yamamoto, K. Toyoshima, and A. E. Smith.** 1988. Peptide antibodies to the human c-fyn gene product demonstrate pp59c-fyn is capable of complex formation with the middle-T antigen of polyomavirus. EMBO J **7:**3845-3855.

31. **Chu, Y., and X. Yang.** 2011. SUMO E3 ligase activity of TRIM proteins. Oncogene **30:**1108-1116.

32. **Ciccia, A., and S. J. Elledge.** 2010. The DNA damage response: making it safe to play with knives. Mol Cell **40:**179-204.

33. **Cimprich, K. A., and D. Cortez.** 2008. ATR: an essential regulator of genome integrity. Nat Rev Mol Cell Biol **9:**616-627.

34. **Courtneidge, S. A., and A. E. Smith.** 1983. Polyoma virus transforming protein associates with the product of the c-src cellular gene. Nature **303:**435-439.

35. **Cripe, T. P., S. E. Delos, P. A. Estes, and R. L. Garcea.** 1995. In vivo and in vitro association of hsc70 with polyomavirus capsid proteins. J Virol **69:**7807-7813.

36. **Dahl, J., H. I. Chen, M. George, and T. L. Benjamin.** 2007. Polyomavirus small T antigen controls viral chromatin modifications through effects on kinetics of virus growth and cell cycle progression. J Virol **81:**10064-10071.

37. **Dahl, J., A. Jurczak, L. A. Cheng, D. C. Baker, and T. L. Benjamin.** 1998. Evidence of a role for phosphatidylinositol 3-kinase activation in the blocking of apoptosis by polyomavirus middle T antigen. J Virol **72:**3221-3226.

38. **Dahl, J., J. You, and T. L. Benjamin.** 2005. Induction and utilization of an ATM signaling pathway by polyomavirus. J Virol **79:**13007-13017.

39. **Daniels, R., N. M. Rusan, P. Wadsworth, and D. N. Hebert.** 2006. SV40 VP2 and VP3 insertion into ER membranes is controlled by the capsid protein VP1: implications for DNA translocation out of the ER. Mol Cell **24:**955-966.

40. **Davison, A. J., M. Benko, and B. Harrach.** 2003. Genetic content and evolution of adenoviruses. J Gen Virol **84:**2895-2908.

41. **Day, P. M., C. C. Baker, D. R. Lowy, and J. T. Schiller.** 2004. Establishment of papillomavirus infection is enhanced by promyelocytic leukemia protein (PML) expression. Proc Natl Acad Sci U S A **101:**14252-14257.

42. **Day, P. M., R. B. Roden, D. R. Lowy, and J. T. Schiller.** 1998. The papillomavirus minor capsid protein, L2, induces localization of the major capsid protein, L1, and the viral transcription/replication protein, E2, to PML oncogenic domains. J Virol **72:**142-150.

43. **de The, H., C. Chomienne, M. Lanotte, L. Degos, and A. Dejean.** 1990. The t(15;17) translocation of acute promyelocytic leukaemia fuses the retinoic acid receptor alpha gene to a novel transcribed locus. Nature **347:**558-561.

44. **de The, H., C. Lavau, A. Marchio, C. Chomienne, L. Degos, and A. Dejean.** 1991. The PML-RAR alpha fusion mRNA generated by the t(15;17) translocation in acute promyelocytic leukemia encodes a functionally altered RAR. Cell **66:**675-684.

45. **DeCaprio, J. A., J. W. Ludlow, J. Figge, J. Y. Shew, C. M. Huang, W. H. Lee, E. Marsilio, E. Paucha, and D. M. Livingston.** 1988. SV40 large tumor antigen forms a

specific complex with the product of the retinoblastoma susceptibility gene. Cell **54:**275-283.

46. **Dellaire, G., R. W. Ching, K. Ahmed, F. Jalali, K. C. Tse, R. G. Bristow, and D. P. Bazett-Jones.** 2006. Promyelocytic leukemia nuclear bodies behave as DNA damage sensors whose response to DNA double-strand breaks is regulated by NBS1 and the kinases ATM, Chk2, and ATR. J Cell Biol **175:**55-66.

47. **Deshpande, R. A., G. J. Williams, O. Limbo, R. S. Williams, J. Kuhnlein, J. H. Lee, S. Classen, G. Guenther, P. Russell, J. A. Tainer, and T. T. Paull.** 2014. ATP-driven Rad50 conformations regulate DNA tethering, end resection, and ATM checkpoint signaling. EMBO J **33:**482-500.

48. **Doucas, V., A. M. Ishov, A. Romo, H. Juguilon, M. D. Weitzman, R. M. Evans, and G. G. Maul.** 1996. Adenovirus replication is coupled with the dynamic properties of the PML nuclear structure. Genes Dev **10:**196-207.

49. **Duprez, E., A. J. Saurin, J. M. Desterro, V. Lallemand-Breitenbach, K. Howe, M. N. Boddy, E. Solomon, H. de The, R. T. Hay, and P. S. Freemont.** 1999. SUMO-1 modification of the acute promyelocytic leukaemia protein PML: implications for nuclear localisation. J Cell Sci **112 (Pt 3):**381-393.

50. **Dyck, J. A., G. G. Maul, W. H. Miller, Jr., J. D. Chen, A. Kakizuka, and R. M. Evans.** 1994. A novel macromolecular structure is a target of the promyelocyte-retinoic acid receptor oncoprotein. Cell **76:**333-343.

51. **Dyson, N., R. Bernards, S. H. Friend, L. R. Gooding, J. A. Hassell, E. O. Major, J. M. Pipas, T. Vandyke, and E. Harlow.** 1990. Large T antigens of many polyomaviruses are able to form complexes with the retinoblastoma protein. J Virol **64:**1353-1356.

52. **Dyson, N., P. M. Howley, K. Munger, and E. Harlow.** 1989. The human papilloma virus-16 E7 oncoprotein is able to bind to the retinoblastoma gene product. Science **243:**934-937.

53. **Egli, A., L. Infanti, A. Dumoulin, A. Buser, J. Samaridis, C. Stebler, R. Gosert, and H. H. Hirsch.** 2009. Prevalence of polyomavirus BK and JC infection and replication in 400 healthy blood donors. J Infect Dis **199:**837-846.

54. **Erickson, K. D., C. Bouchet-Marquis, K. Heiser, E. Szomolanyi-Tsuda, R. Mishra, B. Lamothe, A. Hoenger, and R. L. Garcea.** 2012. Virion assembly factories in the nucleus of polyomavirus-infected cells. PLoS Pathog **8:**e1002630.

55. **Evans, J. D., and P. Hearing.** 2005. Relocalization of the Mre11-Rad50-Nbs1 complex by the adenovirus E4 ORF3 protein is required for viral replication. J Virol **79:**6207-6215.

56. **Fairman, M. P., and B. Stillman.** 1988. Cellular factors required for multiple stages of SV40 DNA replication in vitro. EMBO J **7:**1211-1218.

57. **Fanning, E., and K. Zhao.** 2009. SV40 DNA replication: from the A gene to a nanomachine. Virology **384:**352-359.

58. **Ferenczy, M. W., L. J. Marshall, C. D. Nelson, W. J. Atwood, A. Nath, K. Khalili, and E. O. Major.** 2012. Molecular biology, epidemiology, and pathogenesis of progressive multifocal leukoencephalopathy, the JC virus-induced demyelinating disease of the human brain. Clin Microbiol Rev **25:**471-506.

59. **Fernandez-Capetillo, O., H. T. Chen, A. Celeste, I. Ward, P. J. Romanienko, J. C. Morales, K. Naka, Z. Xia, R. D. Camerini-Otero, N. Motoyama, P. B. Carpenter, W. M. Bonner, J. Chen, and A. Nussenzweig.** 2002. DNA damage-induced G2-M checkpoint activation by histone H2AX and 53BP1. Nat Cell Biol **4:**993-997.

60. **Feunteun, J., L. Sompayrac, M. Fluck, and T. Benjamin.** 1976. Localization of gene functions in polyoma virus DNA. Proc Natl Acad Sci U S A **73:**4169-4173.

61. **Fluck, M. M., and B. S. Schaffhausen.** 2009. Lessons in signaling and tumorigenesis from polyomavirus middle T antigen. Microbiol Mol Biol Rev **73:**542-563.

62. **Garber, E. A., M. M. Seidman, and A. J. Levine.** 1980. Intracellular SV40 nucleoprotein complexes: synthesis to encapsidation. Virology **107:**389-401.

63. **Garcea, R. L.** 2001. SV40: A human pathogen? Dis Markers **17:**149-151.

64. **Garcea, R. L., and T. L. Benjamin.** 1983. Host range transforming gene of polyoma virus plays a role in virus assembly. Proc Natl Acad Sci U S A **80:**3613-3617.

65. **Garcea, R. L., and M. J. Imperiale.** 2003. Simian virus 40 infection of humans. J Virol **77:**5039-5045.

66. **Garcea, R. L., D. A. Talmage, A. Harmatz, R. Freund, and T. L. Benjamin.** 1989. Separation of host range from transformation functions of the hr-t gene of polyomavirus. Virology **168:**312-319.

67. **Gardner, S. D., A. M. Field, D. V. Coleman, and B. Hulme.** 1971. New human papovavirus (B.K.) isolated from urine after renal transplantation. Lancet **1:**1253-1257.

68. **Ginn, S. L., I. E. Alexander, M. L. Edelstein, M. R. Abedi, and J. Wixon.** 2013. Gene therapy clinical trials worldwide to 2012 - an update. J Gene Med **15:**65-77.

69. **Goldman, E., and T. L. Benjamin.** 1975. Analysis of host range of nontransforming polyoma virus mutants. Virology **66:**372-384.

70. **Goodarzi, A. A., and P. A. Jeggo.** 2013. The repair and signaling responses to DNA double-strand breaks. Adv Genet **82:**1-45.

71. **Griffin, B. E., M. Fried, and A. Cowie.** 1974. Polyoma DNA: a physical map. Proc Natl Acad Sci U S A **71:**2077-2081.

72. **Gross, L.** 1953. A filterable agent, recovered from Ak leukemic extracts, causing salivary gland carcinomas in C3H mice. Proc Soc Exp Biol Med **83:**414-421.

73. **Grotzinger, T., T. Sternsdorf, K. Jensen, and H. Will.** 1996. Interferon-modulated expression of genes encoding the nuclear-dot-associated proteins Sp100 and promyelocytic leukemia protein (PML). Eur J Biochem **238:**554-560.

74. **Guy, C. T., S. K. Muthuswamy, R. D. Cardiff, P. Soriano, and W. J. Muller.** 1994. Activation of the c-Src tyrosine kinase is required for the induction of mammary tumors in transgenic mice. Genes Dev **8:**23-32.

75. **Han, R., Z. Li, Y. Fan, and Y. Jiang.** 2013. Recent advances in super-resolution fluorescence imaging and its applications in biology. J Genet Genomics **40:**583-595.

76. **Heino, P., J. Zhou, and P. F. Lambert.** 2000. Interaction of the papillomavirus transcription/replication factor, E2, and the viral capsid protein, L2. Virology **276:**304-314.

77. **Hickson, I., Y. Zhao, C. J. Richardson, S. J. Green, N. M. Martin, A. I. Orr, P. M. Reaper, S. P. Jackson, N. J. Curtin, and G. C. Smith.** 2004. Identification and characterization of a novel and specific inhibitor of the ataxia-telangiectasia mutated kinase ATM. Cancer Res **64:**9152-9159.

78. **Hirao, A., Y. Y. Kong, S. Matsuoka, A. Wakeham, J. Ruland, H. Yoshida, D. Liu, S. J. Elledge, and T. W. Mak.** 2000. DNA damage-induced activation of p53 by the checkpoint kinase Chk2. Science **287:**1824-1827.

79. **Hirt, B.** 1967. Selective extraction of polyoma DNA from infected mouse cell cultures. J Mol Biol **26:**365-369.

80. **Hollenbach, A. D., C. J. McPherson, E. J. Mientjes, R. Iyengar, and G. Grosveld.** 2002. Daxx and histone deacetylase II associate with chromatin through an interaction with core histones and the chromatin-associated protein Dek. J Cell Sci **115:**3319-3330.

81. **Huang, B., S. A. Jones, B. Brandenburg, and X. Zhuang.** 2008. Whole-cell 3D STORM reveals interactions between cellular structures with nanometer-scale resolution. Nat Methods **5:**1047-1052.

82. **Ishov, A. M., and G. G. Maul.** 1996. The periphery of nuclear domain 10 (ND10) as site of DNA virus deposition. J Cell Biol **134:**815-826.

83. **Ishov, A. M., A. G. Sotnikov, D. Negorev, O. V. Vladimirova, N. Neff, T. Kamitani, E. T. H. Yeh, J. F. Strauss, and G. G. Maul.** 1999. PML is critical for ND10 formation and recruits the PML-interacting protein Daxx to this nuclear structure when modified by SUMO-1. Journal of Cell Biology **147:**221-233.

84. **Jensen, E., and D. J. Crossman.** 2014. Technical review: types of imaging-direct STORM. Anat Rec (Hoboken) **297:**2227-2231.

85. **Jensen, K., C. Shiels, and P. S. Freemont.** 2001. PML protein isoforms and the RBCC/TRIM motif. Oncogene **20:**7223-7233.

86. **Jiang, M., P. Entezami, M. Gamez, T. Stamminger, and M. J. Imperiale.** 2011. Functional reorganization of promyelocytic leukemia nuclear bodies during BK virus infection. MBio **2:**e00281-00210.

87. **Jiang, M., L. Zhao, M. Gamez, and M. J. Imperiale.** 2012. Roles of ATM and ATR-mediated DNA damage responses during lytic BK polyomavirus infection. PLoS Pathog **8:**e1002898.

88. **Jiang, X., V. Klimovich, A. I. Arunkumar, E. B. Hysinger, Y. Wang, R. D. Ott, G. D. Guler, B. Weiner, W. J. Chazin, and E. Fanning.** 2006. Structural mechanism of RPA loading on DNA during activation of a simple pre-replication complex. EMBO J **25:**5516-5526.

89. **Jul-Larsen, A., T. Visted, B. O. Karlsen, C. H. Rinaldo, R. Bjerkvig, P. E. Lonning, and S. O. Boe.** 2004. PML-nuclear bodies accumulate DNA in response to polyomavirus BK and simian virus 40 replication. Exp Cell Res **298:**58-73.

90. **Kean, J. M., S. Rao, M. Wang, and R. L. Garcea.** 2009. Seroepidemiology of human polyomaviruses. PLoS Pathog **5:**e1000363.

91. **Koljonen, V., H. Kukko, E. Pukkala, R. Sankila, T. Bohling, E. Tukiainen, H. Sihto, and H. Joensuu.** 2009. Chronic lymphocytic leukaemia patients have a high risk of Merkel-cell polyomavirus DNA-positive Merkel-cell carcinoma. Br J Cancer **101:**1444-1447.

92. **Kornbluth, S., M. Sudol, and H. Hanafusa.** 1987. Association of the polyomavirus middle-T antigen with c-yes protein. Nature **325:**171-173.

93. **Krejci, L., V. Altmannova, M. Spirek, and X. Zhao.** 2012. Homologous recombination and its regulation. Nucleic Acids Res **40:**5795-5818.

94. **Kuypers, D. R.** 2012. Management of polyomavirus-associated nephropathy in renal transplant recipients. Nat Rev Nephrol **8:**390-402.

95. **Lallemand-Breitenbach, V., J. Zhu, F. Puvion, M. Koken, N. Honore, A. Doubeikovsky, E. Duprez, P. P. Pandolfi, E. Puvion, P. Freemont, and H. de The.** 2001. Role of promyelocytic leukemia (PML) sumolation in nuclear body formation, 11S proteasome recruitment, and As2O3-induced PML or PML/retinoic acid receptor alpha degradation. J Exp Med **193:**1361-1371.

96. **LaMorte, V. J., J. A. Dyck, R. L. Ochs, and R. M. Evans.** 1998. Localization of nascent RNA and CREB binding protein with the PML-containing nuclear body. Proc Natl Acad Sci U S A **95:**4991-4996.

97. **Lane, D. P., and L. V. Crawford.** 1979. T antigen is bound to a host protein in SV40-transformed cells. Nature **278:**261-263.

98. **Langerak, P., E. Mejia-Ramirez, O. Limbo, and P. Russell.** 2011. Release of Ku and MRN from DNA ends by Mre11 nuclease activity and Ctp1 is required for homologous recombination repair of double-strand breaks. PLoS Genet **7:**e1002271.

99. **Lau, A., K. M. Swinbank, P. S. Ahmed, D. L. Taylor, S. P. Jackson, G. C. Smith, and M. J. O'Connor.** 2005. Suppression of HIV-1 infection by a small molecule inhibitor of the ATM kinase. Nat Cell Biol **7:**493-500.

100. **Lee, J. H., and T. T. Paull.** 2005. ATM activation by DNA double-strand breaks through the Mre11-Rad50-Nbs1 complex. Science **308:**551-554.

101. **Lee, J. H., and T. T. Paull.** 2004. Direct activation of the ATM protein kinase by the Mre11/Rad50/Nbs1 complex. Science **304:**93-96.

102. **Levine, A. J.** 2009. The common mechanisms of transformation by the small DNA tumor viruses: The inactivation of tumor suppressor gene products: p53. Virology **384:**285-293.

103. **Li, G. M.** 2008. Mechanisms and functions of DNA mismatch repair. Cell Res **18:**85-98.

104. **Liddington, R. C., Y. Yan, J. Moulai, R. Sahli, T. L. Benjamin, and S. C. Harrison.** 1991. Structure of simian virus 40 at 3.8-A resolution. Nature **354:**278-284.

105. **Lilley, B. N., J. M. Gilbert, H. L. Ploegh, and T. L. Benjamin.** 2006. Murine polyomavirus requires the endoplasmic reticulum protein Derlin-2 to initiate infection. J Virol **80:**8739-8744.

106. **Lilley, C. E., C. T. Carson, A. R. Muotri, F. H. Gage, and M. D. Weitzman.** 2005. DNA repair proteins affect the lifecycle of herpes simplex virus 1. Proc Natl Acad Sci U S A **102:**5844-5849.

107. **Lilley, C. E., M. S. Chaurushiya, C. Boutell, R. D. Everett, and M. D. Weitzman.** 2011. The intrinsic antiviral defense to incoming HSV-1 genomes includes specific DNA repair proteins and is counteracted by the viral protein ICP0. PLoS Pathog **7:**e1002084.

108. **Lilley, C. E., R. A. Schwartz, and M. D. Weitzman.** 2007. Using or abusing: viruses and the cellular DNA damage response. Trends Microbiol **15:**119-126.

109. **Lombard, D. B., and L. Guarente.** 2000. Nijmegen breakage syndrome disease protein and MRE11 at PML nuclear bodies and meiotic telomeres. Cancer Res **60:**2331-2334.

110. **Low, J., H. D. Humes, M. Szczypka, and M. Imperiale.** 2004. BKV and SV40 infection of human kidney tubular epithelial cells in vitro. Virology **323:**182-188.

111. **Magnuson, B., E. K. Rainey, T. Benjamin, M. Baryshev, S. Mkrtchian, and B. Tsai.** 2005. ERp29 triggers a conformational change in polyomavirus to stimulate membrane binding. Mol Cell **20:**289-300.

112. **Mahaney, B. L., K. Meek, and S. P. Lees-Miller.** 2009. Repair of ionizing radiation-induced DNA double-strand breaks by non-homologous end-joining. Biochem J **417:**639-650.

113. **Major, E. O.** 2010. Progressive multifocal leukoencephalopathy in patients on immunomodulatory therapies. Annu Rev Med **61:**35-47.

114. **Malkas, L. H., and R. J. Hickey.** 1996. Expression, purification, and characterization of DNA polymerases involved in papovavirus replication. Methods Enzymol **275:**133-167.

115. **Mannova, P., D. Liebl, N. Krauzewicz, A. Fejtova, J. Stokrova, Z. Palkova, B. E. Griffin, and J. Forstova.** 2002. Analysis of mouse polyomavirus mutants with lesions in the minor capsid proteins. J Gen Virol **83:**2309-2319.

116. **Maser, R. S., O. K. Mirzoeva, J. Wells, H. Olivares, B. R. Williams, R. A. Zinkel, P. J. Farnham, and J. H. J. Petrini.** 2001. Mre11 Complex and DNA Replication: Linkage to E2F and Sites of DNA Synthesis. Molecular and Cellular Biology **21:**6006-6016.

117. **Matsumoto, T., T. Eki, and J. Hurwitz.** 1990. Studies on the initiation and elongation reactions in the simian virus 40 DNA replication system. Proc Natl Acad Sci U S A **87:**9712-9716.

118. **Matsuoka, S., B. A. Ballif, A. Smogorzewska, E. R. McDonald, 3rd, K. E. Hurov, J. Luo, C. E. Bakalarski, Z. Zhao, N. Solimini, Y. Lerenthal, Y. Shiloh, S. P. Gygi, and S. J. Elledge.** 2007. ATM and ATR substrate analysis reveals extensive protein networks responsive to DNA damage. Science **316:**1160-1166.

119. **Mattern, C. F., K. K. Takemoto, and W. A. Daniel.** 1966. Replication of polyoma virus in mouse embryo cells: electron microscopic observations. Virology **30:**242-256.

120. **Maul, G. G., H. H. Guldner, and J. G. Spivack.** 1993. Modification of discrete nuclear domains induced by herpes simplex virus type 1 immediate early gene 1 product (ICP0). J Gen Virol **74 (Pt 12):**2679-2690.

121. **Maul, G. G., A. M. Ishov, and R. D. Everett.** 1996. Nuclear domain 10 as preexisting potential replication start sites of herpes simplex virus type-1. Virology **217:**67-75.

122. **Meili, R., P. Cron, B. A. Hemmings, and K. Ballmer-Hofer.** 1998. Protein kinase B/Akt is activated by polyomavirus middle-T antigen via a phosphatidylinositol 3-kinase-dependent mechanism. Oncogene **16:**903-907.

123. **Montross, L., S. Watkins, R. B. Moreland, H. Mamon, D. L. Caspar, and R. L. Garcea.** 1991. Nuclear assembly of polyomavirus capsids in insect cells expressing the major capsid protein VP1. J Virol **65:**4991-4998.

124. **Mutti, L., M. Carbone, G. G. Giordano, and A. Giordano.** 1998. Simian virus 40 and human cancer. Monaldi Arch Chest Dis **53:**198-201.

125. **Nagashima, K., K. Yamaguchi, H. Nakase, and J. Miyazaki.** 1982. Progressive multifocal leukoencephalopathy. A case report and review of the literature. Acta Pathol Jpn **32:**333-343.

126. **Nakanishi, A., N. Itoh, P. P. Li, H. Handa, R. C. Liddington, and H. Kasamatsu.** 2007. Minor capsid proteins of simian virus 40 are dispensable for nucleocapsid assembly and cell entry but are required for nuclear entry of the viral genome. J Virol **81:**3778-3785.

127. **Novoa, R. R., G. Calderita, R. Arranz, J. Fontana, H. Granzow, and C. Risco.** 2005. Virus factories: associations of cell organelles for viral replication and morphogenesis. Biol Cell **97:**147-172.

128. **O'Shea, C. C.** 2005. DNA tumor viruses -- the spies who lyse us. Curr Opin Genet Dev **15:**18-26.

129. **Oakley, G. G., and S. M. Patrick.** 2010. Replication protein A: directing traffic at the intersection of replication and repair. Front Biosci (Landmark Ed) **15:**883-900.

130. **Olson, E., C. J. Nievera, V. Klimovich, E. Fanning, and X. Wu.** 2006. RPA2 is a direct downstream target for ATR to regulate the S-phase checkpoint. J Biol Chem **281:**39517-39533.

131. **Orba, Y., T. Suzuki, Y. Makino, K. Kubota, S. Tanaka, T. Kimura, and H. Sawa.** 2010. Large T antigen promotes JC virus replication in G2-arrested cells by inducing ATM- and ATR-mediated G2 checkpoint signaling. J Biol Chem **285:**1544-1554.

132. **Ostapchuk, P., and P. Hearing.** 2005. Control of adenovirus packaging. J Cell Biochem **96:**25-35.

133. **Ou, H. D., T. J. Deerinck, E. Bushong, M. H. Ellisman, and C. C. O'Shea.** 2015. Visualizing viral protein structures in cells using genetic probes for correlated light and electron microscopy. Methods **90:**39-48.

134. **Padgett, B. L., D. L. Walker, G. M. ZuRhein, R. J. Eckroade, and B. H. Dessel.** 1971. Cultivation of papova-like virus from human brain with progressive multifocal leucoencephalopathy. Lancet **1:**1257-1260.

135. **Pallas, D. C., L. K. Shahrik, B. L. Martin, S. Jaspers, T. B. Miller, D. L. Brautigan, and T. M. Roberts.** 1990. Polyoma small and middle T antigens and SV40 small t antigen form stable complexes with protein phosphatase 2A. Cell **60:**167-176.

136. **Pallas, D. C., W. Weller, S. Jaspers, T. B. Miller, W. S. Lane, and T. M. Roberts.** 1992. The third subunit of protein phosphatase 2A (PP2A), a 55-kilodalton protein which is apparently substituted for by T antigens in complexes with the 36- and 63-kilodalton PP2A subunits, bears little resemblance to T antigens. J Virol **66:**886-893.

137. **Pavani, S. R., and R. Piestun.** 2008. High-efficiency rotating point spread functions. Opt Express **16:**3484-3489.

138. **Pavani, S. R., M. A. Thompson, J. S. Biteen, S. J. Lord, N. Liu, R. J. Twieg, R. Piestun, and W. E. Moerner.** 2009. Three-dimensional, single-molecule fluorescence imaging beyond the diffraction limit by using a double-helix point spread function. Proc Natl Acad Sci U S A **106:**2995-2999.

139. **Peden, K. W., S. L. Spence, L. C. Tack, C. A. Cartwright, A. Srinivasan, and J. M. Pipas.** 1990. A DNA replication-positive mutant of simian virus 40 that is defective for transformation and the production of infectious virions. J Virol **64:**2912-2921.

140. **Polo, S. E., and S. P. Jackson.** 2011. Dynamics of DNA damage response proteins at DNA breaks: a focus on protein modifications. Genes Dev **25:**409-433.

141. **Qian, W., and K. G. Wiman.** 2000. Polyoma virus middle T and small t antigens cooperate to antagonize p53-induced cell cycle arrest and apoptosis. Cell Growth Differ **11:**31-39.

142. **Rajsbaum, R., A. Garcia-Sastre, and G. A. Versteeg.** 2014. TRIMmunity: the roles of the TRIM E3-ubiquitin ligase family in innate antiviral immunity. J Mol Biol **426:**1265-1284.

143. **Rass, E., A. Grabarz, I. Plo, J. Gautier, P. Bertrand, and B. S. Lopez.** 2009. Role of Mre11 in chromosomal nonhomologous end joining in mammalian cells. Nat Struct Mol Biol **16:**819-824.

144. **Regad, T., and M. K. Chelbi-Alix.** 2001. Role and fate of PML nuclear bodies in response to interferon and viral infections. Oncogene **20:**7274-7286.

145. **Rodig, S. J., J. Cheng, J. Wardzala, A. DoRosario, J. J. Scanlon, A. C. Laga, A. Martinez-Fernandez, J. A. Barletta, A. M. Bellizzi, S. Sadasivam, D. T. Holloway, D. J. Cooper, T. S. Kupper, L. C. Wang, and J. A. DeCaprio.** 2012. Improved detection suggests all Merkel cell carcinomas harbor Merkel polyomavirus. J Clin Invest **122:**4645-4653.

146. **Rogakou, E. P., C. Boon, C. Redon, and W. M. Bonner.** 1999. Megabase chromatin domains involved in DNA double-strand breaks in vivo. J Cell Biol **146:**905-916.

147. **Rowe, W. P., R. J. Huebner, L. K. Gilmore, R. H. Parrott, and T. G. Ward.** 1953. Isolation of a cytopathogenic agent from human adenoids undergoing spontaneous degeneration in tissue culture. Proc Soc Exp Biol Med **84:**570-573.

148. **Russell, W. C.** 2009. Adenoviruses: update on structure and function. J Gen Virol **90:**1-20.

149. **Rust, M. J., M. Bates, and X. Zhuang.** 2006. Sub-diffraction-limit imaging by stochastic optical reconstruction microscopy (STORM). Nat Methods **3:**793-795.

150. **Saenz Robles, M. T., C. Shivalila, J. Wano, S. Sorrells, A. Roos, and J. M. Pipas.** 2013. Two independent regions of simian virus 40 T antigen increase CBP/p300 levels, alter patterns of cellular histone acetylation, and immortalize primary cells. J Virol **87:**13499-13509.

151. **Salomoni, P., and A. F. Khelifi.** 2006. Daxx: death or survival protein? Trends Cell Biol **16:**97-104.

152. **Sapp, M., and P. M. Day.** 2009. Structure, attachment and entry of polyoma- and papillomaviruses. Virology **384:**400-409.

153. **Saragosti, S., G. Moyne, and M. Yaniv.** 1980. Absence of nucleosomes in a fraction of SV40 chromatin between the origin of replication and the region coding for the late leader RNA. Cell **20:**65-73.

154. **Schaffhausen, B. S., and T. L. Benjamin.** 1976. Deficiency in histone acetylation in nontransforming host range mutants of polyoma virus. Proc Natl Acad Sci U S A **73:**1092-1096.

155. **Schmid, M., T. Speiseder, T. Dobner, and R. A. Gonzalez.** 2014. DNA virus replication compartments. J Virol **88:**1404-1420.

156. **Schmitt, M., U. Wieland, A. Kreuter, and M. Pawlita.** 2012. C-terminal deletions of Merkel cell polyomavirus large T-antigen, a highly specific surrogate marker for virally induced malignancy. Int J Cancer **131:**2863-2868.

157. **Shah, G. A., and C. C. O'Shea.** 2015. Viral and Cellular Genomes Activate Distinct DNA Damage Responses. Cell **162:**987-1002.

158. **Sheng, Q., D. Denis, M. Ratnofsky, T. M. Roberts, J. A. DeCaprio, and B. Schaffhausen.** 1997. The DnaJ domain of polyomavirus large T antigen is required to regulate Rb family tumor suppressor function. J Virol **71:**9410-9416.

159. **Shi, Y., G. E. Dodson, S. Shaikh, K. Rundell, and R. S. Tibbetts.** 2005. Ataxia-telangiectasia-mutated (ATM) is a T-antigen kinase that controls SV40 viral replication in vivo. J Biol Chem **280:**40195-40200.

160. **Shishido-Hara, Y., S. Ichinose, K. Higuchi, Y. Hara, and K. Yasui.** 2004. Major and minor capsid proteins of human polyomavirus JC cooperatively accumulate to nuclear domain 10 for assembly into virions. J Virol **78:**9890-9903.

161. **Shope, R. E., and E. W. Hurst.** 1933. Infectious Papillomatosis of Rabbits : With a Note on the Histopathology. J Exp Med **58:**607-624.

162. **Silverman, L., and L. J. Rubinstein.** 1965. Electron microscopic observations on a case of progressive multifocal leukoencephalopathy. Acta Neuropathol **5:**215-224.

163. **Smith, A. E., H. Lilie, and A. Helenius.** 2003. Ganglioside-dependent cell attachment and endocytosis of murine polyomavirus-like particles. FEBS Lett **555:**199-203.

164. **Smolka, M. B., C. P. Albuquerque, S. H. Chen, and H. Zhou.** 2007. Proteome-wide identification of in vivo targets of DNA damage checkpoint kinases. Proc Natl Acad Sci U S A **104:**10364-10369.

165. **Sontag, E., S. Fedorov, C. Kamibayashi, D. Robbins, M. Cobb, and M. Mumby.** 1993. The interaction of SV40 small tumor antigen with protein phosphatase 2A stimulates the map kinase pathway and induces cell proliferation. Cell **75:**887-897.

166. **Sowd, G. A., N. Y. Li, and E. Fanning.** 2013. ATM and ATR activities maintain replication fork integrity during SV40 chromatin replication. PLoS Pathog **9:**e1003283.

167. **Sowd, G. A., D. Mody, J. Eggold, D. Cortez, K. L. Friedman, and E. Fanning.** 2014. SV40 utilizes ATM kinase activity to prevent non-homologous end joining of broken viral DNA replication products. PLoS Pathog **10:**e1004536.

168. **Srinivasan, A., A. J. McClellan, J. Vartikar, I. Marks, P. Cantalupo, Y. Li, P. Whyte, K. Rundell, J. L. Brodsky, and J. M. Pipas.** 1997. The amino-terminal transforming region of simian virus 40 large T and small t antigens functions as a J domain. Mol Cell Biol **17:**4761-4773.

169. **Stahl, H., P. Droge, and R. Knippers.** 1986. DNA helicase activity of SV40 large tumor antigen. EMBO J **5:**1939-1944.

170. **Stewart, S. E., B. E. Eddy, A. M. Gochenour, N. G. Borgese, and G. E. Grubbs.** 1957. The induction of neoplasms with a substance released from mouse tumors by tissue culture. Virology **3:**380-400.

171. **Stolz, A., N. Ertych, and H. Bastians.** 2011. Tumor suppressor CHK2: regulator of DNA damage response and mediator of chromosomal stability. Clin Cancer Res **17:**401-405.

172. **Stracker, T. H., C. T. Carson, and M. D. Weitzman.** 2002. Adenovirus oncoproteins inactivate the Mre11-Rad50-NBS1 DNA repair complex. Nature **418:**348-352.

173. **Stracker, T. H., and J. H. Petrini.** 2011. The MRE11 complex: starting from the ends. Nat Rev Mol Cell Biol **12:**90-103.

174. **Su, W., W. Liu, B. S. Schaffhausen, and T. M. Roberts.** 1995. Association of Polyomavirus middle tumor antigen with phospholipase C-gamma 1. J Biol Chem **270:**12331-12334.

175. **Suhy, D. A., T. H. Giddings, Jr., and K. Kirkegaard.** 2000. Remodeling the endoplasmic reticulum by poliovirus infection and by individual viral proteins: an autophagy-like origin for virus-induced vesicles. J Virol **74:**8953-8965.

176. **Sullivan, C. S., A. T. Grundhoff, S. Tevethia, J. M. Pipas, and D. Ganem.** 2005. SV40-encoded microRNAs regulate viral gene expression and reduce susceptibility to cytotoxic T cells. Nature **435:**682-686.

177. **Summers, S. A., L. Lipfert, and M. J. Birnbaum.** 1998. Polyoma middle T antigen activates the Ser/Thr kinase Akt in a PI3-kinase-dependent manner. Biochem Biophys Res Commun **246:**76-81.

178. **Sweet, B. H., and M. R. Hilleman.** 1960. The vacuolating virus, S.V. 40. Proc Soc Exp Biol Med **105:**420-427.

179. **Takahashi, Y., V. Lallemand-Breitenbach, J. Zhu, and H. de The.** 2004. PML nuclear bodies and apoptosis. Oncogene **23:**2819-2824.

180. **Taube, S., M. Jiang, and C. E. Wobus.** 2010. Glycosphingolipids as receptors for non-enveloped viruses. Viruses **2:**1011-1049.

181. **Thomas, M. A., D. L. Lichtenstein, P. Krajcsi, and W. S. Wold.** 2007. A real-time PCR method to rapidly titer adenovirus stocks. Methods Mol Med **130:**185-192.

182. **Thompson, M. R., J. J. Kaminski, E. A. Kurt-Jones, and K. A. Fitzgerald.** 2011. Pattern recognition receptors and the innate immune response to viral infection. Viruses **3:**920-940.

183. **Tittel-Elmer, M., C. Alabert, P. Pasero, and J. A. Cobb.** 2009. The MRX complex stabilizes the replisome independently of the S phase checkpoint during replication stress. EMBO J **28:**1142-1156.

184. **Toker, C.** 1972. Trabecular carcinoma of the skin. Arch Dermatol **105:**107-110.

185. **Tokuyasu, K. T.** 1973. A technique for ultracryotomy of cell suspensions and tissues. J Cell Biol **57:**551-565.

186. **Topalis, D., G. Andrei, and R. Snoeck.** 2013. The large tumor antigen: a "Swiss Army knife" protein possessing the functions required for the polyomavirus life cycle. Antiviral Res **97:**122-136.

187. **Torii, S., D. A. Egan, R. A. Evans, and J. C. Reed.** 1999. Human Daxx regulates Fas-induced apoptosis from nuclear PML oncogenic domains (PODs). EMBO J **18:**6037-6049.

188. **Treisman, R., A. Cowie, J. Favaloro, P. Jat, and R. Kamen.** 1981. The structures of the spliced mRNAs encoding polyoma virus early region proteins. J Mol Appl Genet **1:**83-92.

189. **Trujillo, K. M., D. H. Roh, L. Chen, S. Van Komen, A. Tomkinson, and P. Sung.** 2003. Yeast xrs2 binds DNA and helps target rad50 and mre11 to DNA ends. J Biol Chem **278:**48957-48964.

190. **Trujillo, K. M., S. S. Yuan, E. Y. Lee, and P. Sung.** 1998. Nuclease activities in a complex of human recombination and DNA repair factors Rad50, Mre11, and p95. J Biol Chem **273:**21447-21450.

191. **Truong, L. N., Y. Li, L. Z. Shi, P. Y. Hwang, J. He, H. Wang, N. Razavian, M. W. Berns, and X. Wu.** 2013. Microhomology-mediated End Joining and Homologous Recombination share the initial end resection step to repair DNA double-strand breaks in mammalian cells. Proc Natl Acad Sci U S A **110:**7720-7725.

192. **Tsai, B., J. M. Gilbert, T. Stehle, W. Lencer, T. L. Benjamin, and T. A. Rapoport.** 2003. Gangliosides are receptors for murine polyoma virus and SV40. EMBO J **22:**4346-4355.

193. **Tsang, S. H., X. Wang, J. Li, C. B. Buck, and J. You.** 2014. Host DNA damage response factors localize to merkel cell polyomavirus DNA replication sites to support efficient viral DNA replication. J Virol **88:**3285-3297.

194. **Uziel, T., Y. Lerenthal, L. Moyal, Y. Andegeko, L. Mittelman, and Y. Shiloh.** 2003. Requirement of the MRN complex for ATM activation by DNA damage. EMBO J **22:**5612-5621.

195. **van de Linde, S., A. Loschberger, T. Klein, M. Heidbreder, S. Wolter, M. Heilemann, and M. Sauer.** 2011. Direct stochastic optical reconstruction microscopy with standard fluorescent probes. Nat Protoc **6:**991-1009.

196. **Vassin, V. M., M. S. Wold, and J. A. Borowiec.** 2004. Replication protein A (RPA) phosphorylation prevents RPA association with replication centers. Mol Cell Biol **24:**1930-1943.

197. **Walboomers, J. M., M. V. Jacobs, M. M. Manos, F. X. Bosch, J. A. Kummer, K. V. Shah, P. J. Snijders, J. Peto, C. J. Meijer, and N. Munoz.** 1999. Human papillomavirus is a necessary cause of invasive cervical cancer worldwide. J Pathol **189:**12-19.

198. **Wang, M., J. S. Park, M. Ishiai, J. Hurwitz, and S. H. Lee.** 2000. Species specificity of human RPA in simian virus 40 DNA replication lies in T-antigen-dependent RNA primer synthesis. Nucleic Acids Res **28:**4742-4749.

199. **Wang, Z. G., L. Delva, M. Gaboli, R. Rivi, M. Giorgio, C. Cordon-Cardo, F. Grosveld, and P. P. Pandolfi.** 1998. Role of PML in cell growth and the retinoic acid pathway. Science **279:**1547-1551.

200. **Wang, Z. G., D. Ruggero, S. Ronchetti, S. Zhong, M. Gaboli, R. Rivi, and P. P. Pandolfi.** 1998. PML is essential for multiple apoptotic pathways. Nat Genet **20:**266-272.

201. **Weisshart, K., H. Forster, E. Kremmer, B. Schlott, F. Grosse, and H. P. Nasheuer.** 2000. Protein-protein interactions of the primase subunits p58 and p48 with simian virus 40 T antigen are required for efficient primer synthesis in a cell-free system. J Biol Chem **275:**17328-17337.

202. **Weisshart, K., P. Taneja, and E. Fanning.** 1998. The replication protein A binding site in simian virus 40 (SV40) T antigen and its role in the initial steps of SV40 DNA replication. J Virol **72:**9771-9781.

203. **Werness, B. A., A. J. Levine, and P. M. Howley.** 1990. Association of human papillomavirus types 16 and 18 E6 proteins with p53. Science **248:**76-79.

204. **Wessel, R., J. Schweizer, and H. Stahl.** 1992. Simian virus 40 T-antigen DNA helicase is a hexamer which forms a binary complex during bidirectional unwinding from the viral origin of DNA replication. J Virol **66:**804-815.

205. **Wold, M. S., and T. Kelly.** 1988. Purification and characterization of replication protein A, a cellular protein required for in vitro replication of simian virus 40 DNA. Proc Natl Acad Sci U S A **85:**2523-2527.

206. **Wu, X., D. Avni, T. Chiba, F. Yan, Q. Zhao, Y. Lin, H. Heng, and D. Livingston.** 2004. SV40 T antigen interacts with Nbs1 to disrupt DNA replication control. Genes Dev **18:**1305-1316.

207. **Xue, Y., R. Gibbons, Z. Yan, D. Yang, T. L. McDowell, S. Sechi, J. Qin, S. Zhou, D. Higgs, and W. Wang.** 2003. The ATRX syndrome protein forms a chromatin-remodeling complex with Daxx and localizes in promyelocytic leukemia nuclear bodies. Proc Natl Acad Sci U S A **100:**10635-10640.

208. **Yang, S., C. Kuo, J. E. Bisi, and M. K. Kim.** 2002. PML-dependent apoptosis after DNA damage is regulated by the checkpoint kinase hCds1/Chk2. Nat Cell Biol **4:**865-870.

209. **Yim, E. K., and J. S. Park.** 2005. The role of HPV E6 and E7 oncoproteins in HPV-associated cervical carcinogenesis. Cancer Res Treat **37:**319-324.

210. **Zalvide, J., H. Stubdal, and J. A. DeCaprio.** 1998. The J domain of simian virus 40 large T antigen is required to functionally inactivate RB family proteins. Mol Cell Biol **18:**1408-1415.

211. **Zhao, H., and H. Piwnica-Worms.** 2001. ATR-mediated checkpoint pathways regulate phosphorylation and activation of human Chk1. Mol Cell Biol **21:**4129-4139.

212. **Zhao, X., R. J. Madden-Fuentes, B. X. Lou, J. M. Pipas, J. Gerhardt, C. J. Rigell, and E. Fanning.** 2008. Ataxia telangiectasia-mutated damage-signaling kinase- and proteasome-dependent destruction of Mre11-Rad50-Nbs1 subunits in Simian virus 40-infected primate cells. J Virol **82:**5316-5328.

213. **Zhu, J., V. Lallemand-Breitenbach, and H. de The.** 2001. Pathways of retinoic acid- or arsenic trioxide-induced PML/RARalpha catabolism, role of oncogene degradation in disease remission. Oncogene **20:**7257-7265.

214. **Zou, L., and S. J. Elledge.** 2003. Sensing DNA damage through ATRIP recognition of RPA-ssDNA complexes. Science **300:**1542-1548.

215. **Zurhein, G., and S. M. Chou.** 1965. Particles Resembling Papova Viruses in Human Cerebral Demyelinating Disease. Science **148:**1477-1479.